Application of Liquid Membrane-FTIR in the Investigation of the Mechanism in Degradative Solvent Extraction of Biomass

Watcharakorn Ketren

2018

Graduate School of Energy Science
Kyoto University

ABSTRACT

Application of Liquid Membrane-FTIR in the Investigation of the Mechanism in Degradative Solvent Extraction of Biomass

The aim of this study was to apply spectroscopic analysis techniques to clarify the process reactions and product structures in degradative solvent extraction (DSE). Infrared (IR) absorption spectroscopy was proposed to investigate the mechanism prior in-situ measurement. For this purpose, liquid membrane-Fourier Transform Infrared spectroscopy (FTIR) was utilized to characterize the Soluble product without modification (i.e. under the same conditions as those of the DSE system).

DSE is effective not only in dewatering biomass wastes, but also in upgrading them through the selective removal of oxygen functional groups. However, this conversion mechanism has yet to be fully elucidated. Here, liquid membrane-FTIR spectroscopy was utilized to examine the main liquid product (Solvent-soluble) without sample modification. Rice straw (RS) and 1-methylnaphthalene (1-MN) (as a non-hydrogen donor solvent) were used as materials, and measurements were performed under mild conditions (< 350°C). The spectra of the RS Solvent-soluble were observed at room temperature, and the spectra for the 1-MN solvent were used for baseline correction. Overlapping peaks and peak areas of the functional groups were deconvoluted and determined using Igor Pro 7. In order to avoid the overlapping of CH-containing functional groups due to the 1-MN solvent, the absorbance regions of 3600 to 3100 cm^{-1} and 1800 to 1500 cm^{-1} were used to measure the oxygen-hydrogen (OH) stretching and oxygen-containing groups, respectively.

The applicability of liquid membrane-FTIR spectroscopy to the structural analysis of the RS Solvent-soluble was demonstrated through the quantitative measurement of the oxygen content in the OH stretching region. The RS Solvent-soluble was prepared at 350°C with a 60 min-residence time. The measured oxygen content in wt.% d.a.f of Soluble was realistic is relation to the other oxygen-containing groups in the Soluble. The measured bias between measurement groups was very close to zero and suggested a high degree of repeatability for the measurement technique. Compared to conventional FTIR (pellet method), the liquid membrane-FTIR technique provided for the following advantages: improved control of the analyte volume; reduced potential for analyte contamination; and increased spectral peak definition.

For clarification of the reaction pathway and a better understanding of the transformation of oxygen-containing functional groups during DSE, liquid

membrane-FTIR was used to analyze RS DSE performed at treatment temperatures of 200, 250, 300 and 350°C for 0 min, and at 350°C for 60 min. The Solvent-soluble spectra were quantitatively analyzed, and changes in the oxygen-containing functional groups and hydrogen bonds at each temperature were used to characterize the DSE mechanism. It was determined that the DSE reaction process can be divided into three stages. During the first stage, 200–300°C (0 min), oxygen was removed via dehydration, and aromaticity was observed. In the second stage, 300–350°C (0 min), deoxygenation reactions involving dehydration and decarboxylation were followed by reactions for aromatization. For the third stage, 350°C (0–60 min), further aromatization and dehydration reactions were observed. Intramolecular reactions are indicated as the predominant mechanism for dehydration in RS DSE and it is suggested that the final product is composed of smaller molecular compounds.

The disadvantage of using the liquid membrane-FTIR technique described in this study is that the C-H bond content of the 1-MN solvent limits the degree to which C-H bonds in the RS Solvent-soluble can be accurately measured.

The study demonstrates the usefulness of liquid membrane-FTIR in the quantitative examination of the reaction process of DSE of RS, and could be further developed into a powerful tool for applying to real-time and in-situ analysis of thermal solvent extraction or other solvent processes. In addition, the technique can be applied for the analysis of other solvent–carbon based interactions in a variety of disciplines.

Keywords : biomass, degradative solvent extraction, dewater, FTIR, rice straw, upgrade

ACKNOWLEDGEMENTS

This study would not have been possible without the encouragement and kindly support that I received from my advisor, Prof. Hideaki Ohgaki. I would like to thank him for giving me not only the opportunity to work under his guidance but also for his valuable instruction on conducting quality research. I also feel very lucky to have had the opportunity to work with and learn from the great scientists in the Quantum Radiation Energy laboratory (QRE).

The weekly group meeting policy of the laboratory was also very valuable, as it has helped me to refine and improve my research. I would like to thank Assoc. Prof. Toshiteru Kii, Assist. Prof. Heishun Zen, the QRE laboratory staff, who were always supportive in entertaining and critiquing my ideas in every meeting. Their invaluable advice and suggestions were integral to the completion of my research.

I would like to also give my sincere thanks to Nagaya Yumiko for her patience and generous support in helping me navigate the administrative requirements of my study.

I would like to give special thanks to Professor Kouichi Miura, the specially appointed professor from QRE, for giving me the opportunity to study and work on the fascinating analytical technique that he and his group developed.

I am very grateful to Assoc. Prof. Ryuichi Ashida from the graduate school of engineering for his patience and expertise during our lengthy discussions about my results. His recommendations were instrumental in improving both my study and my understanding of analytical chemistry.

My sincere thanks to Dr. Jingchong Yang, who was always willing to help and provide advice and encouragement during difficult times. Thank you also for carefully reviewing my manuscript.

Also, I would like to send a special thanks to Mr. Supachi Jassadajerm and all the laboratory members who provided help when I needed it. I would especially like to thank Ms. Siriwan Krainara who always provided me with encouragement.

I am very grateful to my friends, Am, Fern and Pee-Ooy for their support and encouragement, and to my friend, Alex, for proofreading some of my work.

I would like to express my deepest appreciation to the Japanese government for providing me with the Ministry of Education, Culture, Sports, Science and Technology (MEXT) scholarship.

Lastly, I would like to thank my loving parents and brothers for their love, inspiration, and their belief in me. This study could not have happened without their love and support.

LIST OF FIGURES

LIST OF TABLES

A SUMMARY OF A THESIS

Understanding the process reactions and product structures of degradative solvent extraction method, the suitable tool for interpreting the reaction simultaneously for improving the method is useful. The aim of this study is to apply spectroscopic method to investigate the mechanism of degradative solvent extraction (DSE). The most popular IR spectroscopy Fourier Transform Infrared spectroscopy (FTIR) is proposed to investigate the mechanism of the method prior in-situ measurement could be applied. For this purpose, an approach using of FTIR spectroscopy to characterize the product without modification (under the same conditions as those of the DSE system) was pursued.

DSE method has succeeded in dewater and upgrade low-rank coal and biomass under mild condition (<350 °C). Low-rank coal and biomass are treated in a non-polar and non-hydrogen donor solvent in the autoclave reactor at the optimum 350°C of treatment temperature. The biomass samples are fractionated into 3 fractions called Soluble, Deposit and Residue. Soluble and Deposit are the extracted products and Residue was the unextracted product from the method. DSE is upgraded a low-rank coal and biomass by the selective removing of oxygen functional groups in the form of H_2O or CO_2 during extraction process. The important fraction, Soluble, recovers high yield of as > 82 wt. %-d.a.f and low oxygen contents. Yet the mechanism of the method has not been in-depth understanding so far. Liquid membrane-FTIR spectroscopy was proposed to quantitative analysis of soluble of the biomass sample dissolving in solvent, called the Solvent-soluble, and investigate the reaction processes of DSE. This technique has not yet been applied to the characterization of biomass structure in the liquid phase.

The main part of this work deals with the application of liquid membrane-FTIR spectroscopy technique to examine Solvent-soluble of rice straw (RS) of DSE. The RS Solvent-soluble sample was obtained from the batch solvent extraction. Owing to the effective protocol of the using the thermal solvent extraction is to dewater of coal/biomass, liquid membrane-FTIR was performed to quantitative analysis of the RS Solvent-soluble spectra to study the evolution of the oxygen-containing functional groups during the solvent treatment. IR spectrum obtained substantial information and the analysis by using liquid membrane-FTIR technique could shed light on the underlying reaction mechanism of degradative solvent extraction of biomass.

Chapter 1 presents the rationale and problems of the study. The background of biomass and the pyrolysis of biomass will be mentioned. The study of DSE of coal

and biomass were summarized. The chosen of IR spectroscopy for liquid sample and the suitable IR spectroscopy technique for this study, liquid membrane-FTIR will be described. The research objective and the thesis map were presented at the end of the chapter.

The analyte considering in this study is a liquid phase. Thus, the requiring of the use of special types of liquid cell is acquired. In the preliminary work to obtain the IR spectra of wavenumber range of 4000 – 400 cm^{-1}, KBr salt plates were chosen to use for forming a film and holding the sample. KBr cell is commonly used, economical and has high transmission 90% of IR light. Because of deliquescence, the windows became clouded and could not provide the quality spectra of the interested range, 3600 – 3100 cm^{-1}. The interference peaks in this studied region was not possible to analyze. The suitable liquid cell CaF_2 was selected, the detail of selection was mentioned in **Chapter 2**. Liquid membrane-FTIR and degradative solvent extraction procedures were described in **Chapter 2**.

A proof of the applicable of liquid membrane-FTIR spectroscopy presents in **Chapter 3** in order to analyze the structural of the RS Solvent-soluble of DSE. RS was performed by thermal solvent extraction at the optimum temperature 350 ^{o}C of treatment temperature with 60 min-residence time. The by-product Solvent-soluble was examined by liquid membrane-FTIR. The technique had been applied to analyze the oxygen-hydrogen stretching region which is the main region indicating the oxygen containing in Solvent-soluble. A quantitative analysis of the oxygen-hydrogen stretching region (3600-3100 cm^{-1} region) in Solvent-soluble have been studied to validate the usage of the liquid membrane-FTIR technique. The oxygen content of the RS Soluble in weight percent of d.a.f-soluble was reasonable regarding the existence of other kinds of oxygen-containing groups in RS solid Soluble. The repeatability of the measurements was also examined, the mean difference (bias) between the measuring values of oxygen contained in hydroxyl groups by liquid membrane-FTIR and the average value of repeating measurement was very close to zero. Comparing to the conventional FTIR, the liquid membrane-FTIR has several advantages to conventional solid membrane FTIR. 1) Easier to prepare and control the volume of the analyte, 2) fewer chance of contamination of analyte, and 3) sharper peaks in the spectra.

The conversion mechanism of the degradative solvent extraction method has not been fully understood so far. In order to observe the influence of solvent treatment temperature, RS was treated in 1-methylnaphthalene (1-MN) at a different solvent treatment temperatures varied from 250 to 350 ^{o}C with the residence time for 60 min. This study was presented in **Chapter 4**. The liquid membrane-FTIR was

applied to study the processing mechanism without separation of the solvent. It has been found that the decrease of the peak area for hydrogen bonds in hydroxyl groups obviously occurred at 300 to 350 ^{o}C, suggesting the removal of hydroxyl due to dehydration reactions or the removal of water began from this temperature range. FTIR spectra in the carbonyl stretching region (1800-1600 cm^{-1}) revealed the carbonyl groups in biomass gradually decrease from 300 to 350 ^{o}C. These carbonyl groups could have been removed by the decarboxylation into producing carbon dioxide (CO_2) or through the producing carbon monoxide (CO). The prevailing of aromatic groups at 350 ^{o}C increased from 300 ^{o}C while the oxygen-containing groups in the carbonyl region decreased showed that the aromatization took place during extraction. The dehydration, decarboxylation and the aromatization reactions occurred from 300 to 350^{o}C. This suggests that liquid membrane-FTIR as a technique was successful in resolving the overlapping IR bands and also helpful in the interpretation of the mechanisms for the degradative solvent extraction of biomass.

The use of liquid membrane-FTIR to interpret the main mechanism of the DSE of RS was proposed in a previous study (Chapter 4). However, the FTIR spectra of the previous study were too noisy to deconvolute the overlap peaks. The experimental conditions were adjusted to reduce the noise in the water vibrational region presenting in **Chapter 5**. The newly obtained IR spectra gave good reproducibility spectra and more information on peak resolving, which were helpful in the quantitative analysis in spectral regions related to the oxygenic functional groups and in depicting the process mechanism of DSE for RS. DSE batches of RS were performed at various treatment temperatures from 200°C to 350°C with the residence time of 0 min and at 350°C with the residence time of 60 min. The FTIR spectra of the RS Solvent-soluble at each treatment temperatures were obtained from liquid membrane-FTIR and were quantitatively analyses. The changes of oxygen-containing functional groups as increased treatment temperature were observed. The adjusted spectra provide the quantitative information in observing the dewater mechanism of RS under DSE, by estimating the number and the strength distribution of hydrogen bonds of the RS Solvent-soluble. The reaction process of DSE of RS was postulated regarding the quantitative results obtained in this work. Specifically, the DSE process was divided by temperature range into three stages: from 200°C to 300°C; from 300°C to 350°C (0 min); and during the prolonged residence time of 60 min at 350°C. The first stage was characterized by the release of hydrogen bonds via dehydration and the presence of aromatic compounds. The second stage was marked by the removal of the main oxygen-containing groups (H_2O, CO and CO_2) through dehydration and decarboxylation, and the occurrence of

aromatization. The third stage occurred during the prolonged residence time at 350°C (0 min to 60 min), and was characterized by aromatization and dehydration reactions. At all stages, dehydration and the presence of aromatic C=C groups were observed. This indicates that intramolecular reactions were the predominant mechanism for dehydration in RS DSE. This also signifies that polymerization of RS during the DSE process was suppressed and that the final product is composed of smaller molecular compounds. The suggestion of dehydration along with the observed presence of aromatic C=C bonds at each stage clarified that intramolecular reactions were the dominant process reactions among hydrogen bonds of RS during DSE.

The observed spectra characteristics of the RS Solvent-soluble are analogous to the spectrum of 1-MN. The peak related to the C-H band of the RS Solvent-soluble displayed significant overlap between the different samples due to the strong C-H band for 1-MN. In order to overcome this interference of the background sample, the aliphatic-aromatic C-H (Ali-Aro CH) in the oxygen-hydrogen stretching and the fingerprint region of the Solvent-soluble were studied. The drawback of the using liquid membrane-FTIR technique to study aliphatic-aromatic CH was presented in the additional unsuccessful protocol at **Appendix A**. Due to the 1-MN solvent is the structural dependence of C-H bond absorptivity. The examination on the overlapping of Ali-Aro CH peaks of the sample spectra was performed by dilution the Solvent-soluble with 1-MN solvent. ZnSe windows cell were selected to examine C-H bond in the fingerprint region (1500-400 cm^{-1}). The validation of using ZnSe liquid cell was confirmed by the average peak height ratio at 1165 and 1214 cm^{-1} of IR spectra of Solvent-soluble obtained by using ZnSe and CaF_2 windows cell. The overlap peak of C-H bond were observed in the common OH stretching region, 3600-2600 cm^{-1}, the average peak area of Ali-CH at 2980 cm^{-1} and Aro-CH at 3050 cm^{-1} suggested the existing of 1-MN in the Solvent-soluble. The evaluation of Ali-Aro CH content can be greatly affected by 1-MN solvent which contains a highly aliphatic material with a high absorptivity of aliphatic C-H bonds. For reliable analysis of C-H bond in the Solvent-soluble by using liquid membrane-FTIR technique was not recommended for the C-H bond-containing solvent. This technique cannot apply to investigate C-H bonds of the Solvent-soluble in this study.

In conclusion, in this study liquid membrane-FTIR could be further developed to a powerful tool for applying to real-time and in-situ analysis for thermal solvent extraction or other solvent processes. The technique could provide a new idea for understanding of the mechanism of DSE.

TABLE OF CONTENTS

CHAPTER 1
INTRODUCTION

1.1. Rationale and Problems

Consumption of energy has increased worldwide which leads to the environmental and energy issue. Moreover, the depletion and limited of fossil fuels resources have affected the global economy [49]. Biomass seems to be one of the interesting choices as a production of carbonaceous material and carbon-neutral fuels for energy resources [50]. Biomass fuels include both energy crops and residues generally represent future fuels resources and opportunity fuels [51,52]. Biomass can be converted to fuels and chemicals and materials through biochemical or thermochemical processes. The main thermochemical processes include combustion, gasification, hydrothermal liquefaction and pyrolysis [53-57]. Notably properties of biomass are generally high moisture content, low bulk density and relatively low heating value. These properties of biomass affect performance of thermal conversion system and energy efficiency [58,59]. Pretreatment by drying or removal of water from biomass is necessary prior to utilize and deliver to any thermal conversion processes. Degradative solvent extraction method has succeeded in dewater and upgrade low-rank coal [13-15] and biomass [16-18] under mild condition. Low-rank coal and biomass were treated in non-polar solvent in the autoclave reactor at 350 oC of treatment temperature. The samples were fractionated into 3 fractions called Soluble, Deposit and Residue. Soluble and Deposit were the extracted products and Residue was the unextracted product from the method. The method is upgraded low-rank coal and biomass by the selective removing of oxygen functional groups in the form of H2O, CO and CO2 during extraction process. Recovered high yield of as > 82 %-d.a.f of soluble, low oxygen contents of soluble [16] and it can be utilized as a raw material of carbon fiber indicated the effective of the method in upgrading [15, 58]. Researchers were studied the reaction process of the method in order to in detail understanding for optimizing the treatment conditions. The main reaction mechanism of the degradative solvent extraction process concluded the thermal extraction, deoxygenation, decarboxylation and aromatization reactions of the raw biomass occurred from 250 oC to 350 oC. [18,55], oxygenation and aromatization reaction further occurred during isothermal process (60 min-retention time) [18]. The intramolecular dehydration reactions of biomass were significantly suppressed and in parallel bond cleavage reactions preceded with intramolecular dehydration

reactions, resulting in the formation of low-molecular- weight compounds, these reactions underwent at 300 oC to 350 oC [17]. However, the mechanisms of the DSE are not yet fully understood so far.

Fourier Transform Infrared (FTIR) spectroscopy is the spectroscopic technique commonly used to identify and study molecular structures of carbonaceous materials. Several methods were proposed in order to obtain IR spectrum of carbonaceous materials, coal [27, 31] and biomass [59-64, 65-66]. Liquid cells for IR absorption is the suitable technique regarding the state of sample of this study and for quantitative analysis.

Since the extraction process in this study involved thermal decomposition, causing the reaction process and products would be very complex. The analysis without modification of the analyte, physically or chemically is preferable in order to avoid interfering and contaminating of sample. According to the biomass sample of the study was liquid product from solvent extracted (soluble in solvent, called solvent-soluble).

The purpose of this study is to apply the spectroscopy technique to in-depth investigating the conversion pathway of the degradative solvent extraction of rice straw. Hence, the measurement should be performed with the soluble without removing solvent thus avoiding the contaminations during the sample preparation. The liquid membrane-FTIR method is proposed to apply in this study.

1.2. Background

1.2.1 Biomass

Biomass is a general term of the organic materials originating from plants, trees and crops. Biomass was characterized into four main types by the moisture content namely wood plants, herbaceous plants or grasses, aquatic plants and manures. Woody plants and grasses which will be the types of biomass investigated in this study which can be divided into high and low-moisture material apart from specific applications. Aquatic plants and manures are high moisture materials. Biomass has rich in oxygen content and low calorific heating value. In comparison with coal; biomass has lower thermal content, higher moisture content which results in energy loss in thermal conversion like combustion, a low bulk density which causes in difficult of storage and burning and the physical form is not homogeneous and free flowing makes difficulty in metering and transportation to the end-use equipment. There are many resources of biomass such as wood and wood wastes, agricultural crops and their waste by-product and/or herbaceous biomass. Biomass resource as an organic matter in which the energy is stored in chemical bonds thus

when the bonds between adjacent carbon, hydrogen and oxygen molecules are broken by digestion, combustion, or decomposition, these substances release their stored, chemical energy. As it is a renewable and potentially sustainable resource, it can be used for energy production and chemical or material production. Biomass can be used directly (e.g. combustion) or indirectly by converted into convenient solid, liquid and gaseous fuels. By completely extracting the energy stored in the chemical bonds its product combined with oxygen, the carbon is oxidized to produce carbon dioxide (CO_2) and water. [1-6].

Lignocellulosic biomass is a plant dry matter. It is raw material for the production of bio-fuels. It generalizes the structure of plants to the three main sugar-based polymeric structures, which are cellulose, hemicellulose (cellulose and hemicelluloses are the carbohydrate polymers) and lignin (aromatic polymers). These three polymeric structures are mainly considered in many studies for the understanding of decomposition mechanisms of woody and herbaceous biomass. Moisture in biomass is presented both as water is contained in the cavity within the dead cell and also as absorbed water. The water within the dead cell can be removed by drying while the absorbed water equilibrates with the ambient relative humidity. The moisture content is normally expressed on a wet basis which refers to the weight of water as a percentage of the total wet fuel weight.

Cellulose is a glucose polymer, generally the largest fraction, representing about 40–50% of the biomass by weight. It is polysaccharide (carbohydrate polymer) having the generic formula $(C_6H_{10}O_5)_n$ and an average molecular weight range of 300,000 to 500,000. Cellulose consists of a linear glucan chains of of D-glucopyranose unit, which are linked together by β-(1,4)-glucosidic bonds. The building block for cellulose is actually cellobiose, the repeating unit of a two-sugar unit as in Figures 1.1 and 1.2. The hydroxyl groups on these glucopyranosyl units have a strong tendency to form intra- and inter- molecular hydrogen bonds among the linear glucan chains, which stiffen the chains and can facilitate cellulose aggregations to form highly ordered or crystalline cellulose fibril structures. Most plant celluloses also contain varying degrees of amorphous domains that are more amenable to chemical and enzymatic attack. [7,8]

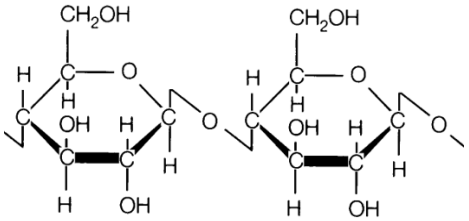

Figure 1.1 Chemical structure of cellobiose

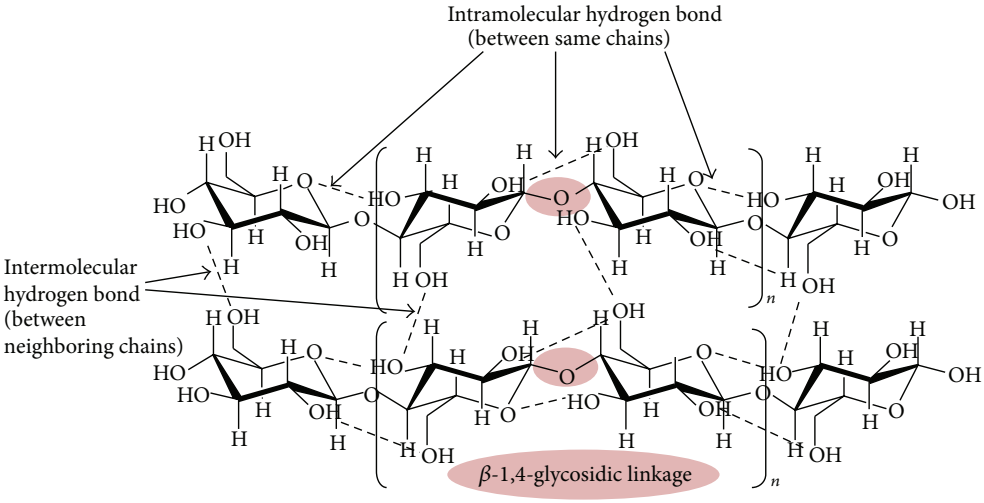

Figure 1.2 Chemical structure of cellulose chains [46]

Hemicellulose represents 20–40% of the material by weight. It contains abundant of polymers; polysaccharides, composed almost entirely of sugars such as glucose, mannose, xylose and arabinose and methylglucuronic and galaturonic acids. Its structure can be understood by first considering the construct of the monomer units. Hemicelluloses usually consist of 50 to 200 monomeric units and a few simple sugar residues. [8,9]. Figure 1.3 is an example of hemicellulose structure.

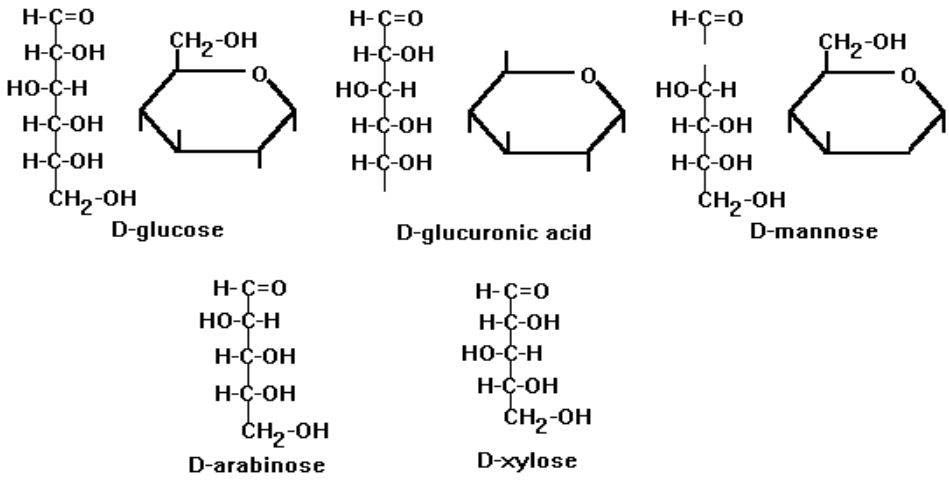

Figure 1.3 The monomer structure in forming of hemicellulose.

Lignin can be regarded as a group of amorphous, high molecular weight, chemically related compounds. It mainly consists of aromatic polymers of phenylpropane units that are considered to be an encrusting substance. The linkages in the polymers occur directly between the rings, between the propane units, and through ether linkages via the hydroxyl groups. The building blocks of lignin are believed to be a three carbon chain attached to rings of six carbon atoms, called phenylpropanes. The small piece of lignin structure illustrates in Figure 1.4. [9,10]

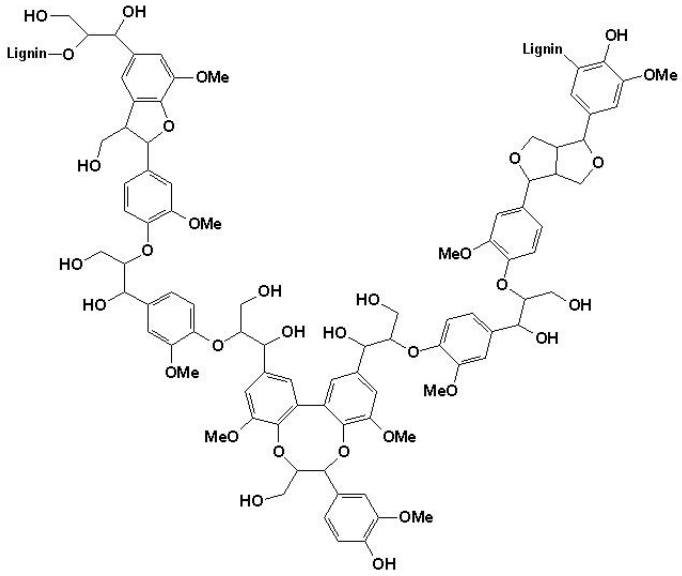

Figure 1.4 Small piece of lignin structure

1.2.2 Pyrolysis of biomass

The literature data report that hemicellulose thermal degradation starts at around 180 °C and finishes at around 350 °C. Cellulose is comparatively more stable than hemicellulose; the temperature of its decomposition ranges from 200 °C to 375 °C, while lignin behaves differently [48]. According to Young et al. 2007 [47], thermal decomposition regions of hemicellulose and cellulose are in ranges of around 220–315 and 315–400 °C, respectively, with maximum mass losses at 268 and 355 °C. Lignin decomposition is in the range from 180 °C up to 900 °C with an undefined maximum mass loss. As was reported in [48], the three main components of wood namely: cellulose, lignin and hemicellulose decompose in temperatures ranging between 240–350, 280–500 and 200–260 °C, respectively.

Generally, thermal decomposition of the organic components is described by the behavior of pyrolysis. Organic components are heated in the absence of oxygen at settle temperature. When biomass is heated to high temperature, biomass is pyrolysed and divided into two fractions. First is a carbon-rich solid residue, called

char, and second is a hydrogen-rich fraction, called volatile matter. The solid residue composes of the non-volatile (or fixed carbon) and the inorganic mineral materials; this fraction is the source in forming ash upon oxidation. The volatile matter is a mixture of low molecular weight compounds such as hydrogen, oxides of carbon, methane and higher molecular weight hydrocarbons such as light oils and tars. The pyrolysis process is usually was significant completed before the gasification or combustion occurred [10].

Pyrolysis is a principal step of biomass thermochemical conversion as it is the initial step of all the processes. Pyrolysis involves in the conversion reaction of biomass by the action of heat in an inert atmosphere into char, gas and a liquid composed of a mixture of hundreds of oxygenated organic compounds. The variety of products and yields were obtained Depending on the operating conditions such as temperature, heating rate, and pressure. Moreover, the diversity in the composition of biomass which constitutes by three main polymers (i.e. cellulose, hemicelluloses and lignin) also contributes to the complexity of the final product. The conventional pyrolysis (slow pyrolysis), cellulose and hemicelluloses are decomposed into volatile matters and chars relating to highly complex reactions. The series of reactions may be classified into the following [10, 11];

1) The temperatures is lower than 300 °C - The reactions at this temperature range produce mainly a char residue. The cellulose is pyrolysed under an inert atmosphere. The reactions include the free radical initiation, the elimination of water, depolymerization, the formation of carbonyl and carboxyl groups and the evolution of carbon monoxide and carbon dioxide gases.

2) The temperature between 300-450°C - The glycosidic linkages of the polysaccharide is broken by substitution of the one of the free hydroxyl groups in order to provide a mixture of the levoglucosan, the derivative of the glucose unit, and oligosaccharides.

3) The temperature is higher than 450°C – A variety of carbonyl compounds is produced by the dehydration reaction, the rearrangement, and the fission of sugar units at this temperature. The produced carbonyl compounds are such as glyoxal, acetaldehyde, and acrolein which they are readily to evaporate. A highly reactive carbonaceous residue containing tapped free radicals occurred by the condensation of the unsaturated products and the cleavage of the side chains through a free radical mechanism. At the temperature above 500 °C, the heating of the cellulosic material produces a mixture of all of these products. As well as, an acidic catalyst or slow heating promotes the dehydration and charring reactions [10,11].

1.2.3 Degradative Solvent Extraction of Coal

Several works studied on the solvent thermal extraction by initial focusing on the fractionation of various types of coals and also various types of biomasses.

The study of Miura *et al*. (2001) presented the extraction of bituminous coals in a flowing stream of non-polar solvent such as tetralin and 1-methylnaphthalene (1-MN) at around 350 °C under 10 MPa. In the study, tetralin and 1-MN were expected not to be involved in chemical reactions with the samples but to act as just a dispersant of the sample. This is also well known and accepted in the field of direct coal liquefaction researches that the used solvent is not involved in chemical reactions even in the presence of catalyst and hydrogen below 350°C. From the results, the method was found to be effective to separate coal into different molecular size fractions without decomposition of coals. The effect of solvent recycling on the extraction was also found to be effective in enhancing the extraction yield and in decreasing further the inorganic fraction in the extracted fraction. In order to obtain the extraction method practically applicable, coal derived oil was also applied for the fractionation of several types of sub bituminous and low-rank coals. It was found that up to 80 wt% of extraction yield was achieved at 350 °C. The yields of residue were plotted against the extraction temperature in Figure 1.5. The fractionation was also performed in the sequential stepwise up to 350 °C for brown coals (Figure 1.6). All the extracted fractions were free from mineral matter and some fractions were found to be fusible like a synthesized pitch when heated [12].

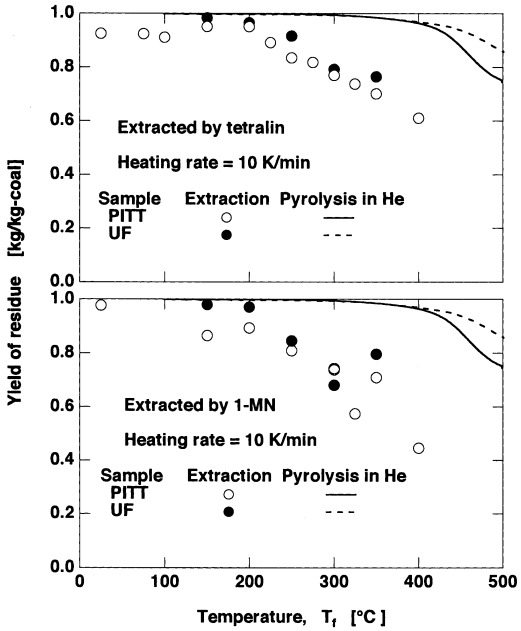

Figure 1.5 Change in the residue yield with the increase of extraction/depolymerization temperature for (a) High rank coals and (b) Low rank coals [12]

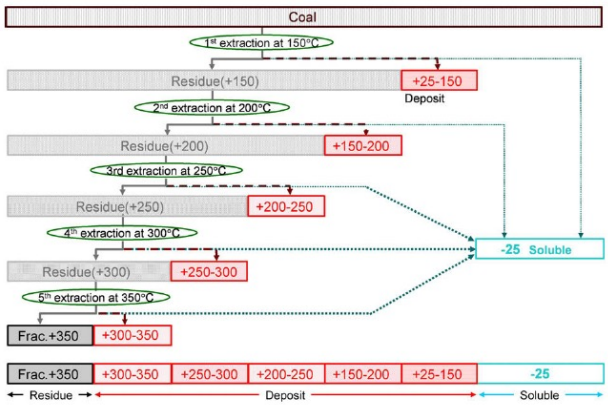

Figure 1.6 Scheme of coal fractionation by solvent extraction [12]

Miura *et al.* [13] presented the solvent extraction method for extracting coal. Twenty coals were extracted by tetralin and two coal derived oil (carbol oil and creosote oil) at 350 °C. The total extraction yields were defined as the sum of the yields of deposit and soluble. Figure 1.7 (a) shows the yield product of twenty coal extracted by tetralin. UF coals reached to 82% for the product yield. The extraction yields exceeded 60% for IL, Mi, Eb, ES and PITT. Using tetralin as solvent is effective to extract some sub-bituminous and bituminous coal. Carbol oil which is a high polar solvent was also used for extract twenty coals which shown in Figure 1.7(b). The extraction yields for lower rank coals were very high such as MW which was the lowest rank coal (its carbon contain only 67.1%) in this study. Its extraction yield high about 70%. Thus, it was showed that carbol oil is effective for extract lower rank coal. Eight coals were extracted by creosote oil as shown in Figure 1.7(c). The extraction yields which extracted by this solvent were close to those in tetralin, but all of the extract were soluble. Polar compounds in the creosote oil were judged to contribute to dissociation of the aggregated structure of the fraction corresponding to the deposit obtained in tetralin. To study the mechanism of the extraction in the carbol oil, a bituminous coal PITT and brown coal MW were chosen as the coal samples and mixed solvents, tetralin/cresol (7/3), tetralin/cresol/naphthalene (5.8/2.5/1.7) and tetralin/phenol (10/1) were also used as a model solvent to examine the extraction behaviors by coal-derived oil. Comparing the extraction yields obtained from the mixed solvents, tetralin/cresol and tetralin/cresol/ naphthalene, with those obtained using tatralin, the carbol oil, and the creosote oil for PITT. Figure 1.8 shows that the amount of deposit decreased significantly by adding cresol to tetralin, and it was null for carbol oil and the creosote extractions. This means that the polar components in solvent contributed to dissociate the aggregated structure of

the components corresponding to the deposit fraction for the tetralin extractions. For brown coal (MW) extraction, tetralin, tetralin/phenol and carbol oil were used as model solvents. The degree of polarity decreases from carbol oil to tetralin. The results are shown in Figure 1.9. The extraction yield increased and the amount of gaseous products decreased when the polarity of solvent increased. It means that the polarity of solvent affected the extraction of low rank coal. The yield of gaseous product decreased, it indicated that the decomposition of brown coal is suppressed by using polar solvent [13].

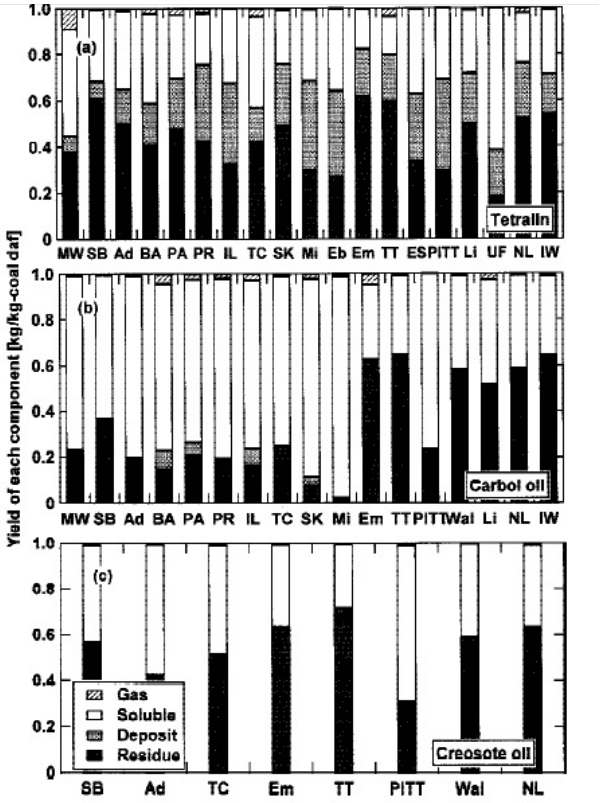

Figure 1.7 Yields of gaseous product, soluble, deposit and residue for various coals through the extraction using (a) tetralin, (b) carbol oil, and (c) creosote oil at 350 °C [13]

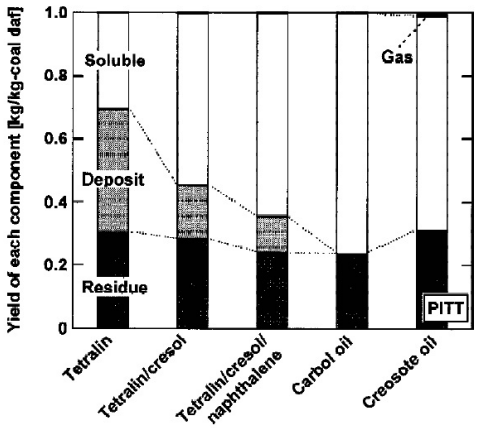

Figure 1.8 Yields of gaseous product, soluble, deposit and residue for PITT through the extraction using various solvents at 350 °C [13]

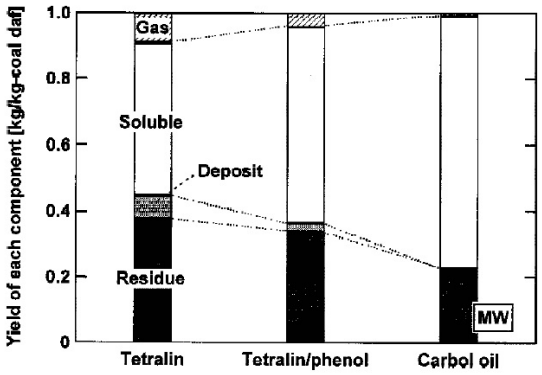

Figure 1.9 Yields of gaseous product, soluble, deposit and residue for MW through the extraction using various solvents at 350 °C [13]

The examination of the coal structure through detailed analyses of the extract and the residue, and the examination of the possibility of preparing clean fuels and/or raw materials for subsequent conversion were studied with various coals including eight Argonne premium coals from 200 °C to 400 °C using a flow-type reactor. It was called the solubilization/ depolymerization experiments. The extraction method is illustrated in Figure 1.10. Coal samples are heated up to around 350 °C from room temperature while a non-polar conventionally used solvent is continuously fed. At room temperature, coals are a little extracted. With increasing temperature, smaller molecule components start being extracted, and most of them are still soluble in the solvent when they are collected at the exit of room temperature. These components are called ''soluble'' hereinafter. With further increasing temperature, larger molecule components are gradually extracted, but those components are precipitated as solids when collected at room temperature. These components are called this fraction ''deposit''. Therefore, the products can be separated into four fractions by the proposed extraction method: soluble, deposit, residue, and gases. The yields of soluble and deposit for bituminous coals, Illinois #6 (IL), PITT (Pittsburgh #8), and UF (Upper Freeport) coals were very large. The extract yields for these coals are as follows: 80% (soluble: 41%, deposit: 39%) for UF, 67% (soluble: 29%, deposit: 38%) for PITT, and 63% (soluble: 27%, deposit: 36%) for IL. 80% of UF coals were extracted at 350 °C. For the lowest rank coal, Beulah Zap lignite (ND), the deposit yield was very small and appreciable amounts of gaseous components were produced. Both the soluble and the deposit yields were small for the highest rank coal, Pochahontus (POC). These results indicate that decomposition reaction occurred for the lowest rank coal ND, but little decomposition reaction occurred for the other higher rank coals. Therefore, most of the soluble and the

deposit for the higher rank coals are judged to be relatively low molecular weight components existent in the original coal. The small molecules could come out because the macromolecular network of coal was relaxed through the heat treatment in the solvent. The comparison of the product yields obtained at the extraction temperature of 350 °C for eight Argonne premium coals is shown in Figure 1.11. Most of the ash was found in the residue. They have also estimated the molecular weight distribution (MWD) of the soluble, the deposit and the residue prepared from PITT coal. The MWDs for the raw coal, the residue and the deposit had peaks at *M* = ca. 300 and ca. 2200. On the other hand, the soluble consists of only small molecules of less than 600 in *M*, and the peak position almost coincides with the peaks w of smaller *M* in the raw coal, the residue and the deposit. This presents the possibility w to prepare clean fuel or clean raw materials in a high yield from bituminous coals by simple extraction.

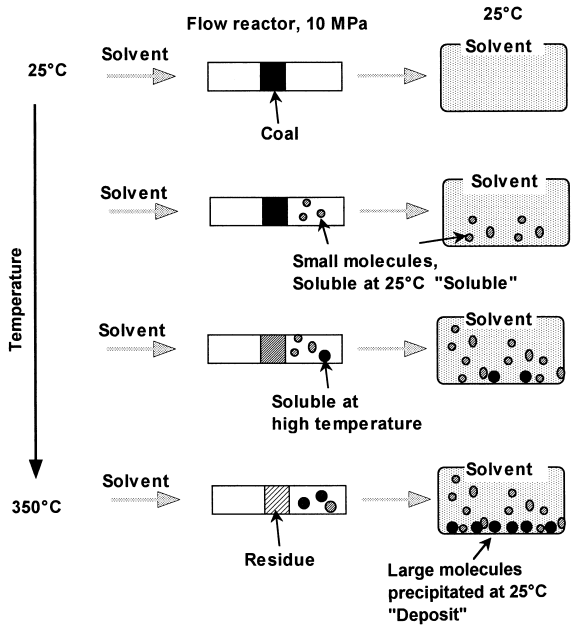

Figure 1.10 Illustration of the extraction of heated coal in a flowing solvent

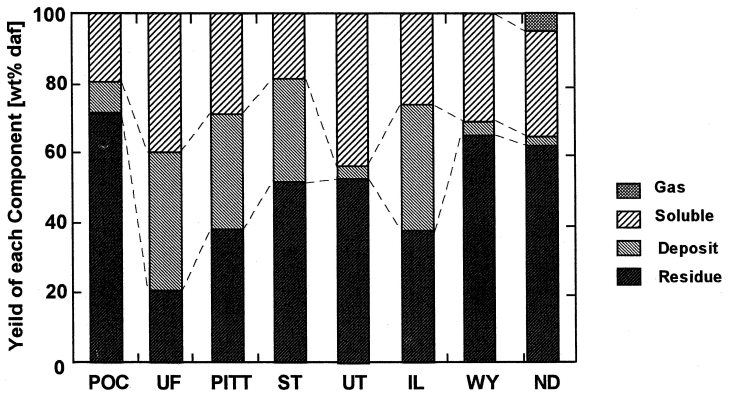

Figure 1.11 Product yields obtained at the extraction temperature of 350 °C for eight Argonne premium coals

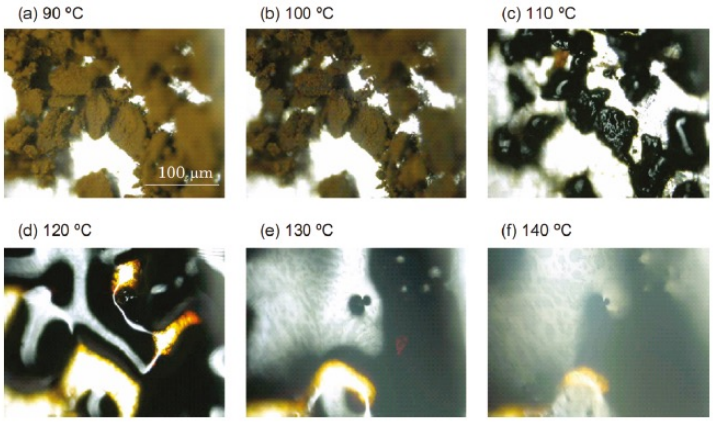

Figure 1.12 Appearance of LY-350-D during heating at 10 °C/min in nitrogen atmosphere

In order to obtain the extraction method practically applicable, coal derived oil was also applied for the fractionation of several types of sub bituminous and low-rank coals. It was found that up to 80 wt% of extraction yield was achieved at 350 °C. The hydrothermal extraction of brown coals at around 350 °C and less than 20 MPa was found to recover as much organic compounds as possible as water soluble fraction. The upgraded coals were found to have the low self-ignition tendencies because of the reductions in the volatile content and the changes in the properties. The extraction of low-rank coals in a stream of hot water at 300-350 °C was also found to obtain the extracted fraction having the higher calorific value and compounds having the thermoplastic property. Almost all Deposits produced by this method were found to melt completely at less than 200 °C. Figure 1.12 showed the images taken during the melting of the Deposit of Australian brown coal treated at 350 °C (LY-350-D). The melting started around 110 °C and became liquid-like at 130 °C. [13]

Miura *et al.* (2010) presented a degradative extraction method at around 350 °C in 1-methylnephalene in a batch type reactor of wide ranges of low-rank coals. The results showed that this method did not lose any calorific values of coals and was effective to recover several fractions having similar chemical and physical properties [14].

Li *et al.* (2012) studied the production of degradative solvent extraction by using eight kinds of low-rank coals including lignites and sub-bituminous coals. The coals included lignites from Thailand and the Philippines, brown coals from Indonesia, Australia and Malaysia, and two sub-bituminous coals from Indonesia. This experimental was subjected in a batch reactor (autoclave) at 350 °C by using 1-methylnapthalene which is the non-hydrogen donor as a solvent. The product yields was shown in Figure 1.13, the yields of solid product were 16.9-27.2 wt%, 3.5-16.9

wt% and 49.7-63.6 wt% on dry and ash free basis for soluble, deposits and residue respectively. The gaseous product was generated about 2.8- 8.7 wt % which mainly was CO_2 which is common in low rank coal. The liquid yields which consisted mainly of water reached to 10.6 wt% on dry and ash free basis that relate to carbon content of the raw coals. The results were showed that 21.8-40.7 wt% of selected coals can be extracted and more than 94.4% of carbon was recovered as solid fractions. Both the Solubles and Deposits were free from water and ash. Elemental compositions of Solubles were C = 81.8−84.8 wt %, H = 7.5−8.1 wt %, and O = 6.5−10.2 wt %. The carbon content of the Solubles was very high which were rather close to the elemental composition of bituminous coal. Moreover the Soluble and Deposit products which were extracted from low rank coal were completely free from water, and almost completely free from ash. [15]

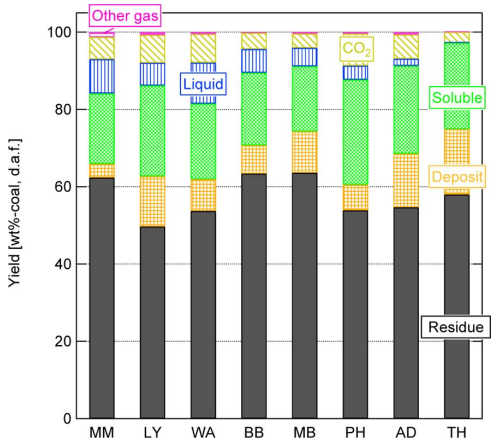

Figure 1.13 Product yields obtained by degradative solvent extraction [15]

1.2.4 Degradative Solvent Extraction of Biomass

Wannapeera *et al.* (2012) studied the production of degradative solvent extraction method by using 8 biomasses, namely Leucaena (abbreviated to LC), eucalyptus (EUCA), oil palm empty fruit bunches (EFB), jatropha trunk (JT) and cassava rhizome (CR), rice husk (RH), napier grass (NP) and rice straw (RS). In addition to the eight types of biomass, a microcrystalline cellulose, a hemicelluloses and a lignin were also collected. This experiment was subjected in a batch reactor (autoclave) at 350 °C by using 1-methylnapthalene as a solvent. For solid product, the carbon-based yield of Solubles, Deposites and Residues were 36.8-71.6%, 4.4-10.6% and 15.1-27.5% respectively. The element distributions of product are showed in Figure 1.14. The elemental compositions of the Solubles from the various biomasses were C = 81.0−83.3 wt %, H = 6.1−7.3 wt %, and O = 7.3−11.1 wt %. It was found that, the Soluble fractions which were extracted from various biomass

contained the highest carbon. The oxygen about 82.5-88.4% was present in gaseous and Liquid fraction. This means that more than 80% of structural oxygen was removed as CO_2, CO and H_2O at 350 °C. Furthermore, most of the ash was concentrated in the Residues, whereas the Solubles were completely free from ash [16].

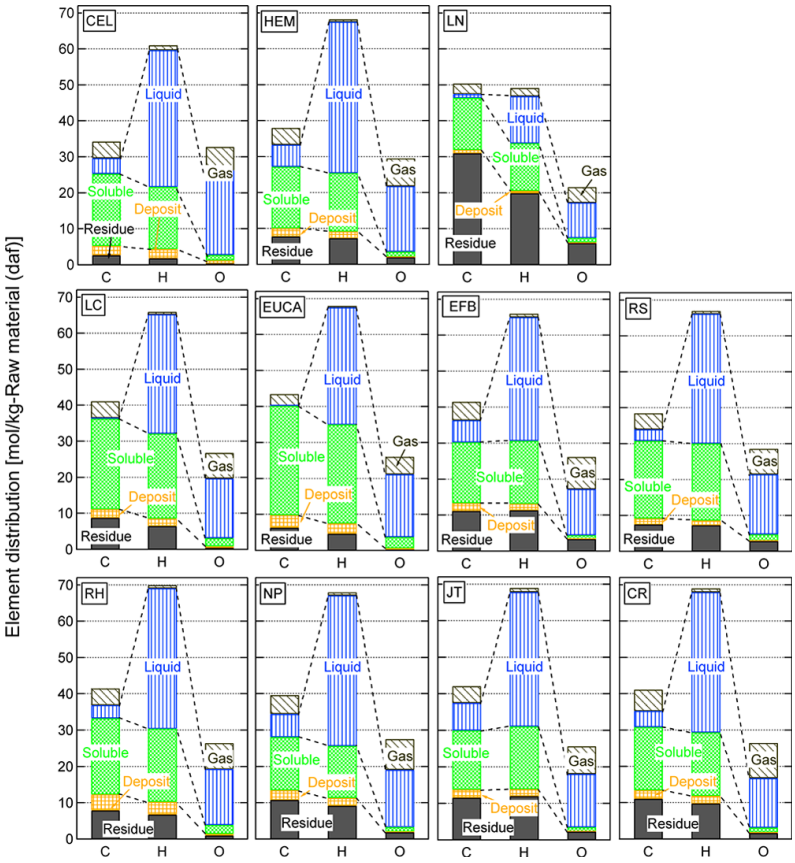

Figure 1.14 Element distribution in the products obtained by solvent treatment of all biomass samples at 350 °C [16]

Wannapeera et al. studied the effects of the solvent-treatment temperature on the product yield was examined at 250, 300, and 350 °C using EFB and RS. The results showed that increasing the solvent-treatment temperature, the Solubles from EFB and RS will increase. Figure 1.15 showed the effect of solvent treatment temperature on the element distribution in the product for (a) EFB and for (b) RS. For the EFB, at 350 °C, oxygen distribution about 82.5% contained the gaseous product or the Liquid. These results indicated that more than 80% of the oxygen in the samples was removed as CO_2, CO, and H2O at 350 °C. The carbon from EFB was distributed to the Soluble, Deposit, and Residue fractions at about 40.7%, 5.3%, and 27.0% respectively, indicating that 73.0% of the carbon was retained in the solid product. The similar trend in the case of rice straw, 350 °C, oxygen distribution about 83.8%

contained the gaseous product or the Liquid. The carbon about 80.0% from RS was retained in the solid product. From these results, the oxygen distribution in the gaseous product and Liquid increased when increasing treatment temperature for both EFB and RS and more than 80% of the oxygen in the samples was removed as CO_2, CO, and H2O at 350 °C. The loss of carbon to gaseous products was mainly due to the formation of CO_2. These results indicated that the thermal reactions are deoxygenation reactions involving dehydration and decarboxylation. It clearly show that the proposed solvent treatment at 350 °C is very effective for simultaneous deoxygenation and recovery of a solid product having a high carbon content and low oxygen content in rather high yield from both EFB and RS [16].

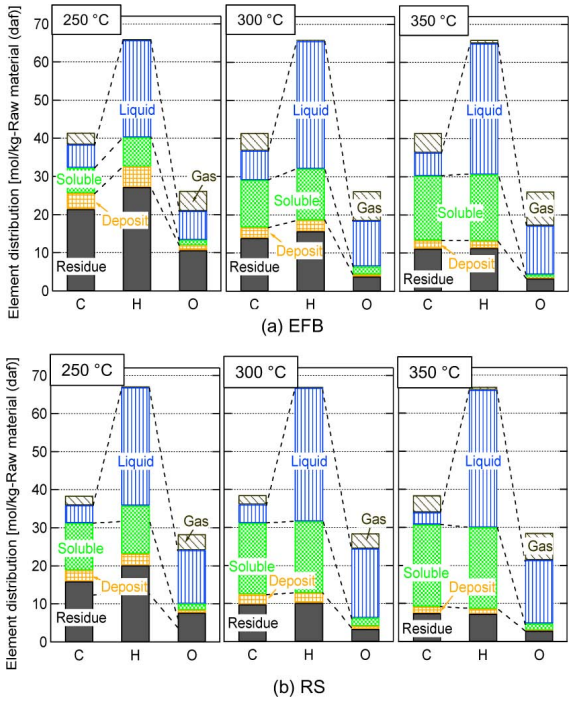

Figure 1.15 Effect of solvent treatment temperature on the element distribution in the product for (a) EFB and for (b) RS [16]

Ashida et al. (2015) studied the mechanism in degradative solvent extraction of biomass wastes. A reagent grade cellulose was used as biomass wastes sample and 1-methylnaphalene (1-MN) was used as non-hydrogen donor solvent. The degradative solvent extraction of the cellulose was conducted using a stainless steel autoclave at temperature lower 350 °C. 15 g (d.a.f.) of sample and 300 cm^3 of 1-MN was used. The reactor was heated up to 300 °C (without holding time) or 350 °C (without holding time or with holding time of 60 min). The product yields of the degradative solvent extraction and N_2 treatment were showed in Figure 1.16. From the results, the soluble yield from the solvent treatment was 36 wt% (d.a.f.) and the

carbon based yield of soluble was as large as 66 wt% (d.a.f.) at 350 °C. Moreover, the soluble yield slightly decreased when it was held at 350 °C for 1 hr. In order to compare the upgrading behaviors between solvent treatment and non-solvent treatment, heat treatment under N_2 atmosphere was examined. It was found that the soluble yield from solvent treatment was higher than the one from N_2 treatment [17].

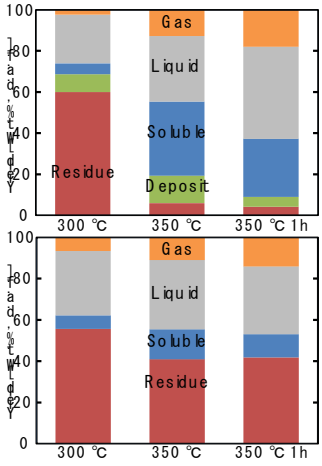

Figure 1.16 Product yields for the degradative solvent extraction (upper) or treatment in N_2 (lower) [17]

Figure 1.17 showed FTIR spectra of the products. It was found that the residue product obtained by solvent treatment at 300 °C retained its original cellulose structure whereas dehydration reactions of OH groups proceeded significantly for N_2 treatment. The soluble product obtained from solvent treatment at 350 °C show that the main dehydration reactions took place at temperature between 300 and 350 °C. The soluble yield increased dramatically in this temperature range for solvent treatment and the bond cleavage reactions occurred. The FTIR spectrum of the soluble obtained by solvent treatment at 350 °C had a distinct peak at 3030 cm^{-3} which is attributed to aromatic CH bonds whereas this peak was not found for the residue from N_2 treatment at the same temperature. The results showed that the existence of the solvent highly suppressed intermolecular dehydration reactions to from cross links at temperature lower than 300 °C which were dominant in the N_2 treatment. Contrary to solvent treatment, the intramolecular dehydration reactions occur in parallel with bond cleavage reactions between 300 and 350 °C which it increase the yield of aromatic rich and low-molecular-weight compounds (soluble). The mechanism of degradative solvent extraction of cellulose was summarized in Figure 1.18 [17].

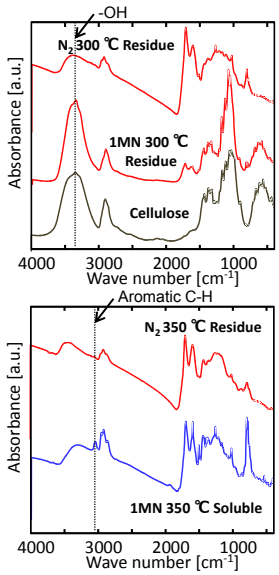

Figure 1.17 FTIR spectra of the main solid products [17]

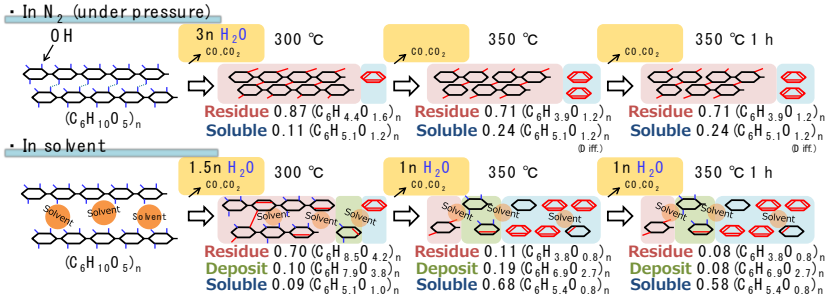

Figure 1.18 Upgrading mechanism of cellulose [17]

Zhu et al. (2015) studied the mechanism of degradative solvent extraction of a fir sawdust (abbreviated as SD) was employed as a raw material. The degradative solvent extraction was conducted at 350 C at an average heating rate of 5 K/min. The residence time at 350 C were 0, 15, 30, 45, 60, and 90 min. The product yield distributions of degradative solvent extraction of SD at different residence time (0–90 min) are given in Figure 1.19. The results implied that the Deposit decomposed to generate Soluble with prolonging the residence time and the short residence time is sufficient to obtain the extracts. Figure 1.20 showed the carbon and oxygen distributions in products obtained at different residence time. As the results the author concluded that the main transformation of carbon during the extraction was from Deposit to Soluble. The carbon distributions in Liquids obtained from 45 min to 90 min were less than those from 0 min to 30 min. This may be caused by the condensation reactions of the small organic molecules in Liquid. But overall, the condensation reactions were slight. Carbon was transferred into Gas and formed CO_2 mainly, independent of the residence time. The result of the oxygen distribution, more than 73.10% of the oxygen in raw SD was removed as water in the

Liquid or CO_2 in Gas. The prolonging of the residence time enhanced the oxygen removal and transformation from raw SD to Liquid.

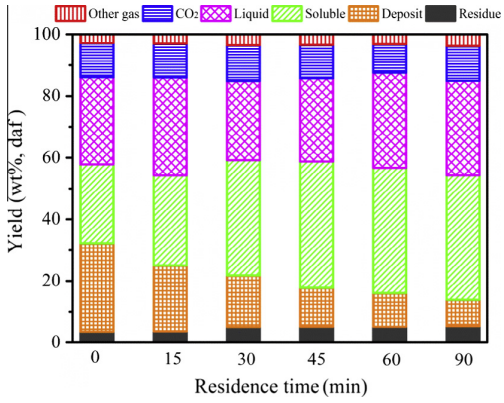

Figure 1.19. Product distributions of degradative solvent extraction of SD at different residence time [18]

The thermal decomposition behaviors of Solubles and Deposits, were studied by using a thermogravimetric analyzer. Soluble obtained at 90 min appeared slight different. The weight decrease of all Solubles mainly took place at the temperature range of 200–450 C. It was judged that the weight loss of the Solubles at the temperature lower than 350 C was caused by the devolatilization of the Solubles therefore the Soluble was obtained by the extraction at 350 C. FTIR analysis was performed to investigate the variation of chemical structure of Solubles and Deposits with residence time as shown in Figure 1.20. The spectrum of raw SD mainly consisted of OH stretching vibration (3100–3600 cm^{-1}), aliphatic C-H stretching vibration (2850–2970 cm^{-1}) and C-O stretching vibration (1030 cm^{-1}), which were the typical structure of biomass. The wide band of all Solubles and Deposits centered at 3406 cm^{-1} attributed to C-OH group apparently weakened that suggesting the removal of hydroxyls or carboxyls due to the dehydration and decarboxylation reactions. The aromatization reactions significantly took place during the extraction of biomass, the aromatic groups prevailed in the spectra of Solubles and Deposits: aromatic out-of-plane C-H bending at 750–875 cm^{-1}, aromatic C=C stretching vibration at 1460–1600 cm^{-1} and aromatic C-H stretching vibration at 3050 cm^{-1}. Moreover, the spectra of Solubles obtained at different residence time seemingly resembled each other, except the slight enhancement of the peaks attributed to the aromatic compounds (750–875 cm^{-1}, 3050 cm^{-1}). It suggests the chemical structure of the soluble was almost constant and independent of the varying residence time. So the Soluble should be a stable and final product of the

degradative solvent extraction of the biomass. So the removal of C-OH groups dominated, leading to the reduction of C-OH group content in Deposit. On the other hand, the region between 1600 cm^{-1} and 1460 cm^{-1} assigned to aromatic structure also increased with the residence time increasing from 0 to 90 min for the Deposit. Therefore, the Deposit underwent further complex reaction process with the residence time increasing, such as decomposition, aromatization, and dehydration [18].

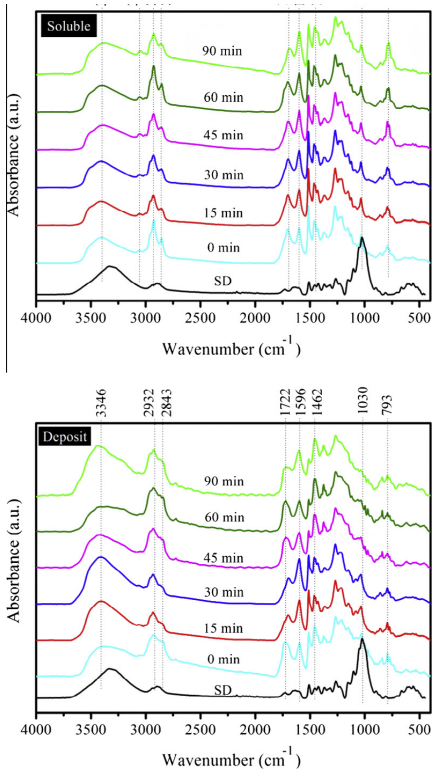

Figure 1.20 FTIR spectra of raw SD, Solubles and Deposits prepared at 0–90 min [18]

The ^{13}C NMR studied results showed the carbonyl carbon found in Solubles and Deposits which should be caused by the removal of C-OH from carboxyl groups. The aromaticity of Souble and Deposit obtained in Table 1.5 showed that the amount of aromatic carbon increased dramatically during degradative solvent extraction suggesting that significant aromatization reactions occurred during degradative solvent extraction of biomass.

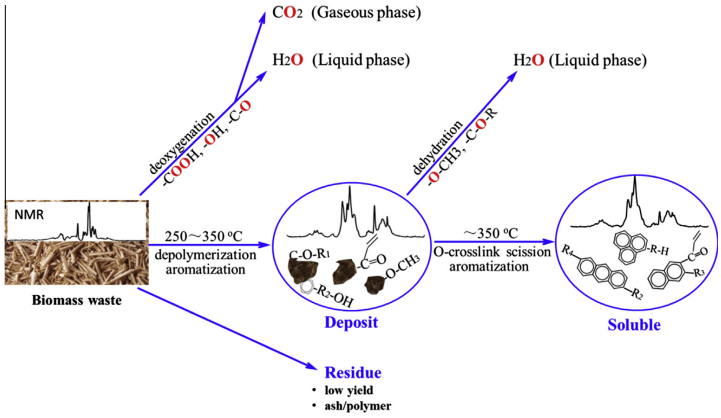

Figure 1.21. Proposal of conversion pathway of the degradative solvent extraction of biomass [18]

The conversion pathway of the degradative solvent extraction of biomass was proposed by the author (Figure 1.21). The author divided the whole process into two stages. The first stage took place at heating up stage from 250 to 350 C and the beginning of the isothermal stage at 350 C (0 min - 60 min). At first stage, the thermal extraction, deoxygenation and aromatization reactions of the raw biomass occurred significantly. At the second stage, the Deposit was further deoxygenated and converted into Soluble. This stage Deposit was found as the main product, it underwent complex reactions, such as the cleavages of oxygen containing cross-links and aromatization reactions. The oxygen was mainly removed as HO_2 at the second stage. The reactions in this process were mainly intramolecular. This is the main difference between degradative solvent extraction [18].

1.2.5 Infrared (IR) Spectroscopy for Liquid Sample

Infrared (IR) spectroscopy is one of the most common spectroscopic techniques used to characterize the organic and inorganic materials. The main objective of IR spectroscopic analysis is to define the chemical functional groups of a sample. Basically technique is the absorption measurement of different IR frequencies of the sample by placing it in the path of IR beam. The different functional groups in the sample absorb frequencies of IR radiation. Clearly, IR spectroscopy is non-destructive technique. It can measure many forms of the sample such as solid, liquid and gas. Thus, IR spectroscopy is the important and effective tool for identifying and interpreting the structural and chemical compound of the analyte.

The absorption of IR is generally presented as wavenumbers defining the number of waves per unit length which is the proportional to frequency as well as

the IR absorption energy. Its unit is cm^{-1}. IR absorption information is presented in the form of spectrum with wavenumber as the x-axis and the percent transmission or the absorption intensity as the y-axis.

Transmittance (T) is the ratio of the IR light intensity transmitted through the sample (I) to the light intensity from the IR source (I_0). Figure 1.22 illustrated the schematic of IR transmission.

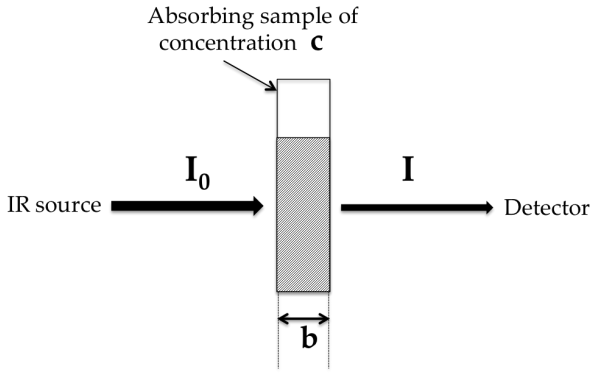

Figure 1.22 Schematic illustration of the transmission IR principle.

The sample is a thin disk with an IR transparent disk or a thin film liquid or gas in the IR permeable windows. The appropriate window is important and depends on the wavenumber range to be study. The IR light intensity passing through the sample decreases due to the absorption by the vibrating molecules in sample. Clearly, the IR intensity at the detector depends on the absorption cross-section (a), sample thickness (b) and its concentration (c) which describe by the Beer Lambert Law as Equation 1. Absorbance (A) is the logarithm to the base 10 of the reciprocal of the transmittance. Transmittance range is from 0 to 100% of T and absorbance is from 0 to unity. Transmission and absorption relative to the incident light are as the wavenumber-dependent intensity.

$$I = I_0 e^{(-abc)} \quad (1)$$

$$T = I/I_0,\ A = -\log_{10}(I_0/I) = abc \quad (2)$$

The molecules absorb the IR radiation when the frequency of the specific vibration is equal to the frequency of the IR radiation radiated on the molecule. The IR active and detectable undergo with only the vibrational transition mode depending on its wavelength, IR light used to excite the transition. The IR region is commonly divided into three smaller areas: near IR, mid IR, and far IR as Table 1.1

Table 1.1
IR Region

IR region	Near-IR	Mid-IR	Far-IR
Wavenumber (cm^{-1})	13,000–4,000	4,000–400	200–10
Wavelength (μm)	0.78–2.5	2.5–50	50–1,000

Mid-IR range (4,000–400 cm^{-1}) was selected in this study as it covers the vibrational transition of functional groups of organic molecules. IR spectra are obtained by detecting changes in absorption intensity as a function of frequency. The most instrument uses to measure IR radiation is Fourier Transform spectrometers.

Acquiring acceptable IR spectra of liquid samples in this study requires the use of special types of liquid cells. Most techniques for liquid sample measurements can also be accomplished with Attenuated Total Reflectance (ATR) accessories which is discussed later in this chapter and Fourier Transform-Infrared spectroscopy (FTIR) for liquid sample measurement.

ATR accessories are especially useful for obtaining IR spectra. They are suitable for studying highly absorbing solid and liquid materials, aqueous samples, powders, polymers including films. It's one of the most versatile sampling techniques which require little sample preparation. ATR occurs when a light of radiation enters from a higher refractive index into a low refractive index. Basically, the reflected of the incidence beam fraction increases when the angle of incidence increases. All incident radiation will be completely reflected at the interface when the angle of incidence is greater than the critical angle. The IR beam penetrates into the interface with a very short distance and a low refractive index medium before the reflection occurs. The penetration of incidence light is called the evanescent wave. The intensity is attenuated by the sample in the IR region where the sample absorbs. The sample is placed in close contact with a high refractive index crystal such as ZnSe, Ge or KRS-5. The IR radiation is directed to the beveled edge of the ATR crystal and internally reflected through the crystal with a single or multiple reflections. The higher length-to-thickness ratio of the ATR crystal angle gives higher numbers of reflections. The obtained spectra of ATR-IR looks like the conventional IR spectrum, however the absorption band positions are identical in the two spectra but the relative intensities of corresponding bands are different [19, 20]. However, a suitable contact and the appropriate incident angle between the reflection crystal cells and the refractive index of the solid/liquid sample and medium are important

for this technique. Figure 1.23 illustrates the basic of ATR principle.

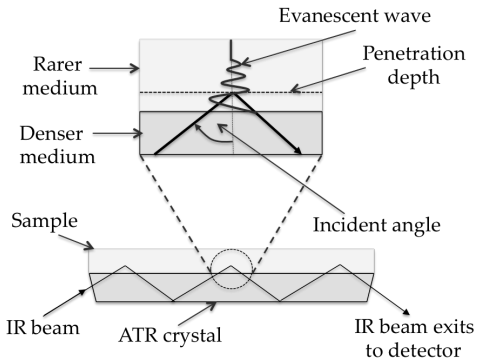

Figure 1.23 the schematic of ATR transmission.

There are three basic components in a FTIR spectrometer: an IR source, an interferometer and a detector. FTIR spectroscopy is the basically of the two-beam interferometer designed by Michelson, the schematic is presented by Figure 1.24 (A). The IR beam generated by the IR source falls onto the splitter ideally the radiation transmits half and the other half reflects. The reflection after traversing a distance L falls onto a fixed mirror M1. The radiation is reflected back to the beam splitter again by M1 with distance L. The transmission follows the same path and same distance. A mirror M2 is moved constantly along the optical axis with distance X therefore the transmission path length is equal 2(L+X). On the recombination at the beam splitter the optical path difference of the two beams is 2X. Two spatial coherent beams interfere on recombination. The movement of the mirror modulates the beam. The interferometer passes through the sample and is focused on the detector. The detector processes the interferogram in term of the intensity (I) as a function of X-displacement of the moving of the mirror M2 from the distance L (Figure 1.24 (B)). The interferogram is transformed by Fourier Transform function processing by the computer. The single-beam spectrum then is obtained by the comparing the measured reference IR spectrum without sample to the measured IR spectrum by the conventional dispersive method. The obtained IR spectrum is stored digitally in the computer (Figure 1.24 (C)).

Quantitative analysis in Mid-IR measurement, the spectral response of a sample relates by a mathematical function to changes in concentration of the sample. Ideally, the measured spectrum varies linearly with concentration. The fundamental equation for IR spectrometric quantitative analysis is know as Beer-Lambert Law as mentioned in Equation 1. A simple chemical mixture can consists of one component or more than one component. It is assumed that the radiation absorption by one

chemical component is not affected by the other components. The quantitative of the spectra in this study is used of the integrated absorption spectrum or peak area in order to avoid the intrinsic instrument error. It is possible to give absorption ranges where the characteristic frequencies of the most common groups subject to IR radiation. IR spectrum can divide in to four regions [21].

4000-2500 cm^{-1} : the absorption of single bonds to hydrogen, e.g. C-H, O- H, and N-H

2500-2000 cm^{-1}: the absorption of triple bonds, e.g. CC and CN

2000-1500 cm^{-1}: the absorption of double bonds, e.g. C=C and C=O

1500-400 cm^{-1}: absorption owing to other bond deformations (complex interacting vibrations, e.g. rotating, scissoring, and bending)

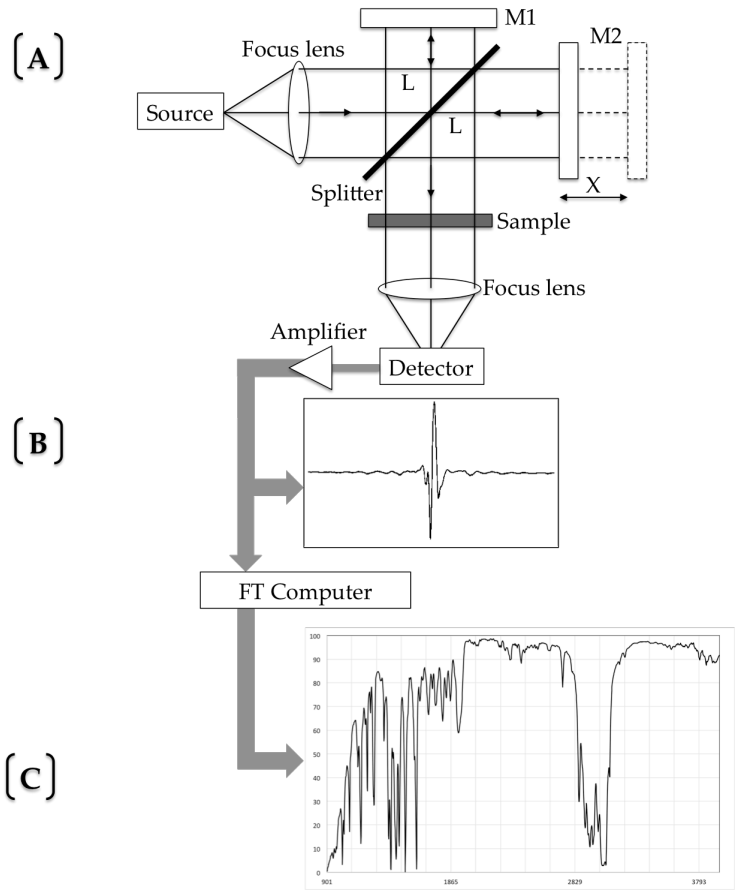

Figure 1.24 (a) Schematic diagram of Michelson interferometer (b) Interferogram (c) Spectrum obtained by Fourier Transform (FT) of the interferogram

For the oxygen-containing absorption bands which is the interest in this study, the main absorption in the IR region is in between 3600-2500 cm^{-1} and 1800-1500 cm^{-1}. The important functional groups of the interest region will be assigned and descripted in Chapter 3 and 4.

FTIR is a rapid and non-destructive technique applied for qualitative and quantitative determination of biomass components [45]. Most samples of biomass for FTIR are in solid state even though the obstacle in FTIR of biomass is the interference of absorbance background of water.

In order to understand the chemical composition and structure, the main compounds of coal/biomass have in the past been intensively studied by FTIR spectroscopy in cellulose [22, 23], lignin [24, 25], and hemicellulose [26] and in analysis of coal structure [27-32]. Most FTIR studies on coal/biomass measure from KBr pellet by mixing KBr powder with sample powder and pressing these into transparent discs that subsequently were IR radiated. KBr pellet needs fine grinding of the sample until it gets to a suitable size that reaches the maximum absorption. Furthermore, grinding for long period and hygroscopic property of KBr can produce contamination that causes problems of background absorbance and scattering. [33 - 35]. The factors that affect the IR spectrum are physical states of the sample, measuring conditions, and particularly, the lack of reproducibility is inconvenient in application [36-39]. A quantitative analysis with IR is preferable to be conducted without modification of the analyte, neither physically nor chemically.

1.2.6 Liquid Membrane-FTIR Spectroscopy

The sample liquid cells for IR absorption measurement is illustrated in Figure 1.25. It commonly composts of two IR-transmitting windows, the gasket that determines the path length of the cells which are the variable-thickness liquid cell or the fixed-thickness with the liquid filled-area and metal frame plates for holding the liquid cells. A drop of liquid sample is squeezed between two optical windows to form a film of approximately of the thickness. The windows held together by capillary attraction and together held with the metal plates holder which be clamped in a screw-tightened in order to form a good contact of liquid cells.

Liquid samples are a challenge for optical measurements as strongly absorbing on optical access measurement. The application of a liquid cell in the FTIR measurement has been applied in characterizing the liquid hydrocarbon fuel [40,41] in liquid organic compounds, such as protein structural determination [42-44]. The IR measurement using liquid cell was applied in this work to analyze the structure of liquid sample obtained from degradative solvent extraction (solvent-soluble of

biomass) which has not yet been applied to the characterization of biomass structure in the liquid state.

The liquid cells for FTIR measurement in this study is named 'Liquid Membrane-FTIR spectroscopy' hereafter.

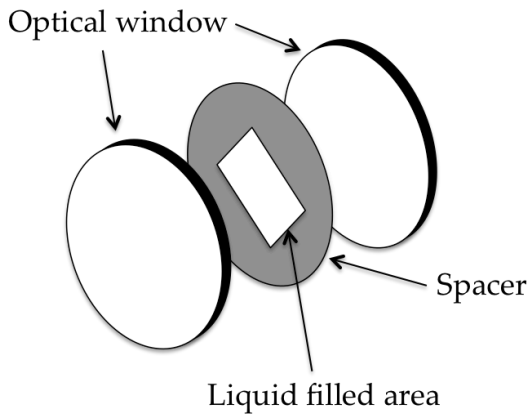

Figure 1. 25 Liquid cell used in absorption measurement.

1.3 Research Objective

The overall objectives for the research that formed the foundation of this thesis were to study the applicability of the IR spectroscopy technique for characterizing and investigation on mechanism of degradative solvent extraction of biomass materials.

Specific objectives were to

- Study the suitability of using liquid membrane-FTIR in order to characterize the biomass product during degradative solvent extraction. (Paper I)
- Use liquid membrane-FTIR spectroscopy for quantitative analysis and the applicable in predicting the mechanism of degradative solvent extraction. (Paper II)
- To develop and extend liquid membrane-FTIR spectroscopy in quantitative analysis for the important functional groups related to product of degradative solvent extraction and interpretation the reaction pathway of degradative solvent extraction (Paper III – submitted)

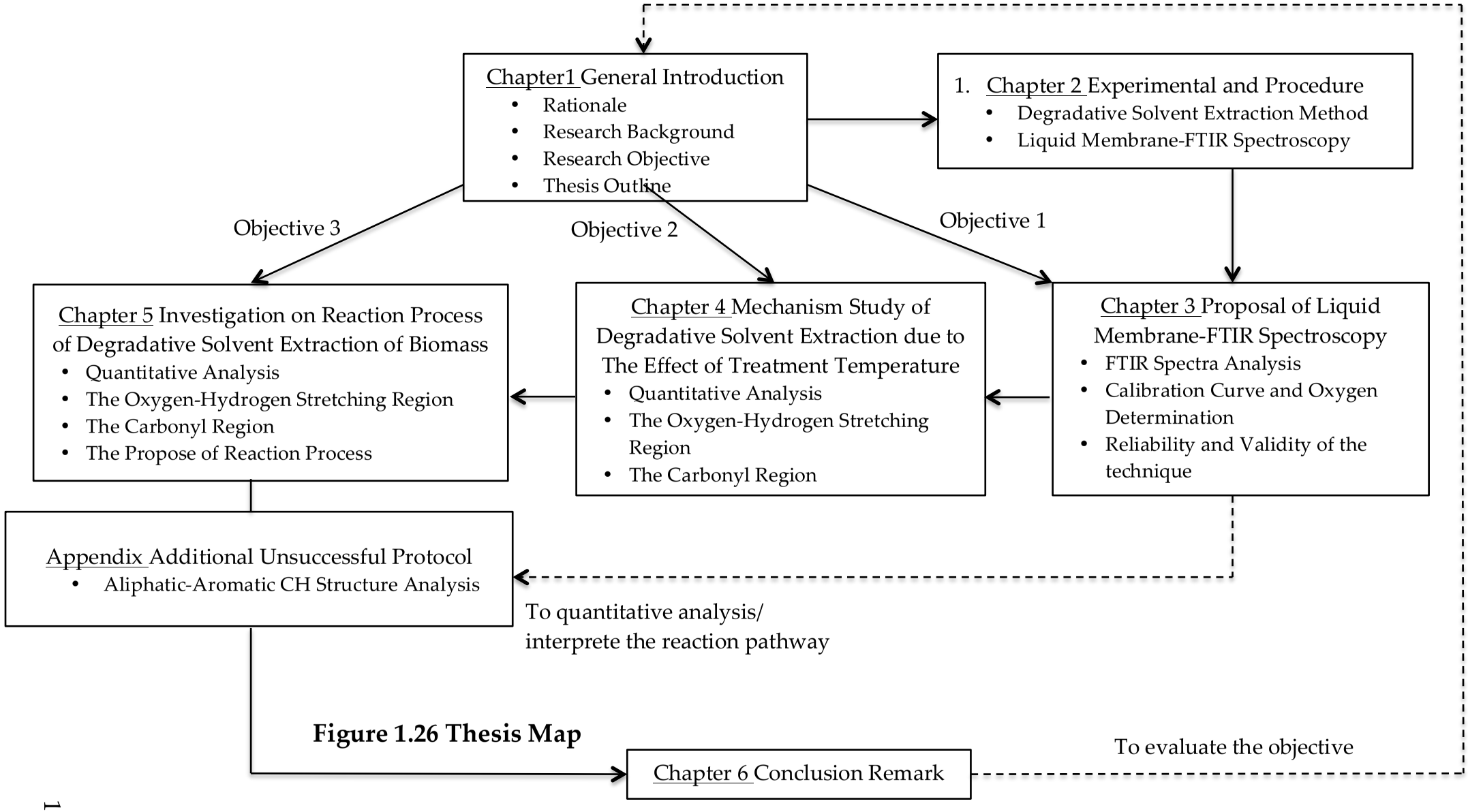

Figure 1.26 Thesis Map

References

[1]Klass D. 1998. Biomass for Renewable Energy, Fuels, and Chemical. San Diego, CA.

[2]Kumar P., Diane M. B., Michael J. D., Pieter S. 2009. "Methods for pretreatment of lignocellulosic biomass for efficient hydrolysis and biofuel production." Ind. Eng. Chem. Res. 48 (8): 3713–3729.

[3]Crocker M. 2010. Thermochemical Conversion of Biomass to Liquid Fuels and Chemicals. Cambridge, U.K.: RSC Publishing.

[4]Bergeron C., Danielle J. C., Shri R. 2012. Biorefinery Co-Products: Phytochemicals, Primary Metabolites and Value-Added Biomass Processing.

[5]Jiang J., Junming X., Zhanqian S. 2015. "Review of the direct thermochemical conversion of lignocellulosic biomass for liquid fuels." Agr. Sci. Eng. 2 (1): 13-27.

[6]Peter McKendry Energy production from biomass (part 1): overview of biomass 83, 2002, 37-46

[7]Zugenmaier P. Conformation and packing of various crystalline cellulose fibers. Prog Polym Sci 2001;26:1341–417.

[8]Klemm, D., Heublein, B., Fink, H.-B., Bohn, A. 2005. Cellulose: Fascinating biopolymer and sustainable raw material. Angewandte Chemie-International Edition, 44, 3358–3393.

[9]Ragauskas, A.J., Williams, C.K., Davison, B.H. 2006. The path forward for biofuels and biomaterials. Science, 311, 484–489.

[10]Collard, F. X., Blin, J. 2014. A review on pyrolysis of biomass constituents: Mechanisms and composition of the products obtained from the conversion of ce0lulose, hemicelluloses andlignin. Renewable and Sustainable Energy Reviews , 38, 594–608.

[11]Haiping Y., Rong Y., Hanping C., Dong H. L., Chuguang Z. 2007. Characteristics of hemicellulose, cellulose and lignin pyrolysis Fuel 86, 1781–1788

[12]Miura K., Shimada M., Mae, K., Sock H. Y. 2001. Fuel.,80, 1573-1582.

[13]Miura K., Kazuhiro M., Hiroyuki S., Ryuichi A., Takayuki I. 2003. "Extraction of low rank coals by coal derived oils at 350 °C for producing clean fuels." J Chemical Engineering of Japan 36 (7): 742-750.

[14]Miura, K., Hasegawa, Y., Ashida R. 2010. American Chemical Society, Division of Fuel Chemistry, 55, 212-212.

[15]Xian L., Ashida R., Miura K. 2012. "Preparation of high-grade carbonaceous materials having similar chemical and physical properties from various low-rank coals by degradative solvent extraction." Energy Fuels 26: 6897-6904.

[16]Wannapeera J., Xian L., Nakorn W., Ryuichi A., Miura K. 2012. "Production of high-grade carbonaceous materials and fuel having similar chemical and physical

properties from various types of biomass by degradative solvent extraction." Energy Fuels 26: 4521-4531.

[17]Ashida R., Takahashi R., Kawase M., Miura K. 2015. "Upgrading mechanism in degradative solvent extraction of biomass wastes," 12thEMSES.

[18]Zhu, X., Xue, Y., Li, X., Zhang, Z., Sun, W., Ashida, R., Miura, K., Yao, H., 2016. Mechanism study of degradative solvent extraction of biomass. Fuel 165, 10–18.

[19]Thomasson J., Coin C., Kahraman H., and Fredericks P.M. 2000. Attenuated total reflectance infrared microspectroscopy of coal, Fuel, 79, 685.

[20]Fran A. S. 1997. Handbook Of Instrumental Techniques For Analytical Chemistry prentice hall, New Jersy.

[21]Faust, B. 1992. Modern Chemical Techniques. The Royal Society of Chemistry, London, UK.

[22]Fengel, D. & Ludwig, M. 1991. Possibilities and limits of the FTIR spectroscopy for the characterization of cellulose. 1. Comparison of various cellulose fibers and bacteria cellulose. Das Papier, 45, 45-51.

[23]Kataoka, Y., Kondo, T. 1998. FT-IR microscopic analysis of changing cellulose crystalline structure during wood cell wall formation. Macromolecules, 31, 760-764.

[24]Hergert, H.L. Sarkanen, K.V., Ludwig, C.H. 1971. Infrared Spectra. In: Lignins Occurrence, formation, structure and reactions. John Wiley & Sons, New York, NY, pp. 267-297.

[25]Faix, O. 1991. Classifcation of lignins from different botanical origins by FT-IR spectroscopy. Holzfor- schung, 45, 21–27.

[26]Marchessault, R.H. 1962. Application of infra-red spectroscopy to cellulose and wood polysaccharides. Pure and Applied Chemistry, 5, 107-129.

[27]Painter P. C., Snyder R. W., Starsinic M., Coleman M. M., Kuehn D. W., Davis A. 1981. Concerning the Application of FT-IR to the Study of Coal: A Critical Assessment of Band Assignments and the Application of Spectral Analysis Programs. Applied Spectroscopy, 35, 5, 475-485.

[28]Painter P. C., Starsinic M., Squires E. and Davis A. 1983. Concerning the 1600 cm^{-1} region in the i.r. spectrum of coal. Fuel, 62, 6, 742-744.

[29]Solomon P. R. 1981. Relation between coal aromatic carbon concentration and proximate analysis fixed carbon. Fuel, 60, 1, 3-6.

[30]Solomon P.R. and Carangelo R.M., 1988. FT-ir analysis of coal: 2. Aliphatic and aromatic hydrogen concentration, Fuel, 67, 949.

[31]Sobkowiak M. and Painter P.A. 1995. A comparison of drift and KBr pellet methodologies for the quantitative analysis of functional groups in coal by infrared spectroscopy, Energy & Fuels, 9, 359.

[32]Solomon P.R., and Carangelo R.M. 1982. FTIR analaysis of coal. 1. Techniques and determination of hydroxyl concentrations, Fuel, 61.

[33]Sobkowiak M. and Painter P.A. 1995. A comparison of drift and KBr pellet methodologies for the quantitative analysis of functional groups in coal by infrared spectroscopy, Energy & Fuels, 9, 359.

[34]Friedel R.A., Retcofsky H.L., and Queiser J.A. 1967. Advance in coal spectrometry, absorption spectrometry. U.S. Dept. of the Interior, Bureau of Mines, Bulletin 640.

[35]John C., Interpretation of Infrared Spectra, A Practical Approach, Encyclopedia of Analytical Chemistry, R.A. Meyers (Ed.) Copyright John Wiley & Sons Ltd.

[36]Sobkowiak M., Painter P.A. 1995. A comparison of drift and KBr pellet methodologies for the quantitative analysis of functional groups in coal by infrared spectroscopy, Energy Fuels, 9, 359.

[37]Glover G., van der Walt T.J., Glasser D., Prinsloo N.M., Hildebrandt D. 1995. DRIFT spectroscopy and optical reflectance of heat-treated coal from a quenched gasifier, Fuel, 74, 1216.

[38]Thomasson J., Coin C., Kahraman H., Fredericks P.M. 2000. Attenuated total reflectance infrared microspectroscopy of coal, Fuel, 79, 685.

[39]Jorge A. Orrego-Ruiz, Rafael C., Enrique Mejía-O. 2011. Study of Colombian coals using photoacoustic Fourier transform infrared spectroscopy, Int J of Coal Geology, 85,307–310.

[40]J. E. Bertie, C. D. Keefe, and R. N. Jones. 1991. Infrared intensities of liquids VIII. accurate baseline correction of transmission spectra of liquids for computation of absolute intensities, and the 1036 cm^{-1} band of benzene as a potential intensity standard. Can. J. Chem., 69:1609–1618.

[41]Jason M. Porter, Jay. B. Jeffries, and Ronald. K. Hanson. 2009. Mid-infrared absorption measurements of liquid hydrocarbon fuels near 3.4 μm. Journal of Quantitative Spectroscopy and Radiative Transfer, 110:2135–2147.

[42]Dong, A., Huang, P., Caughey, W.S. 1990. Protein secondary structures in water from second-derivative amide I infrared spectra. Biochemistry, 29, 3303–3308.

[43]Yu S., Wuu A., Basu R., Holbrook M. R., Barrett A. D. T., Lee J. C. 2004. Solution structure and structural dynamics of envelope protein domain III of mosquito-and tick-borne flaviviruses. Biochemistry, 43, 9168–9176.

[44]Yu S., Mei F.C., Lee J.C.m Cheng, X. 2004. Probing cAMP-dependent protein kinase holoenzyme complexes Iá and IIâ by FT-IR and chemical protein footprinting. Biochemistry, 43, 1908–1920.

[45]Tucker M. P., Nguyen Q. A., Eddy F. P., Kadam K. L., Gedvilas L. M., Webb J. D. 2001. Fourier transform infrared quantitative analysis of sugars and lignin in pretreated softwood solid residues. Appl Biochem Biotechnol, 91, 51–61.

[46]Lee H. V., Hamid S. B. A., Zain S. K. 2014. Conversion of Lignocellulosic Biomass to Nanocellulose: Structure and Chemical Processe Scientific World Journal Volume, 20.

[47]Yang H., Yan R., Chen H., Lee D. H., Zheng C. 2007. Characteristics of hemicellulose, cellulose and lignin pyrolysis. Fuel. 86, 1781–8.

[48]Tarrio S. J., Naya S., Francisco F. M., Lopez B. J., Artiaga R. 2011. Functional nonparametric of wood species from thermal data. J Therm Anal Calorim. 104, 87–100.

[49]Edenhofer O., Pichs-Madruga R., Sokona Y., Seyboth K., Matschoss P., Kadner S., Zwickel T., Eickemeier P., Hansen G., Schlömer S., Stechow von C., *IPCC, 2011: Summary for Policymakers. In: IPCC Special Report on Renewable Energy Sources and Climate Change Mitigation*. Cambridge: Cambridge University Press.

[50]Bridgwater A. V., "Renewable fuels and chemicals by thermal processing of biomass", *Chem. Eng,* vol. 91, pp.87-102, 2003.

[51]Zhou C. H, Xia X., Lin C. X., Tong D. S., Beltramini J. 2011. Catalytic conversion of lignocellu- losic biomass to fine chemicals and fuels. Chem Soc Rev, 40, 5588–617.

[52]Taarning E., Osmundsen C. M., Yang X. B., Voss B., Andersen S. I., Christensen C. H. 2011. Zeo- lite-catalyzed biomass conversion to fuels and chemicals. Energy Environ Sci ,4, 793–804.

[53]Kwietniewska E., Tys J. 2014. Process characteristics, inhibition factors and methane yields of anaerobic digestion process, with particular focus on microalgal bio- mass fermentation. Renewable Sustainable Energy Rev, 34, 491–500.

[54]Limayem A, Ricke S. C. 2012. Lignocellulosic biomass for bioethanol production: cur- rent perspectives, potential issues and future prospects. Prog Energy Combust Sci, 38, 449–67.

[55]Biomass pyrolysis—A review of modeling, process parameters and catalytic studies

[56]Mckendry P., 2002. Energy production from biomass (part 2): Conversion Technologies. Bioresour Technol, 83, 1, 47–54.

[57]Liu Y., Aziz M., Fushimi C., Kansha Y., Mochidzuki K., Kaneko S., Tsutsumi A., Yokohama K., Myoyo K., Oura K., Matsuo K., Sawa S., Shinoda K., 2012. Exergy analysis of biomass drying based on self-heat recuperation technology and its application to industry : a simulation and experimental study," Industrial and Engineering Chemistry Research, 51, 9997-10007.

[58]Wannapeera, J., Ashida, R., Ohgaki, H., Miura, K. 2017. Production of carbon fiber and activated carbon fiber from the extract produced from the degradative solvent extraction of biomass. International Conference on Coal Science & Technology and 2017 Australia-China Symposium on Energy (pp. No. O9-5) Beijing, China.

[59]Xiaoxiang J., Naoko E., Dekui S., Jianchun J., Weidi D., Zhaping Z. 2011. Thermogravimetric-FTIR analysis of pyrolysis of pyrolytic lignin extracted from bio-oil" Chemical Engineering and Technology, 35, 5, 827-833.

[60]Qian L., Shurong W., Yun Z., Zhongyang L. and Kefa C. 2008. Mechanism study of wood lignin pyrolysis by using TG-FTIR analysis" Journal of Analytical and Applied Pyrolysis, 82, 1, 170-177.

[61]Luo S., Bao G., Wang H., Li F., Li Y. 2012. TG-DSC- FTIR analysis of cyanobacteria pyrolysis, Physics Procedia, 33, 657-662.

[62]Hui Z., Ai H. M., Yan Q. L., Qing H. L., Yan G. Z. 2014. Interactions of municipal solid waste components during pyrolysis a TG-FTIR study, Journal of Analytical and Applied Pyrolysis, 108, 19-25.

[63]Qian L., Zhaoping Z. S., Wang Z., Yang L. 2011. Interactions of biomass components during pyrolysis: A TG-FTIR study, Journal of Analytical and Applied Pyrolysis, 90, 213–218.

[64]Bassilakis R., Carangelo R.M., Wo M.A. 2001. TG-FTIR analysis of biomass pyrolysis, Fuel, 80, 1765-1786.

[65]Lu H. B., Zhang G. Y., JIA C. X. 2009. Analysis on TG-FTIR and kinetics of biomass pyrolysis, International Conference on Sustainable Power Generation and Supply Publication Year, 1 – 29.

[66]Ravindra K. A. 1988. Kinetics of reactions involved in pyrolysis of cellulose I. The three reaction model, The Canadian Journal of Chemical Engineering, 66, 3, 403-412.

CHAPTER 2

EXPERIMENTS AND PROCEDURES

2.1. Degradative Solvent Extraction

2.1.1 Materials and Solvent

A rice straw was used as a biomass sample in the study. Rice straw samples were shredded by a cutting mill, the suitable size was selected by filtering from 150 μm – 425 μm of a wire tray before serving to the experiment without drying (Figure 2.1).

1-methylnapthalene (1-MN) was used as the solvent for degradative solvent extraction process. The 90-percent-purity colorless solvent which was provided by SAFC was used. Its chemical structure is represented in Figure 2.2. 1-Methylnaphthalene is derived from coal tar. Boiling point and molecular weight of 1-MN is 240-243 °C and 142 g/mol, respectively. This solvent is well known as a non-hydrogen donor solvent and non-polar solvent. This solvent does not react with the sample at about 350 °C, this property is very important for the degradative solvent extraction method.

Figure 2.1 Rice straw sample with 150 μm – 425 μm of particle size

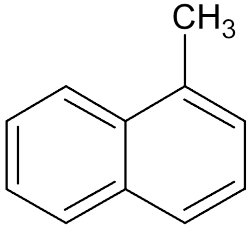

Figure 2.2 Chemical structure of 1-Methylnaphthalene

2.1.2 Experimental Procedure

Figure 2.3 shows the schematic diagram of the apparatus used for the degradative solvent extraction in this study. The apparatuses of experiment showed in Figure 2.4. The parts of the extraction system consist of a 130 mL-stainless steel reactor. A stainless steel filter, whose O.D. and mesh size were 65 mm and 0.5 mm, was equipped at the lower end of the autoclave reactor. A stainless steel reservoir (volume of 130 mL) was connected at the bottom of the reactor through a ball valve. The magnet-driven impeller connected to the agitator would be continuously stirred the content throughout the treatment. The thermocouple and the pressure gauge were equipped connecting to the autoclave reactor in order to monitor and control the temperature and pressure during extraction. On each run, 0.5 MPa of helium gas purged into the autoclave reactor and reservoir several times on each run in order to be sure the oxygen was removed from the system. Rice straw sample (approximate 6 g, d.a.f) and 80 mL of 1-MN were carefully served into the autoclave reactor, and heated up to the investigated extraction temperature by an electric furnace equipped at the autoclave reactor with the average heating rate of 5 K/min. The extraction temperatures were varied from 200, 250, 300 and 350 ^{o}C. The residence time performing at each extraction temperatures were 0 and 60 min in order to characterize the changes in chemical compositions of Solvent-soluble of rice straw (biomass) during extraction process and the effect of the extraction temperature. After the desired residence time, the furnace was stopped and the connecting valve was opened immediately allowing the extracted products with solvent through the reservoir. Rice straw was fractionated into three fractions by the degradative solvent extraction process. The unextracted product called Residue was filtrated by the filter equipped at the bottom of the reactor. The reservoir was cooling down till room temperature. The mixture composed of the solid extracted after precipitation at room temperature called Deposit and the extracted dissolving in the solvent (liquid phase) called Solvent-soluble which was the main and important fraction of the experiment. The mixture was separated by a vacuum filtration by using 0.5 μm-PTFE filter. The filtered solution (Solvent-soluble) at each treatment temperature was the sample using for mechanism study. The experiments exactly followed the procedure above until the end of the treatment temperature.

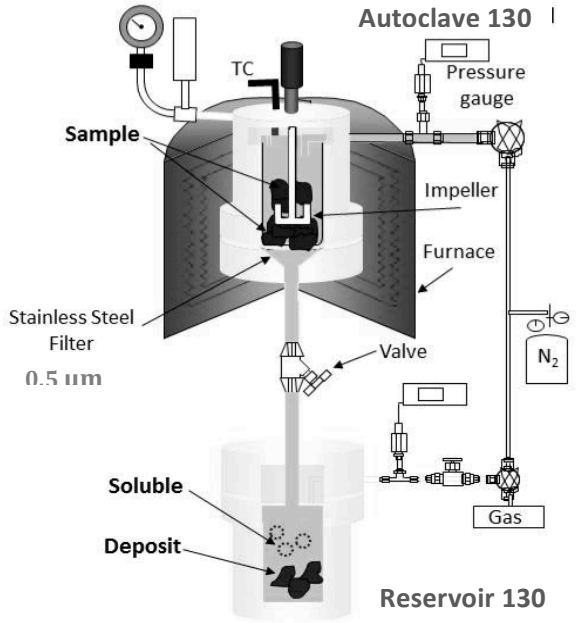

Figure 2.3 Schematic diagram of degradative solvent extraction system.

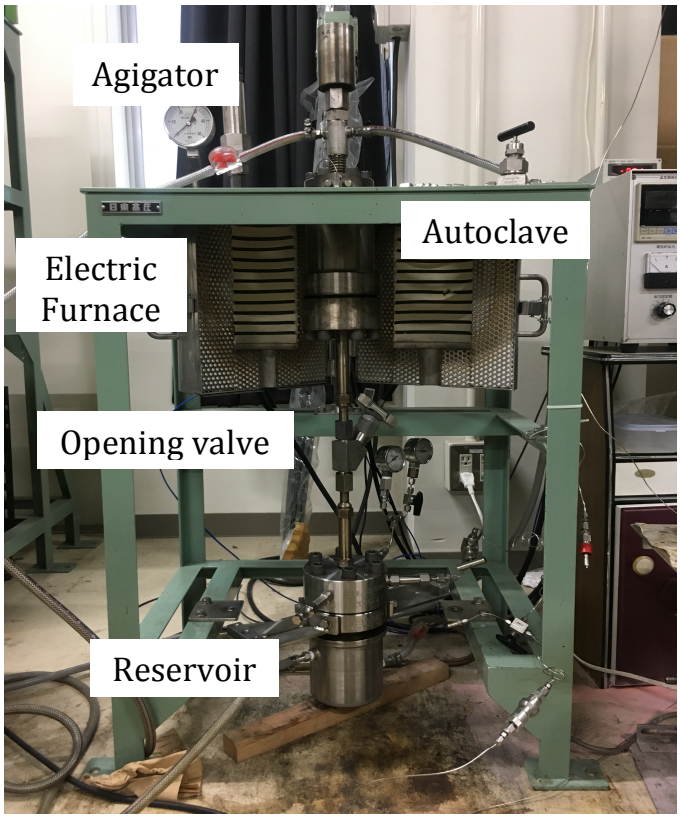

Figure 2.4 Photograph of apparatuses of degradative solvent extraction experiment

2.2. Liquid Membrane-Fourier Transform Infrared (FTIR) Spectroscopy

2.2.1 Liquid Membrane-FTIR equipment

Figure 2.6 shows the apparatuses for liquid membrane-FTIR experiment in this study. The cell used for infrared (IR) spectroscopy should be made of a transparent material that over the spectral range in the study. There are many factors to consider in order to choose the appropriate window material for infrared transmission. The spectral range to be studied, the chemical properties of sample to the window, the physical properties of the window and the cost are needed to consider. This study involving the organic liquid sample, the infrared transmission range window cells must provide in the range of 4000 - 400 cm^{-1}, water and solvent insolubility and easily polished. Table 2.1 shows the list of transmission window with its properties available in the market. Calcium Fluoride (CaF_2) flat windows (Figure 2.6 (d)) with the transmission range from 50,000 – 1,025 cm^{-1} was chose and used as the window material of liquid cell because of its very low water solubility and resistance to most acids and alkalides. Other window materials are not suitable for precise quantitative analysis to compare the CaF_2 window owing to their water solubility (e.g., KBr, NaCl) or to spectral dispersion (e.g., BaF_2, ZnS) [1-3]. CaF_2 is a non–hygroscopic cubic crystal resulting in very small water absorption from the atmosphere. A lead spacer with a rectangular space of 22x10 mm^2 at the middle was used to adjust the thickness of the cell. The thickness of the lead spacer used in this study was 0.05 mm (Figure 2.6 (c)). The demountable metal plates used for holding the windows and metal screws for fixing were shown in Figure 2.6 (a) and Figure 2.6 (b), respectively.

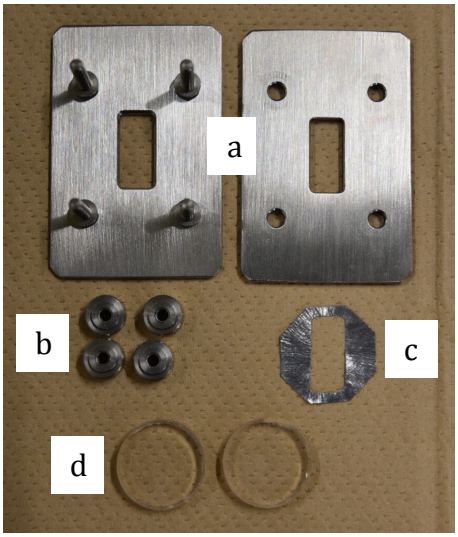

Figure 2.5 Photograph of Liquid membrane-FTIR transmission cells apparatuses; (a) the metal demountable plates (b) the machine screws (c) a lead spacer (d) CaF2 window cells

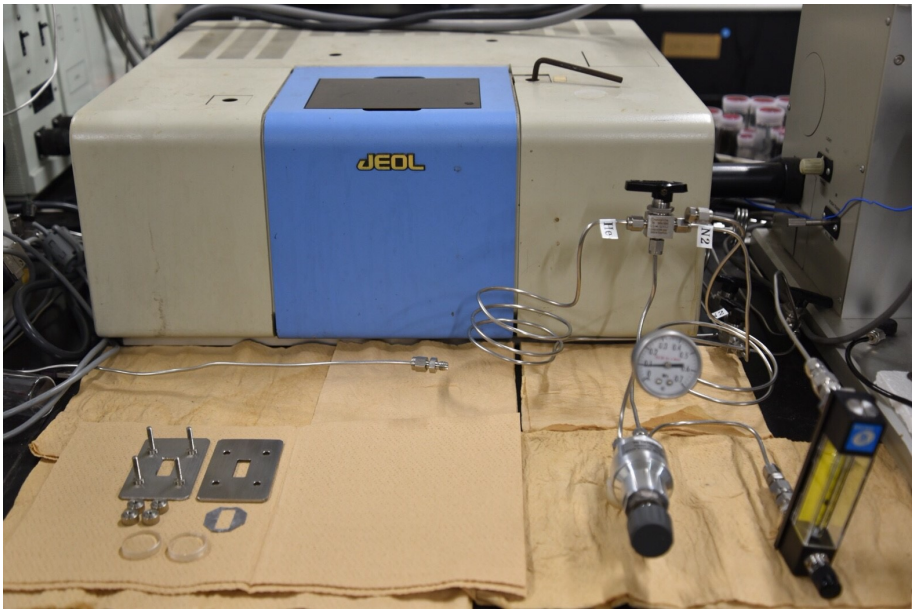

Figure 2.6 Photograph of FTIR spectrometer and flow rate controller.

2.2.2 Experimental Procedure

IR spectra measurement of all samples in this study were performed by using FTIR spectrometer with a spectral range from 4000 – 1000 cm^{-1}. The accumulation of spectra was 64 scans with 4 cm^{-1} of resolution. The time acquiring for 64 scans is approximately 160 seconds. The solvent-soluble in the liquid state was measured by the liquid membrane-FTIR method. 1-mm thick CaF_2 windows were cleaned by using acetone and wiped three times before usage. The equipment for liquid membrane-FTIR composed of two demountable metal plates for holding cell windows and the sample, two CaF_2-windows and a 0.05 mm-thickness lead spacer. The assembling procedure of liquid membrane-FTIR consists of, putting the spacer on the first CaF_2 window and using a clean disposable spatula placing a few drops of liquid sample into a rectangular space of a spacer. During filling, we have made sure that the sample covered the entire space in order to avoid any empty cell area or the presence of air bubbles then slowly sliding the second plate window over the sample-containing lead spacer. After windows and spacer were positioned properly, the demountable metal plates were used to hold the cell and were assembled with four machine screws by tightening screws diagonally and carefully checked the formation of air bubbles or unfilled space. In the case of the leakage of the sample from the cell, the window cell will be dismounted and correctly reassembled then the sample will need to be reloaded and remeasured at the end of the data acquisition. To eliminate moisture and to improve the stability of the measurement, two liters per minute of nitrogen gas was continuously purged into the sample compartment of the FTIR spectrometer. The agreement and reliability of technique

by quantifying the repeatability of measurement were tested by replicating seven measurements of solvent-soluble and were performed by liquid membrane-FTIR under the same measurement condition.

References

[1] Application Note-0602, Spectroscopic creativity, PIKE technologies

[2] Katsumi H., FTIR and water, *FTIR Talk Letter Vol.19*, Shimadzu.

[3] Nasse, M.J., Ratti, S., Giordano, M. & Hirschmugl, C.J. (2009). Demountable liquid/flow cell for *in vivo* infrared microspectroscopy of biological specimens. *Appl. Spectrosc.*, 63, 1181–1186.

[4] 'The Correct Material for Infrared (IR) Applications'
https://www.edmundoptics.com/resources/application-notes/optics/the-correct-material-for-infrared-applications/

[5] 'Optical element – window overview '
http://pdf.directindustry.com/pdf/union-optic-inc/union-optic-window/173804-678434.htm

TABLE 2.1

List of Transmittion Cell Window and Its Properties [4,5]

Window material	ZnS	NaCl	ZnSe	BaF2	CaF2	Ge	KBr
Transmission range (1/cm)	17,000-720	40,000-625	20,000-454	50,000-740	50,000-1,025	5,500-475	40,000-400
Refractive index	2.2	1.49	2.4	1.42	1.4	4	1.52
% Transmittance	70 (1.0 mm)	91.5 (4.0 mm)	65 (1.0 mm)	90 (3.0 mm)	90 (4.0 mm)	50 (2 mm)	90.5 (4.0 mm)
Cleaning Agents	alcohol, acetone	anhydrous alcohols	alcohol, acetone, water	alcohol, acetone	alcohol, acetone	alcohol, acetone, water	anhydrous alcohols
Solubility in water (100g H2O@25 oC)	insoluble	35.7 g	insoluble	0.17 g.	insoluble	insoluble	53.5 g.
Solvents with attack	acids	lower alcohol,wet solvents	acids, strong alkalines	salts, acids	salts, acids	hot sulfuric acid	lower alcohol,wet solvents
Max. Temp in air (oC)	300	400	300	500	900	125	300
Melting point (oC)	1830	801	1520	1280	1360	936	730
Hardness (kg/sq.mm)	178	15	137	82	158	550	7
Crystal class	cubic	simple cubic, cleaves on planes	cubic	cubic	cubic	cubic	cubic, cleaves on planes

CHAPTER 3

THE PROPOSAL OF LIQUID MEMBRANE-FTIR SPECTROSCOPY

3.1. Introduction

Degradative solvent extraction method has been proposed to dewater and upgrade low rank coals and biomass waste at mild conditions (around 350 ^{o}C) [1]. At this temperature, the macromolecular structure of biomass is relaxed, and small molecules are extracted. Three fractions obtained from the degradative solvent extraction as described in Chapter 2 are the unextractable fraction called Residue, the solid extracted fraction precipitated at room temperature called Deposit and the extracted fraction dissolving in the solvent at ambient temperature called Soluble. Soluble has unique properties such as high carbon content (81.0 to 83.3 wt.% and low oxygen content in the range of 7.3-11 wt.%) [1]. The study by Wannapeera et al. [1] showed that the effective treatment temperature for deoxygenation and recovery of high carbon content in the solid product is 350 ^{o}C. Extensive studies have been conducted such as Ashida et. al. (2015) and Zhu et al. (2016) to investigate the mechanism of the DSE method [5,6]. To identify molecular components and structure of products from the DSE method, the researchers analyzed the composition of the solid state of the initial reactant (coal, biomass) and final products [6]. The main reactions of DSE method of biomass are thermal degradation, deoxygenation, and aromatization, however, the mechanism of the DSE method has not been fully understood so far. Therefore, a new technique that consists of identifying the extraction product without separation. This technique would be promising in real-time and in-situ analysis. The knowledge of optical properties is obviously significant for the investigation of chemical structures. The relationship between the absorption spectra and the molar fraction are directly related to the structural feature of molecules. Infrared (IR) spectroscopy provides the important information of the absorption spectra of the structure both organic or inorganic constituent. Therefore, various methods were developed to obtain IR spectrum of coals and carbonaceous materials. Fourier Transform Infrared (FTIR) spectroscopy is the most common spectroscopic technique used to obtain IR spectrum for molecular structure determination. Numerous FTIR studies have been conducted to investigate coal structure during the 1980s [7-11] and the band assignment of various specific

functional groups of coals [10, 12]. So far, the conventional method known as KBr pellet or disk method is the most common method to obtain IR spectra for coals. The method needs fine grinding of the sample until it gets to a suitable size that reaches the maximum absorption. Furthermore, grinding for long period and hygroscopic property of KBr can produce contamination that causes problems of background absorbance and scattering. [11, 13, 14]. In order to reduce the sample preparation, the reflectance method of measurement was developed to obtain IR spectra of coals from the surface of the sample. The common methods are diffuse reflectance (DRIFT), attenuated total reflectance (ATR) and photoacoustic (PAS) method. DRIFT was applied to determine the relation of various band intensities to coal rank [15], including the product of coal from pyrolysis and heat treatment [16, 17]. DRIFT method requires highly scattered sample and a thin optical path length for quantitative measurement. In addition, band distortions could be caused by sample surface and refractive index phenomena [16]. To avoid the scattering of radiation interaction with the sample and optical thickness limitation in DRIFT, ATR technique was applied to perform a quantitative analysis of coal. Although ATR spectroscopy minimizes scattering effects involved, sample limitations have impacts on quantitative studies. The solid samples has to be of similar size and homogeneous grain, as well as have a suitable contact and the appropriate incident angle between the reflection crystal cells [18]. PAS is another technique providing good IR spectra in quantitative analysis of coal without sample modification. The method is particularly good for naturally high absorption and good thermal conduction of the sample [19]. In coal analysis, the factors that affect the IR spectrum are physical states of the sample, measuring conditions, and particularly, the lack of reproducibility is inconvenient in application [16-19]. A quantitative analysis with IR is preferable to be conducted without modification of the analyte, neither physically nor chemically.

This work focuses on the IR measurement technique to analyze the structure of soluble of biomass, which is obtained by the degradative solvent extraction. The proposed technique, called 'liquid membrane-FTIR', has not yet been applied to the characterization of biomass structure in the liquid state, even though the application of a liquid cell in the FTIR measurement has been commonly performed for liquid organic compounds, such as protein structural determination [20-23. The quantitative determination of the absolute amount of oxygen content presented in absorbance spectra of solvent-soluble by using the liquid membrane-FTIR. The result was validated with the analytical value studied by Wannapeera et al.[1].

3.2. Materials and Methods

The degradative solvent extraction in this study was performed as a batch experiment, the detailed procedure of the extraction experiments has been described in Chapter 2. The degradative solvent extraction was performed at treatment temperature at 350 ^{o}C with 60 min-holding time. After the autoclave reactor was heated up to the desired temperature, the extracted products; the mixture composed of the solid extracted after precipitation at room temperature called Deposit and the extracted dissolving in the solvent (liquid phase) called Solvent-soluble, were transferred immediately to the reservoir through the opening valve. The mixture was then separated into Solvent-soluble and Deposit by a vacuum filter using 0.5 μm-PTFE filter. Some amount of the solvent-soluble was prepared into solid phase for FTIR experiment. The solvent-soluble was sampled and evaporated by a rotary evaporator at around 140°C under reduced pressure to remove 1-MN and to recover the extract as the solid phase. Then, the sample was dried in the vacuum oven to further minimize the solvent and the other liquid product.

FTIR experiments were performed IR spectra measurement of all samples were performed by using JEOL, JIR-WINSPEC50 with a spectral range from 4000 – 1000 cm^{-1}. The accumulation of spectra was 64 scans with 4 cm^{-1} of resolution. The time acquiring for 64 scans is approximately 150 seconds. Soluble in the solid state was measured by KBr pellet method while solvent-soluble in the liquid state and the reagents were measured by the liquid membrane-FTIR method. A small solid sample (typically 1.25 mg) was weighed and ground together with 500 mg-KBr. Fine ground soluble and KBr have been dried again in a vacuum oven for 10 hours before being pressed into a pellet for FTIR measurement in order to minimize the water content in the sample. In liquid membrane-FTIR method, the CaF_2 windows were cleaned by using acetone and wiped three times before usage. The assembling procedure of liquid membrane-FTIR followed the description in Chapter 2. The agreement and reliability of technique by quantifying the repeatability of measurement were tested by replicating five measurements of solvent-soluble and were performed by liquid membrane-FTIR under the same measurement condition.

TABLE 3.1

Band assignments of sub-peak and variation rang of positions and widths of solvent-soluble [27, 28]

No	Band position (CM^{-1})	Width (CM^{-1})	Band assignments of hydrogen bonds
1	3611	30	Free OH groups
2	3530±10	50±20	OH-π hydrogen bonds
3	3400	100±10	self-associated *n*-mers (n>3)
4	3280±35	70±15	OH-ether O hydrogen bonds
5	3150±50	60±10	tightly bound cyclic OH tetramers
6	3100-2800	-	OH-N (acid/base structure)
7	2640	-	COOH dimers

3.3. FTIR spectra analysis

IR spectra of the liquid sample were obtained from the liquid membrane-FTIR method and the conventional KBr pellet method for the solid sample. Figure 1 shows the FTIR spectra of the solvent-soluble and the soluble in solid phase performed at 350°C of treatment temperature. The measurement was done at room temperature. The measurements provided the OH region (3750-2400 cm^{-1}) and also the aromatic-aliphatic region (3200-1360 cm^{-1}). It is clear that the spectrum obtained by liquid membrane-FTIR provides more structural information, as the peaks of the liquid membrane-FTIR are sharper and more distinct than those obtained by the conventional KBr pellet method. Regarding the sudden peaks obtained from liquid membrane-FTIR spectrum (upper-spectra) results from 1-MN spectrum, and the slight mismatch between the background spectrum and the sample spectrum, these sudden peaks effect are thought to be one of the drawbacks of liquid-membrane FTIR in the measuring of the sample within the solvent.

Figure 3.2 shows the results of peak deconvolution by curve-fitting and the hydrogen bonds of solvent-soluble and phenol in 1-MN as an example in Figure 3.3. The peak of hydrogen bonds in FTIR spectrum of the solvent-soluble and the reagent phenol appeared in the region of 3650-3100 cm^{-1} and 3650-3400 cm^{-1}, respectively. The peak positions were slightly changed, depending on the sample by referring to curve fitting of each spectrum. The four types of hydrogen bonds in solvent-soluble were found as OH-π at 3540 cm^{-1}, self-associated OH *n*-mers at 3400 cm^{-1}, OH-ether at 3300 cm^{-1} and cyclic OH tetramers at 3200 cm^{-1}. Free OH at 3558 cm^{-1}, OH dimer at

3530 cm^{-1} and OH trimer at 3470 cm^{-1} were resolved from phenol reagent in 1-MN solvent. By curve resolving, the calibration curve of the free OH can be obtained.

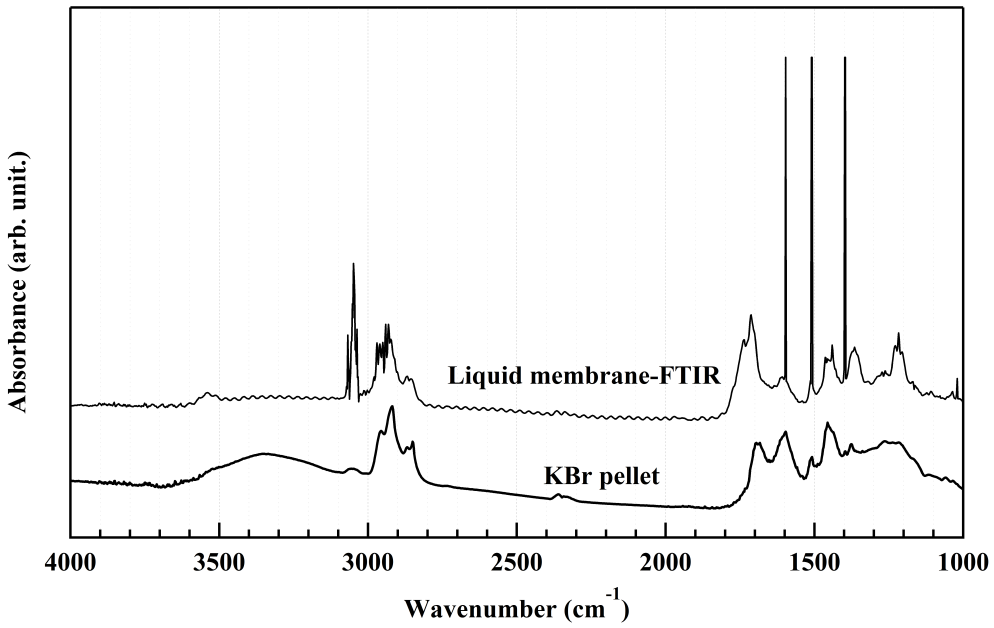

Figure 3.1 The typical FTIR spectra of soluble obtained from liquid membrane-FTIR and KBr pellet

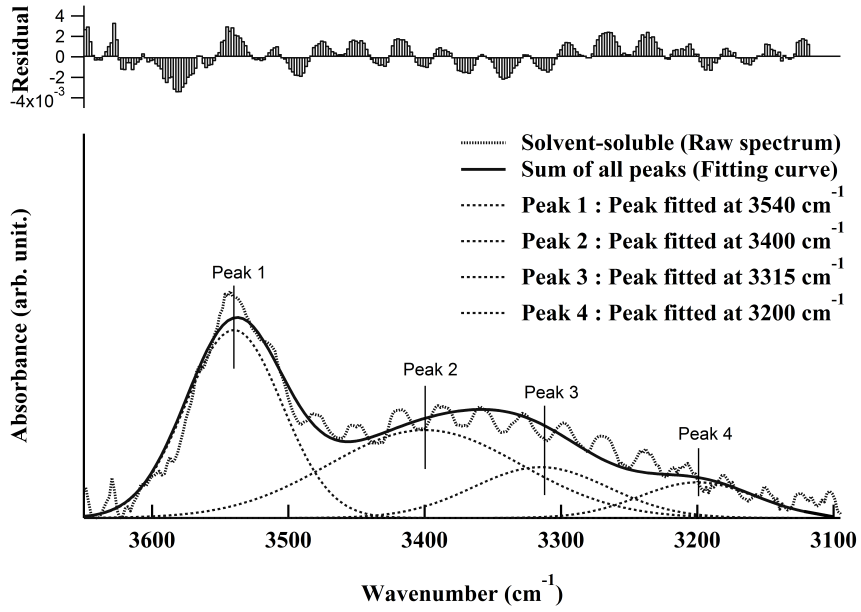

Figure 3.2 FTIR spectrum of solvent-soluble performed at 350 °C-treatment temperature

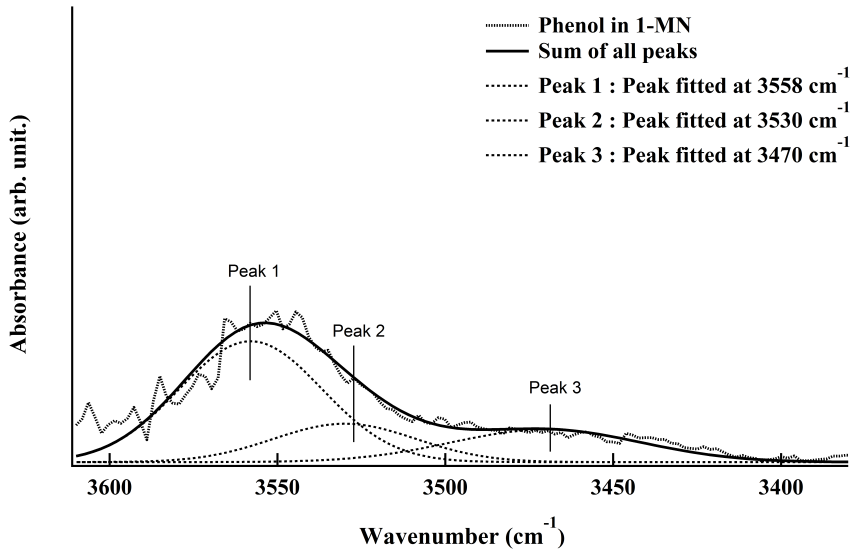

Figure 3.3 FTIR spectrum of 0.2 mg/mL of phenol in 1-MN

3.4. Calibration Curve and Oxygen Determination

The main reaction of degradative solvent extraction method is the deoxygenating [5, 6], the oxygen containing groups in solvent-soluble was examined. In order to quantify the oxygen in solvent-soluble, phenol reagent prepared at various concentrations in 1-MN was used for establishing the calibration curve. The data from the spectral region associated with phenolic groups, namely, the oxygen-hydrogen stretching region was presented in this study. Based on the study of Painter et al. 1987 and Miura K. et al. 1992 [27, 28], there are hydrogen bonds formed by hydroxyl groups, acid/base complex base, and carboxylic acid dimers. The band assignment and chemical structure of OH stretching bands were illustrated in Table 3.1. Background spectra of air were collected for every sample immediately before collecting the single-beam spectrum of the sample. The IR spectra of all samples were subtracted with 1-MN spectrum and the linear baseline was corrected. The spectrum of OH-stretching vibration relates to the hydrogen bonding appearing between 3650-3100 cm^{-1} and 3650-3400 cm^{-1} of solvent soluble and phenol, respectively, therefore the straight baseline was drawn between these wavenumbers by setting the y-intercept and slope as a baseline correction. The baseline was drawn at the inflection point from around 3640 cm^{-1} to the absorbance minima between 3050 and 3000 cm^{-1} for solvent soluble and between 3390 and 3350 cm^{-1} for the reagent phenol. The number, the sub-peak position, the width and their variation ranges were assigned in Table 3.1 [27-28]. Gaussian distribution was adopted as a peak shape which was considered as effective enough for each absorption band by Miura and co-workers [29-31]. All parameters were used as the

initial guesses of each sample; samples which used a set of preselected peaks, whose position and width were held and whose amplitude is varied to reproduce the experimental spectrum. A spectrum was processed by a multi-peak fit function by software IGOR Pro 7. This analysis function uses the Levenberg-Marquardt algorithm, which is a form of least squares fitting. The fitting finished when the rate at which Chi-square decreases is small enough. The peaks were derived from the fitted spectrum and the peak areas were obtained from this function analysis.

In absorption spectroscopy, the absorbance obtained from the measurement is the relationship known as the Beer-Lambert law;

$$I = I_0 * 10^{-(\frac{\alpha}{Lc})} \quad (\mathrm{W.cm^{-2}}) \quad (1)$$

where I and I_0 are the intensity of light passing through the absorbing sample and incident on the sample, respectively, α is the absorptivity or the absorption coefficient, L is the path-length of absorption and c is the concentration of the sample. The measured value of I and I_0 were used to compute the absorbance, A, defined as

$$A = \log (I/ I_0) = \alpha Lc \quad (2)$$

The equation states a linear relationship between the absorbance and the concentration of the absorbing species. The plot between the measured absorbance (y-axis) and concentrations (x-axis) is called a calibration curve. The resulting slope is the absorptivity dividing by the path-length. If the absorbance is obtained by measuring from the known concentration compound at a certain path-length, the absorptivity of the compound can be calculated.

It is known that several researchers attempted to estimate hydrogen bonds in coal by various methods. In order to quantify the amount of oxygen in OH stretching region (3650 – 3100 $\mathrm{cm^{-1}}$) of our sample spectrum, the study has adopted the method developed by Miura and co-workers [29-31] to investigate the distribution of hydrogen bonds in the OH-stretching band of coal by analyzing FTIR spectra. According to the Beer-Lambert law, the analytical equation can be written as

$$A_i = \alpha_i n_{\mathrm{OH},i} , \quad (3)$$

where A_i is the integral intensity or the sub-peak area of the hydrogen bond i from the curve fitting result, α_i is the absorptivity of the ith peak and $n_{\mathrm{OH},i}$ is the estimated amount of OH for the ith peak. Therefore the estimated amount of OH for the ith

peak is

$$n_{\mathrm{OH},i} = \frac{A_i}{\alpha_i} \qquad (\mathrm{mg.ml^{-1}}) \qquad (4)$$

Regarding consist of absorption band in OH stretching region as Table 1; 6 OH stretch bands. The absorptivity of each band, the *i*th, must be determined to convert the individual intensities to corresponding amounts of OH groups. The studies of Miura and co-workers [29-31] arbitrarily assumed that there was a similar relationship for the change in absorption intensity of hydrogen-bonded OH, and estimated the proportional constant from the intensity and the $\Delta\nu_{\mathrm{OH}}$ values on the basis of the work of Detoni and co-workers [32]. The absorptivity of hydrogen bands is as

$$\alpha_{OH} = \alpha_{OH,0}(1 + 0.0147\Delta\nu_{OH}) \qquad (\mathrm{ml.mg^{-1}.cm^{-1}}) \qquad (5)$$

where α_{OH} is the absorptivity of hydrogen-bonded OH, $\alpha_{OH,0}$ is the absorptivity of the free OH and $\Delta\upsilon_{\mathrm{OH}}$ is the wavenumber shift to hydroxyl groups in hydrogen bonds relative to the position of free OH groups (3611 $\mathrm{cm^{-1}}$). Thus the amounts of OH contributing to the different hydrogen bonds can be calculated if $\alpha_{OH,0}$ can be estimated. [31]. Therefore the absorptivity of each hydrogen bond was assumed to be represented by Equation (5) in this analysis as

$$\alpha_i = \alpha_{OH,0}(1 + 0.0147(\Delta\nu_{OH,i})) \qquad (\mathrm{ml.mg^{-1}.cm^{-1}}) \qquad (6)$$

Then the amount of the OH corresponding to the *i*th peak, $n_{\mathrm{OH},i}$, is given by

$$n_{\mathrm{OH},i} = A_i/\{\alpha_{\mathrm{OH},0}(1 + 0.0147(\Delta\nu_{OH,i}))\}.(\mathrm{mg.ml^{-1}}) \qquad (7)$$

The total amount of OH, ($n_{\mathrm{OH,Total}}$), related to the intensity of each absorption band can be calculated by

$$n_{\mathrm{OH,Total}} = \sum_i n_{\mathrm{OH,i}} . \qquad (\mathrm{mg.ml^{-1}}) \qquad (8)$$

In order to determine the total amount of OH in the solvent-soluble, the absorptivity of free OH, $\alpha_{OH,0}$, is needed to estimate. Due to $\alpha_{OH,0}$ is the slope between the absorbance and the concentration of free OH hence the calibration curve of free OH is established. In our study, phenol treated in 1-MN was used as a

reagent of known concentration substance of hydroxyl groups (OH). By applying curve fitting and by peak resolving the spectra of the reagent at different concentrations, the calibration curve of free OH can be established. The absorptivity of free OH, $\alpha_{OH,0}$, is determined from the value of the slope at a certain path-length of the plot between the absorbance of free OH (y-axis) and the concentration of free OH (x-axis) presented as Figure 3.4. Least squares curve fitting techniques and residual standard deviation have been used to improve the calibration curve of free OH.

The calibration curve of the free OH of phenol in the 1-MN solvent and the percent residuals of least squares fitting as shown in Figure 3.4. The regression coefficient of the fitting line of peak area to OH concentration represented the free OH absorptivity. As the absorptivity of free OH, $\alpha_{OH,0}$ is obtained and the sub-peak area of the hydrogen bond of solvent-soluble in OH region results from the curve fitting, by applying Equation (8) the total amount of OH in solvent-soluble can be obtained. By excluding the estimated value of the moisture and ash content and the oxygen containing in OH in solvent-soluble is determined, the oxygen content in weight percent of soluble on dry ash free basis is obtained.

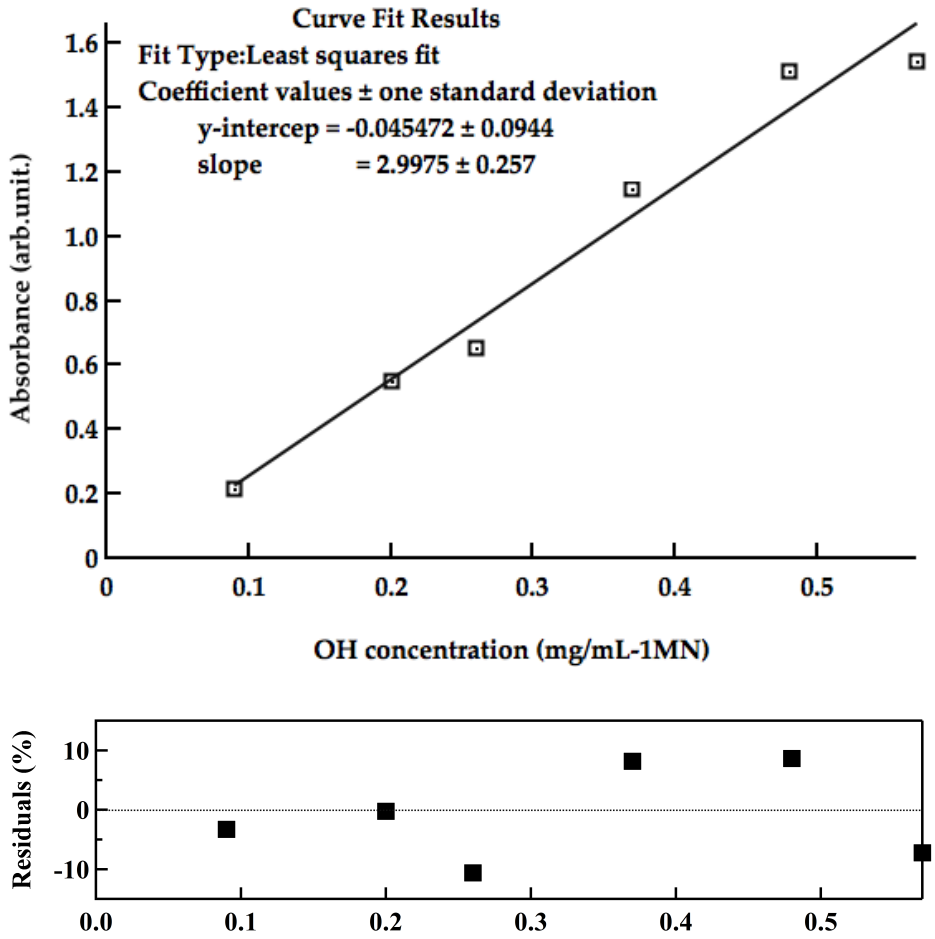

Figure 3.4 Calibration curve of the free OH of phenol treated in the 1-MN solvent and the percent residuals of least squares fitting

3.5. Reliability and Validaty of the Technique

The repeatability of the method was accessed of five measurements by calculated from the spectra and the calibration curve. The results in weight percent of soluble on dry ash free basis were 3.60, 3.77, 3.58, 3.96 and 3.61. The estimated amount of oxygen obtained from hydroxyl groups in solvent-soluble with the precision was 3.70 ± 0.17%. Considering the existence of other oxygen-containing functionalities, the oxygen from hydroxyl group in the solvent soluble should be less than 7.3-11% which is deduced from literature [1]. The distribution of oxygen-containing functional group in carbonaceous material is not only comprised of phenolic (C_{ar}-OH) and alcoholic (C_{al}-OH) hydroxyl groups, but also of carboxyl groups (R-COOH), carbonyl groups (R-CO), ethers (R-O-R') and quinone groups (C_{ar}=O) [39]. The reproducibility of measurements, the agreement between different measurements in the same sample can be represented as reliability indices in Table 3.2.

TABLE 3.2

Descriptive of reliability [38-40]

Statistic indices					
Number of replicated	Mean	Varian	Standard deviation	Standard Error of the Mean	*p*-value (Shapiro-Wilk)
5	3.70	0.03	0.17	0.07	0.12

Relative and absolute reliability indices					
Mean diff (Bias)	SD diff (between subject)	95%LOA (95%CI) LB	95%LOA (95%CI) UB	Within-subject Variance	CR
0.0024	0.16	-0.31	0.32	0.03	$\pm$0.44

- Mean diff is the mean of the difference between the measured values and the average value
- SD diff is the standard deviation of the different value
- 95% LOA = Mean diff $\pm$ 1.96xSD diff
- 95% LOA LB (95% CI of the LOA) = 95% Limits of agreement Lower Boundary (95% Confidence intervals of the limits of agreement)
- 95% LOA UB (95% CI of the LOA) = 95% Limits of agreement Upper Boundary (95% Confidence intervals of the limits of agreement)
- CR (Repeatability Coefficient) = SD diff x1.96$\sqrt{2}$ = the smallest real different

In order to test the repeatability of the method, the measurements remain consistent over repeated tests of the same sample under same conditions in the study. An experiment is reliable if it yields consistent results of the same measure. We used a plot of a Bland Altman as shown in Figure 3.5 in order to see their difference between the repeated measurement values by this method. If there is agreement and the result in a 95% prediction interval, the differences are assumed normally distributed. The normally distribute of data used Shapiro-Wilk test which can perform the number of sample from 3 to 50 elements. We arrived at 0.12 of p-value interpolated from Shapiro-Wilk test. Since p-value is more than 0.05, we retained the null hypothesis that the differences are normally distributed. The mean difference between the measuring values of oxygen contained in hydroxyl groups by liquid membrane-FTIR and the average value of repeating measurement (bias) was very close to zero, 0.0024. It indicated that this average discrepancy between the measurement values with the mean value was very small. The estimated limits of

agreement range within expected 95% of the confidence interval for the bias was [-0.31, 0.32]. The smallest possible change of the bias or the repeatability coefficient (CR) was $\pm$ 0.44. The diagram as plotted in Figure 3.5 illustrated the repeatability of the method by comparing repeated measurements by liquid membrane-FTIR within the same sample. The average difference points were found to be close to the bias (baseline), within the 95% confidence interval.

References

[1] Wannapeera J, Li X, Worasuwannarak N, Ashida R, Miura K. (2012). Production of high-grade carbonaceous materials and fuel having similar chemical and physical properties from various types of biomass by degradative solvent extraction. *Energy Fuels*, 26, 4521–31.

[2] Li X, Ashida R, Miura K. (2012). Preparation of high-grade carbonaceous materials having similar chemical and physical properties from various low-rank coals by degradative solvent extraction. *Energy Fuels*, 26, 6897–904.

[3] Li X., Zhu X., Xiao L., Ashida R., Miura K., Luo G., Yao H. (2014). Degradative solvent extraction of demineralized and ion-exchanged low-rank coals. *J Fuel Chem Technol*, 42, 97–904

[4] Zhu X., Zhang Z., Zhou Q., Cai T., Qiao E., Li X., Yao H. (2015). Upgrading and multistage separation of rice straw by degradative solvent extraction. *J Fuel Chem Technol*, 43, 422–8.

[5] Ashida R., Takahashi R., Kawase M., Miura K. (2015, June). Upgrading mechanism in degradative solvent extraction of biomass wastes.12thEMSES.

[6] Zhu X., Xue Y., Li X, Zhang Z., Sun W., Ashida R., Miura K., Yao H. (2016). Mechanism study of degradative solvent extraction of biomass. *Fuel*, 165, 10-18.

[7] Painter P. C., Snyder R. W., Starsinic M., Coleman M. M., Kuehn D. W., Davis A. (1981). Concerning the Application of FT-IR to the Study of Coal: A Critical Assessment of Band Assignments and the Application of Spectral Analysis Programs. *Applied Spectroscopy*, 35, 5, 475-485.

[8] Painter P. C., Starsinic M., Squires E. and Davis A. (1983). Concerning the 1600 cm^{-1} region in the i.r. spectrum of coal. *Fuel*, 62, 6, 742-744.

[9] Solomon P. R. (1981). Relation between coal aromatic carbon concentration and proximate analysis fixed carbon. *Fuel*, 60, 1, 3-6.

[10] Solomon P.R. and Carangelo R.M., (1988). FT-ir analysis of coal: 2. Aliphatic and aromatic hydrogen concentration, *Fuel*, 67, 949.

[11] Sobkowiak M. and Painter P.A. (1995). A comparison of drift and KBr pellet methodologies for the quantitative analysis of functional groups in coal by infrared spectroscopy, *Energy & Fuels*, 9, 359.

[12] Solomon P.R., and Carangelo R.M., (1982) FTIR analaysis of coal. 1. Techniques and determination of hydroxyl concentrations, *Fuel*, 61.

[13] Friedel R.A., Retcofsky H.L., and Queiser J.A. (1967). Advance in coal spectrometry, absorption spectrometry. U.S. Dept. of the Interior, Bureau of Mines, Bulletin 640.

[14] John C., Interpretation of Infrared Spectra, A Practical Approach, *Encyclopedia of Analytical Chemistry,* R.A. Meyers (Ed.) Copyright John Wiley & Sons Ltd.

[15] Fuller M.R. and Griffiths P.R., (1978) Diffuse reflectance measurements by infrared Fourier transform spectrometry, *Anal. Chem*, 50, 1906.

[16] Sobkowiak M. and Painter P.A., (1995). A comparison of drift and KBr pellet methodologies for the quantitative analysis of functional groups in coal by infrared spectroscopy, *Energy Fuels*, 9, 359.

[17] Glover G., van der Walt T.J., Glasser D., Prinsloo N.M., and Hildebrandt D. (1995) DRIFT spectroscopy and optical reflectance of heat-treated coal from a quenched gasifier, *Fuel*, 74, 1216.

[18] Thomasson J., Coin C., Kahraman H., and Fredericks P.M. (2000) Attenuated total reflectance infrared microspectroscopy of coal, *Fuel*, 79, 685.

[19] Jorge A. Orrego-Ruiz, Rafael C., Enrique Mejía-O. (2011) Study of Colombian coals using photoacoustic Fourier transform infrared spectroscopy, *Int J of Coal Geology*, 85,307–310.

[20] Dong, A., Huang, P., Caughey, W.S. (1990). Protein secondary structures in water from second-derivative amide I infrared spectra. *Biochemistry,* 29, 3303–3308.

[21] Yu S., Wuu A., Basu R., Holbrook M. R., Barrett A. D. T., Lee J. C. (2004). Solution structure and structural dynamics of envelope protein domain III of mosquito-and tick-borne flaviviruses. *Biochemistry,* 43, 9168–9176.

[22] Yu S., Mei F.C., Lee J.C.m Cheng, X. (2004). Probing cAMP-dependent protein kinase holoenzyme complexes Iá and IIâ by FT-IR and chemical protein footprinting. *Biochemistry,* 43, 1908–1920.

[23] Huayan Y., Shouning Y., Jilie K., Aichun D., and Shaoning Y., (2015) Obtaining information about protein secondary structures in aqueous solution using Fourier transform IR spectroscopy, *Nature Protocols10*, 382–396.

[24] Application Note-0602, Spectroscopic creativity, PIKE technologies

[25] Katsumi H., FTIR and water, *FTIR Talk Letter Vol.19*, Shimadzu.

[26] Nasse, M.J., Ratti, S., Giordano, M. & Hirschmugl, C.J. (2009). Demountable liquid/flow cell for *in vivo* infrared microspectroscopy of biological specimens. *Appl. Spectrosc.*, 63, 1181–1186.

[27] Painter P.C., Sobkowiak M., Youtcheff J., (1987). FT-i.r. study of hydrogen bonding in coal, *Fuel*, 66, 973-978.

[28] Miura K., Mae K., Sakurada K. (1992) Flash pyrolysis of coal following thermal pretreatment at low temperature. *Energy Fuels*, 6, 1, 16–21.

[29] Miura K., Kazuhiro M., Li W., Takumi K. and Akido K. (1999) In Situ FTIR Measurement of the change in hydrogen bonding of coal through heat treatment. *ASC*

Fuel Div, 44, 3, 642-646.

[30] Miura K., Kazuhiro M., Fumi-aki M. (1997) A new method to estimate hydrogen bonds in coal by utilizing ftir and dsc. *Am. Chem. Soc. Fuel Div*, 42, 1, 209-213.

[31] Miura K., Mae K., Li W., Kusakawa T., Morozumi F., Kumano A. (2001). Estimation of hydrogen bond distribution in coal through the analysis of OH stretching bands in Diffuse Reflectance Infrared Spectrum Measured by in-situ technique. *Energy Fuels*, 15, 599-610.

[32] Detoni S., Hadzi D., Smerkolj R. (1970) Hydrogen bonding in some adducts of oxygen bases with acids. Part VI. Infrared and dielectric studies of adducts with isothiocyanic acid, *J. Chem. Soc. (A)*, 2851-2859).

[33] De V. H. C.W., Terwee C.B., Knol D.L., Bouter L.M. (2006). When to use agreement versus reliability measures. *J Clin Epidemiol*, 59, 1033 – 1039.

[34] National Institute for Standards and Technology. Guidelines for Evaluating and Expressing the Uncertainty of NIST Measure- ment Results. http://physics.nist.gov/Pubs/guidelines/contents. html [18 December 2007].

[35] Bartlet J.W., Frost C. (2008). Reliability, repeatability and reproducibility: analysis of measurement errors in continuous variables, *Ultrasound Obstete Gynecol*, 31, 466-475.

[36] Krevelen D. W. V. (1993) Coal, typology-physics-chemistry-constitution. 3rd ed. Elsevier Science Publishers B.V.

CHAPTER 4

MECHANISM STUDY OF DEGRADATIVE SOLVENT EXTRACTION OF BIOMASS BY LIQUID MEMBRANE-FTIR

4.1. Introduction

Degradative solvent extraction, a recently developed method, successfully upgrades and fractionates biomasses [1], [5]-[8]. It was used for dewatering and upgrading of low rank coals and biomass waste at mild conditions (around 350 ^{o}C). The raw material was treated in a batch autoclave using a non-polar solvent below 350 ^{o}C. Two extracted fractions in the reservoir were obtained at room temperature; the deposit as a solid fraction was obtained after precipitation and the solvent soluble was obtained in the dissolved fraction. The carbon content of soluble was as high as 81.0 to 83.3 wt.% and its oxygen content was as low as 7.3 to 11 wt.% [1]. The effective treatment temperature of biomass by using this method was around 350 ^{o}C [1]. Extensive studies have been conducted such as [6] and [8] to investigate the mechanism of the degradative solvent extraction method. The researchers studied molecular components and structure of products by analyzing the solid state of the initial reactant (coal, biomass) and final products [8]. The main reactions involved in the degradative solvent extraction method of biomass are thermal degradation, deoxygenation, and aromatization. However, the mechanisms of the degradative solvent extraction method are not yet fully understood so far.

FTIR spectroscopy is the spectroscopic technique commonly used to obtain infrared spectrum, identify and study molecular structures. Several methods were proposed in order to obtain IR spectrum of carbonaceous materials and coal. As of the 1980s, FTIR has been used in several studies in order to investigate coal [9]-[13] and the band assignment of functional groups of coals [11], [14]. When applied to coal analysis, the lack of reproducibility due to factors that affect the IR spectrum such as the physical states of the sample and measuring conditions prove to be particularly inconvenient [15]-[18]. Quantitative analysis using IR is preferable without modification of the analyte, physically or chemically. The liquid membrane-FTIR technique was proposed to characterize biomass structure in the liquid state. It was successful in quantitative analysis of solvent-soluble fraction obtained from the degradative solvent extraction [19]. The measurement can be performed with the

soluble without removing solvent thus avoiding the contaminations during the sample preparation.

One of the main reactions of degradative solvent extraction method is the deoxygenation [6], [8], as such the present study was conducted to investigate the main oxygen-containing groups in solvent-soluble; hydroxyl and carbonyl groups were involved. To study the mechanism of the degradative solvent extraction process mechanism in-depth, the liquid membrane-FTIR technique was applied. The rice straw sample was treated in 1-MN at different solvent-treatment temperatures from 200-350 ^{o}C with a 60 min residence time. The oxygen functional groups investigated in the FTIR spectrum of the solvent-soluble are the oxygen-hydrogen stretching region (3700-3100 cm^{-1}) and the carbonyl stretching region (1800-1500 cm^{-1}). The obtained IR spectrum was deconvoluted into a series of bands in each region and the peak areas for each band are obtained.

4.2. Materials and Methods

The experiments performed in this study consisted of two parts; degradative solvent extraction and liquid membrane-FTIR.

In order to observe the influence of treatment temperature of biomass by solvent extraction, the degradative solvent extraction was performed at various extraction temperatures, the detailed procedure of the extraction experiments has been described in Chapter 2. Thermo gravimetric (TG) curve of rice straw was test to observe the thermal decomposition behaviors of rice straw from 0 to 400 oC as shown in Figure 4.1 Based on the result of TG curve, the degradative solvent extraction was performed at four different treatment temperatures from 200, 250, 300 and 350 ^{o}C with 60-min retention time. In addition, the study of the thermal decomposition behaviors of soluble showed that the sample weight decrease mainly occurred at 200 to 400 ^{o}C. The solvent-soluble of each treatment temperatures was used as the sample in this study.

Liquid membrane-FTIR was performed to investigate the variation of chemical structure in the main oxygen-containing groups in solvent-soluble which are the hydroxyl and carbonyl groups [30]. The FTIR experiment was replicated seven measurements of solvent-soluble under the same measurement condition. The error bars of the measured peak area of seven samplings of each functional group were also shown to illuminate the effects of errors on the experimental results. The infrared spectra of each treatment temperatures (200, 250, 300 and 350 ^{o}C with 60-min retention time) were measured with FTIR spectrometer (JEOL, JIR-WINSPEC50), with a spectral range 4000-1000 cm^{-1}. The FTIR spectra were obtained

at 4 cm^{-1} of resolution and 64 scans. The procedure of measurement has been described in Chaperter 2. The spectra of all samples were performed at room temperature.

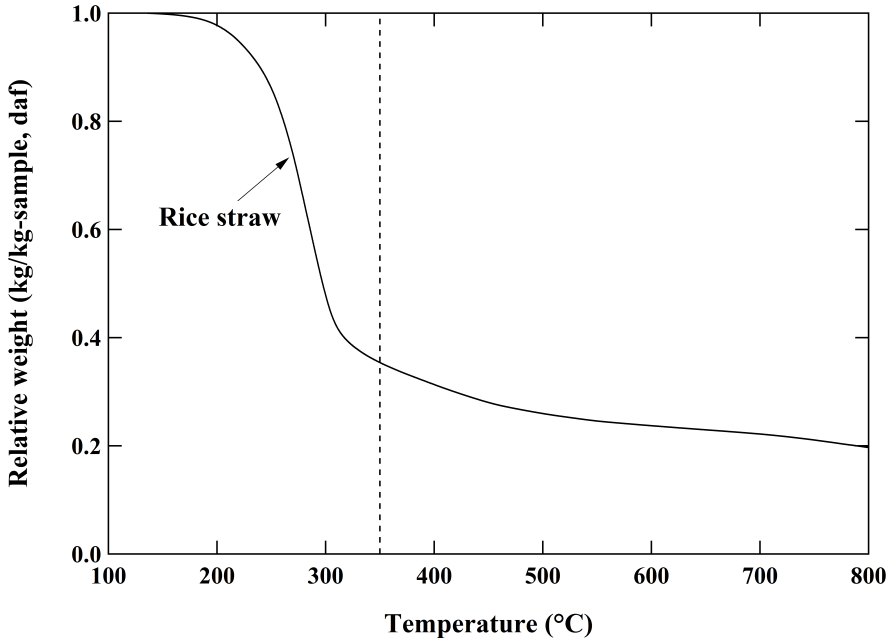

Figure 4.1 TG curve of rice straw

4.3 Quantitative Analysis

4.3.1 FTIR Spectra Analysis

The IR spectra of all samples were subtracted with 1-MN spectrum. Background spectra of the air were collected for every sample immediately before collecting the single-beam spectrum of the sample. The measurement spectrum was divided into two regions; oxygen-hydrogen stretching (3700-3100 cm^{-1}) (Figure 4.2) and the carbonyl stretching (1800-1500 cm^{-1}) regions as shown in Figure 4.3. Since the baseline of spectra changed with the treatment temperature due to the change in the reflectance of the samples, a baseline correction was performed as follows: A straight line was drawn through two points, which passed two minima of absorption at around 3650 and 3150 cm^{-1} for the OH stretching region, and around 1800 and 1550 cm^{-1} for the carbonyl stretching region. After baseline variation was corrected, the IR spectrum was deconvoluted. A spectrum was processed by a multi-peak fit function via the software IGOR Pro 6.31 using the least squares fitting algorithm. A Gaussian function was used for peak shapes [22], [23], [25]-[28]. The number, sub-peak position, width and their variation ranges were assigned in Table 4.1 [22]-[28].

Comparing the obtained spectral to the FTIR analysis of coal and to characteristic group frequencies [26]-[32], the band deconvolution was assigned. The band assignment in the hydroxyl region [22], [23] and the seven bands in carbonyl region (anhydride, carboxylic acids, ester, ketone, etc.) were assigned to resolve [24]-[28]. The peaks were derived from seven spectrum and the peak areas were obtained. The relative amount of functional groups was measured using the integrated area of the peaks as obtained by the peak-fitting process. Each functional group can be quantified using integral area of relevant absorption peaks. Each sample was prepared and analyzed of seven measurements to ensure the reliability and reproducibility of the method employed. The standard deviations of the functional groups at different temperatures were obtained.

TABLE 4.1

PEAK ASSIGNMENTS OF THE MAIN FUNCTIONAL GROUPS

Number	Peak Position (cm^{-1})	Assignments
1	3530±10	OH-π hydrogen bonds[a,b]
2	3400	self-associated *n*-mers (n>3) [a,b]
3	3280±35	OH-ether O hydrogen bonds[a,b]
4	3150±50	tightly bound cyclic OH tetramers[a,b]
5	1770±6	ester groups (-COO)[c,d,e,g]
6	1740±2	aldehydes (-CHO) [e,f,g]
7	1710±5	carboxylic acids (COOH) [c,d,e,f,g]
8	1670±20	conjugated aromatic ketone [c,d,e,f,g] (conjugated carbonyl)
9	1650±10	highly conjugated aromatic ketone [f,g] (highly conjugated carbonyl)
10	1600±7	Aromatics C=C [c,d,e,f,g,j]

[a] [22], [b] [23], [c] [24], [d] [25], [e] [26], [f] [27], [g] [28], [h] [29], [i] [30] and [j][10]

4.3.1.1 The Oxygen-Hydrogen Stretching Region

The IR spectrum in the OH stretching vibration region (3650-3100 cm^{-1}) was shown in Figure 4.2. The wide band of the region was centered at around 3400 cm^{-1} which was attributed to the self-associated *n*-mers. Figure 4.3 showed the profiles of the associated OH bonds at different treatment temperatures. The peak at 3400 cm^{-1} decreased more rapidly than the peak of 3530 cm^{-1} in the temperature region 200 to

300 °C. On the other hand, the peak at 3530 cm^{-1} decreased markedly at 300-350 °C. In this study, tightly bound cyclic OH tetramers are not found in the OH stretching region at 200 °C. At 200 to 300 °C, can be observed that the hydrogen bonds of biomass began released into solvent. The decrease of the peak area for hydrogen bonds in hydroxyl group obviously occurred at 300 to 350 °C, suggesting the removal of hydroxyl due to dehydration reactions [1], [8] or the removal of water began from this temperature range.

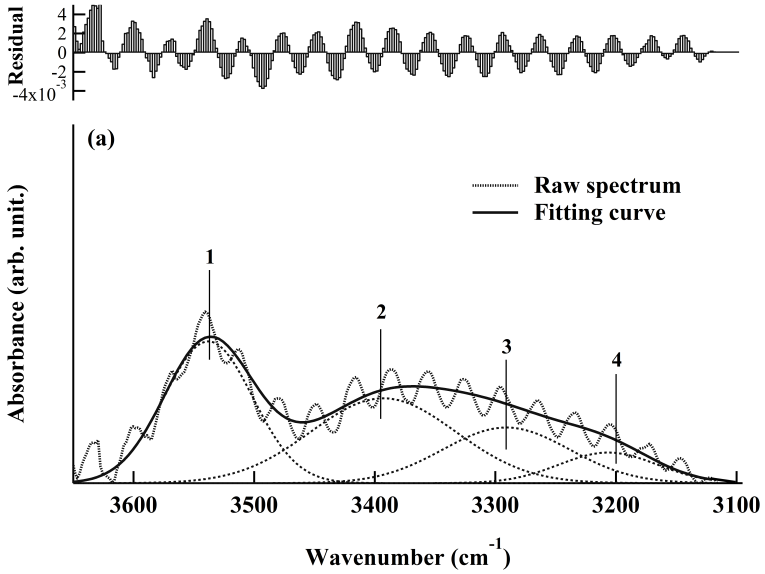

Figure 4.2 The curve-fitting results for solvent-soluble of 350 °C-treatment temperature between 3650 and 3100 cm^{-1}

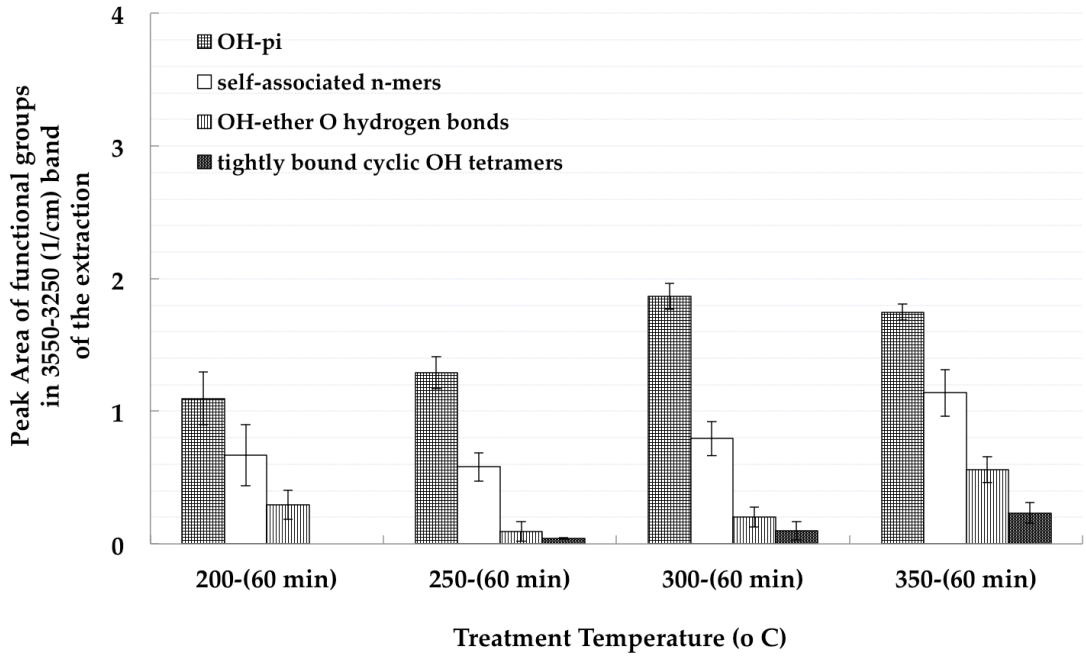

Figure 4.3 Variation of hydrogen bond in the OH stretching region (range 3650 – 3100 cm^{-1}) of solvent-soluble of biomass

4.3.1.2 The Carbonyl Stretching Region

The obtained IR spectra in the carbonyl stretching region (1850-1530 cm^{-1}) of solvent-soluble of rice straw showed two prominent peaks that centered around 1710 and 1601 cm^{-1}. Nine bands were resolved for the region as shown in Figure 4. Six bands at approximately 1800, 1770, 1740, 1710, 1670 and 1650 cm^{-1} can be ascribed to carbonyl functional groups. The band at 1601 cm^{-1} is associated with the aromatic C=C and two bands of aromatic stretching band; 1586 cm^{-1} and 1565 cm^{-1} [24]-[28]. The strongest absorption band at 1710 cm^{-1} was attributed to carboxylic acid while a shoulder with the bands at 1800, 1770 and 1740 cm^{-1} were assigned to assymetric anhydride (-$C(O)_2O$-), ester groups; (-COO) and aldehydes (-CHO), respectively. Relatively weak bands to carboxylic acid at 1670 and 1650 cm^{-1} were attributed to conjugated carbonyl and highly conjugated carbonyl groups or ketonic structure groups [24]-[28].

Figure 4.5 showed the variation of functional groups in the carbonyl stretching region with varied treatment temperature. The prevailing of aromatic groups at 1601 cm^{-1}, 1586 cm^{-1} and 1565 cm^{-1} in Figure 4.5 clearly demonstrated that the aromatization reaction took place during degradative extraction from treatment temperature at 300 ^oC [1], [6]-[8].

A functional group associates in the carbonyl stretching region in Figure 4.6 illustrated the deconvoluted peak area relative to that obtained at 200 ^oC. The peak of ester, carboxylic acid, anhydride, conjugated carbonyl and highly conjugated carbonyl decreased gradually decreased with increasing treatment temperature from 300^oC. On the contrary, at 250 ^oC of aldehydes showed as higher as at 300 ^oC by comparing the standard deviation of both temperature and the total carbonyl groups could conclude that aldehydes groups tend to decrease from 300 ^oC. The decrease was usually attributed to the decomposition of oxygen-containing functional groups or the formation of small molecules with oxygen-containing functional groups during the extraction reaction. The carbonyl groups consisting of the peak area at 1800, 1770, 1740, 1670 and 1650 cm^{-1} relatives to that obtained at 200 ^oC were presented on the right axes of Figure 4.6. The figure showed that the carbonyl groups in biomass gradually decreased with increasing extraction temperature from 300 to 350 ^oC. These carbonyl groups could have been removed by the decarboxylation into producing carbon dioxide (CO_2) or through the producing carbon monoxide (CO). These suggestions corroborated with the studies of Janewit et al. [1], in which more than 80% of the oxygen was observed to be removed as CO_2, CO, and water. In this study, ester groups were discovered to be one of the functional groups, contributing to the carbonyl group, esters could be the other

sources of CO_2 during the extraction process.

From the results and discussion, the deoxygenation, decarboxylation and the aromatization reactions occurred from 300 to 350°C which was consistent with the previous publications [1], [6]-[8]. This suggests that liquid membrane-FTIR as a technique was successful in resolving the overlapping IR bands and also helpful in the interpretation of the mechanisms for the degradative solvent extraction of biomass.

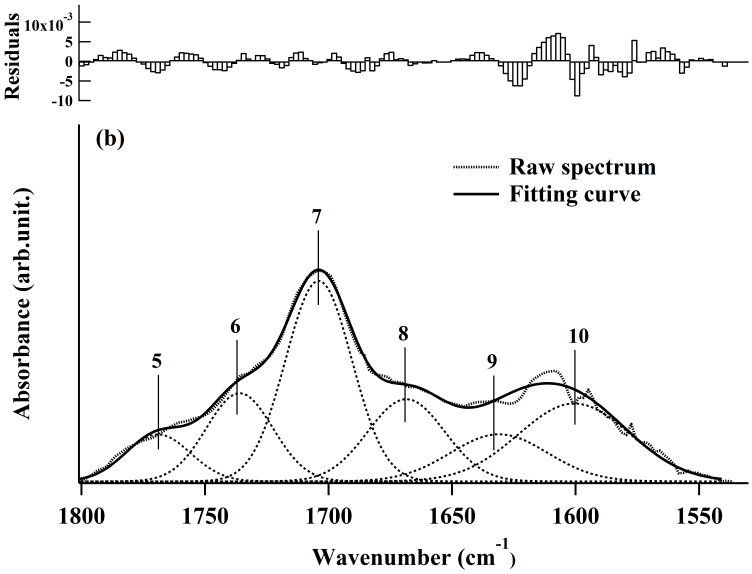

Figure 4.4 The curve-fitting results for solvent-soluble of 350 °C-treatment temperature between 1850 and 1530 cm^{-1}

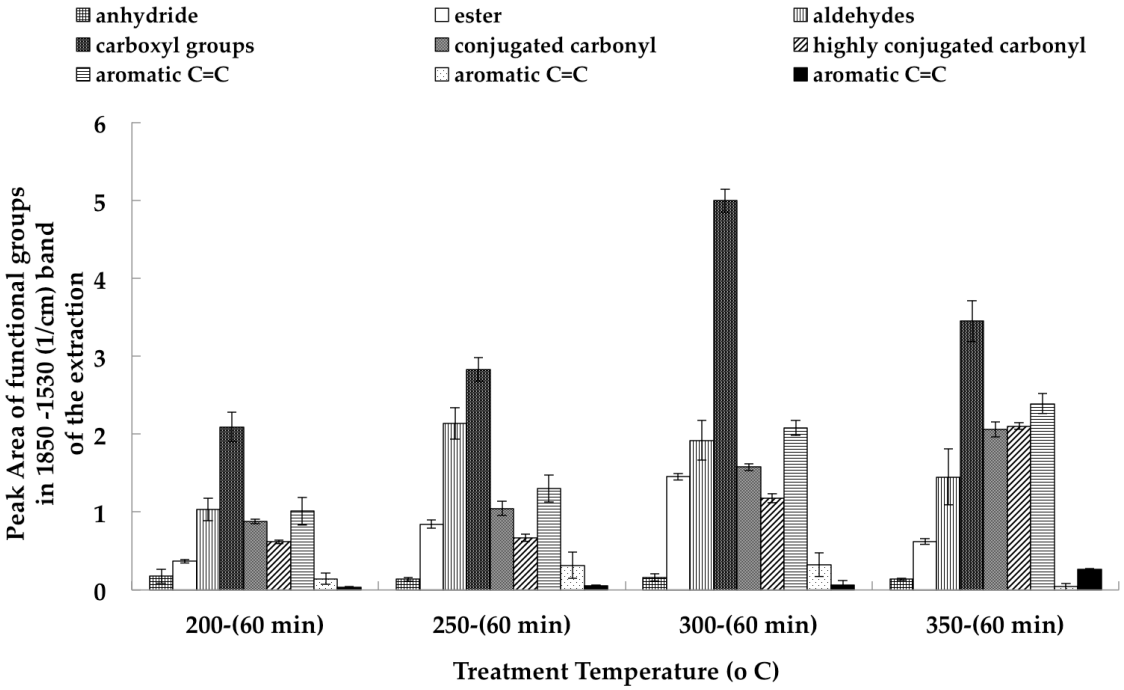

Figure 4.5 Variation of functional groups in the carbonyl region (range 1850 – 1530 cm^{-1}) of solvent-soluble of biomass

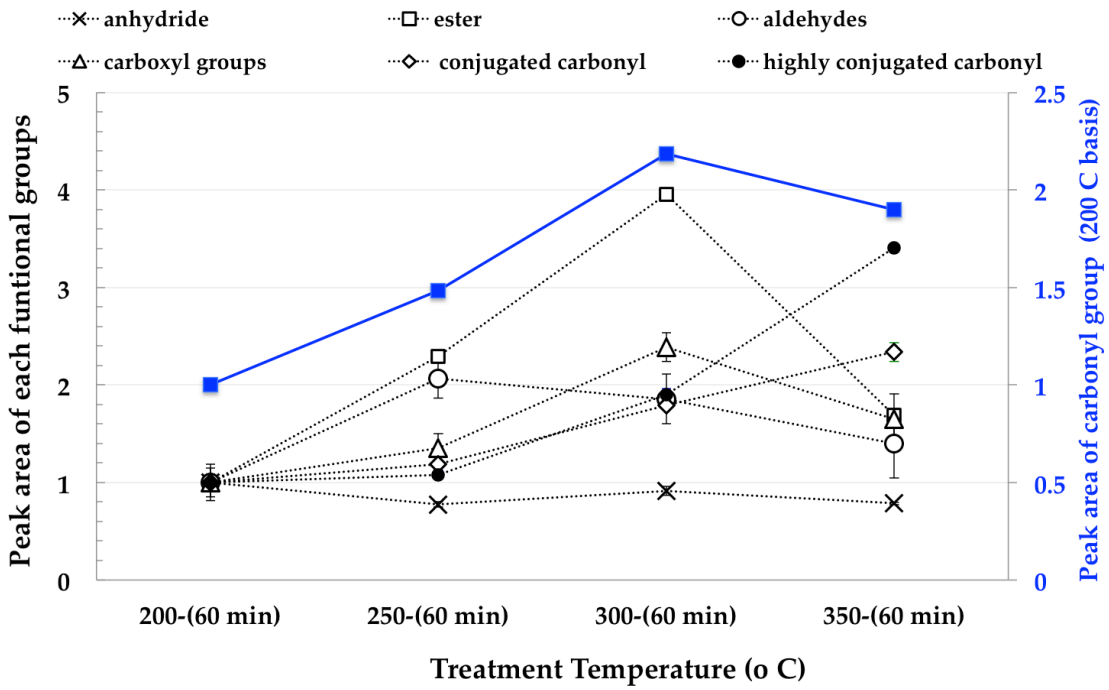

Figure 4.6 Variation in peak area of carboxylic acid and their derivatives relative to that obtained at 200 °C; variation of carbonyl band (1800, 1770, 1740, 1710, 1670 and 1650 cm^{-1})

References

[1] Janewit W., Li X., Nakorn W., Ashida R., Miura K., "Production of high-grade carbonaceous materials and fuel having similar chemical and physical properties from various types of biomass by degradative solvent extraction," *Energy Fuels*, vol. 26, pp. 4521–31, 2012.

[2] Li X., Ashida R., Miura K., "Preparation of high-grade carbonaceous materials having similar chemical and physical properties from various low-rank coals by degradative solvent extraction," *Energy Fuels*, vol.26, 11, pp. 6897–6904, 2012.

[3] Fujitsuka H., Ashida R., Miura K., "Upgrading and dewatering of low rank coals through solvent treatment at around 350°C and low temperature oxygen reactivity of the treated coals." *Fuel*, vol. 114, pp. 16–20, 2013.

[4] Li X., Zhu X., Xiao L., Ashida R., Miura K., Luo G., Yao H., "Degradative solvent extraction of demineralized and ion-exchanged low-rank coals," *J Fuel Chem Technol*, vol. 42, 8, pp. 897–904, 2014.

[5] Li X., Ashida R., Makino M., Nishida A., Yao H., Miura K., "Enhancement of gasification reactivity of low-rank coal through high-temperature solvent treatment," *Energy Fuels*, vol. 28, 9, pp. 5690–5695, 2014.

[6] Ashida R., Takahashi R., Kawase M., Miura K., "Upgrading mechanism in degradative solvent extraction of biomass wastes," 12thEMSES, 2015.

[7] Zhu X., Zhang Z., Zhou Qi, Cai T., Qiao E., Li X, Yao H. "Upgrading and multistage separation of rice straw by degradative solvent extraction," *J Fuel Chem Technol*, vol. 43, 4, pp. 422-428, 2015.

[8] Zhu X., Xue Y., Li X., Zhang Z., Sun W., Ashida R., Miura K., Yao H., "Mechanism study of degradative solvent extraction of biomass," *Fuel*, vol. 165, pp. 10-18, 2016.

[9] Painter P. C., Snyder R. W., Starsinic M., Coleman M. M., Kuehn D. W., Davis A., "Concerning the Application of FT-IR to the Study of Coal: A Critical Assessment of Band Assignments and the Application of Spectral Analysis Programs," *Applied Spectroscopy*, vol. 35, 5, pp. 475-485, 1981.

[10] Painter P. C., Starsinic M., Squires E., Davis A., "Concerning the 1600 cm^{-1} region in the i.r. spectrum of coal," *Fuel*, vol. 62, 6, pp. 742-744, 1983.

[11] Solomon P. R., "Relation between coal aromatic carbon concentration and proximate analysis fixed carbon," *Fuel*, vol. 60, 1, pp. 3-61981.

[12] Solomon P.R., Carangelo R.M., "FT-ir analysis of coal: 2. Aliphatic and aromatic hydrogen concentration," *Fuel*, vol. 67, pp. 949, 1988.

[13] Sobkowiak M., Painter P.A., "A comparison of drift and KBr pellet methodologies for the quantitative analysis of functional groups in coal by infrared spectroscopy," *Energy & Fuels*, vol. 9, pp.359, 1995.

[14] Solomon P.R., Carangelo R.M., "FTIR analaysis of coal. 1. Techniques and determination of hydroxyl concentrations," *Fuel*, vol. 61, 1982.

[15] Sobkowiak M., Painter P.A., "A comparison of drift and KBr pellet methodologies for the quantitative analysis of functional groups in coal by infrared spectroscopy," *Energy Fuels*, vol. 9, pp. 359, 1995.

[16] Glover G., van der Walt T.J., Glasser D., Prinsloo N.M., Hildebrandt D., "DRIFT spectroscopy and optical reflectance of heat-treated coal from a quenched gasifier," *Fuel*, vol. 74, pp. 1216, 1995.

[17] Thomasson J., Coin C., Kahraman H., Fredericks P.M., "Attenuated total reflectance infrared microspectroscopy of coal," *Fuel*, vol. 79, 685, 2000.

[18] Jorge A., Orrego-Ruiz, Rafael C., Enrique Mejía-O., "Study of colombian coals using photoacoustic Fourier transform infrared spectroscopy," *Int J of Coal Geology*, vol. 85, pp. 307–310, 2011.

[19] Watcharakorn K., Trirat M., Janewit W., Zen H., Kii T., Miura K., Ohgaki H., "Proposal of Liquid Membrane-FTIR Spectroscopy to Quantify the Oxygen Content in Soluble Fraction of Degradative Solvent-Extraction," *Int. J. Exp. Spectroscopic Tech.*, pp. 2-10, 2017.

[20] Ibarra J.V., Munoz E., Moliner R., "FTIR study of the evolution of coal structure during the coalification process," *Org. Geochem.*, vol. 24, pp. 725–735, 1996.

[21] Wenhua Geng, Tsunemori Nakajima, Hirokazu Takanashi, Akira Ohki, "Analysis of carboxyl group in coal and coal aromaticity by Fourier transform infrared (FT-IR) spectroscopy," *Fuel*, vol. 88, pp.139-144, 2009.

[22] Painter P.C., Sobkowiak M., Youtcheff J., "FT-i.r. study of hydrogen bonding in coal," *Fuel*, vol. 66, pp. 973-978, 1987.

[23]Miura K., Mae K., Li W., Kusakawa T., Morozumi F., Kumano A., "Estimation of hydrogen bond distribution in coal through the analysis of OH stretching bands in Diffuse Reflectance Infrared Spectrum Measured by in-situ technique," *Energy Fuels*, vol. 15, pp. 599-610, 2001.

[24]Ibarra J.V., Munoz E., Moliner R., "FTIR study of the evolution of coal structure during the coalification process," *Org. Geochem.*, vol. 24, pp. 725–735, 1996.

[25]Murakami K., Shirato H., Nishiyama Y., "In situ infrared spectroscopic study of the effects of exchanged cations on the thermal decomposition of a brown coal," *Fuel*, vol. 76, pp. 655-661, 1997.

[26]Supaluknari S., Larkins F.P., "An FTIR study of Australian coals: characterization of oxygen functional groups," *Fuel Processing Technology*, vol. 19, pp. 123-140, 1988.

[27]Wenhua Geng, Tsunemori Nakajima, Hirokazu Takanashi, Akira Ohki, "Analysis of carboxyl group in coal and coal aromaticity by Fourier transform infrared (FT-IR) spectroscopy," *Fuel*, vol. 88, pp.139-144, 2009.

[28]Wang Y., Wu J., Xue Sh., Wang J., Zhang Y., "Experimental Study on the Molecular Hydrogen Release Mechanism during Low-Temperature Oxidation of Coal," *Energy Fuel*, vol. 31, pp. 5498-5506, 2017.

[29]Painter P.C., Starsinic M., Coleman M.M. Determination of functional groups in coal by Fourier transform interferometry. In: Ferraro J.R., Basile L.J., editors. Fourier Transform Infrared Spectroscopy. Academic Press; New York, NY, USA: 1985. pp. 169–240

[30]The application of fourier transform infrared spectroscopy to the characterization of coal structure Paul C. Painter and R. W. Snyder FUEL, 1979, Vol 58, April pp.301-308

CHAPTER 5

INVESTIGATION ON REACTION PROCESS OF DEGRADATIVE SOLVENT EXTRACTION

5.1. Introduction

Researchers have studied the reaction process in order to optimize the treatment conditions. The main reactions in the DSE process have been identified as thermal extraction, deoxygenation, decarboxylation, and aromatization [1, 2]. Further investigation also identified deoxygenation and slight aromatization reactions during an isothermal stage at 350°C [2]. The intermolecular dehydration reactions of cellulose are significantly suppressed. The bond cleavage reactions precede parallel with intramolecular dehydration reactions, which results in more unsaturated double bonds [3]. However, the mechanism of DSE is still not yet fully understood.

Since the solvent extraction process involves thermal decomposition, the reaction process and products will be very complex. Besides, the analysis of the analyte under the same conditions as those of the DSE system, without physical or chemical modification, is preferable in order to avoid interfering with and contaminating the sample.

Regarding the obtained analyte of the study, the liquid state by solvent extraction (soluble in solvent including the dissolved fraction in solvent called Liquid), is called Solvent-soluble hereafter. Hence, measurement should be performed to examine the Soluble without removing the solvent, thus avoiding contamination during the sample preparation.

Liquid samples are a challenge for optical measurements as they are strongly absorbing during optical access measurement. A liquid cell in the FTIR measurement has been applied in characterizing the liquid hydrocarbon fuel [4, 5] in liquid organic compounds, such as by using protein structural determination [6, 7].

To acquire acceptable IR spectra of the analyte in the liquid state, Solvent-soluble, we developed special types of liquid cells and applied these to analyze the Solvent-soluble of rice straw (RS). Liquid cells for absorption measurement, called liquid membrane-FTIR, is a suitable and reproducible technique for the characterization and quantitative analysis of the Solvent-soluble of RS regarding the state of the sample [8] The technique proposed the use of liquid membrane-FTIR to

interpret the main mechanism of the DSE of RS in a previous study [9] (Chapter 4). However, the FTIR spectra of the previous study were too noisy to deconvolute the overlap peaks. We have improved the experimental conditions to reduce the noise in the water vibrational region. The newly obtained IR spectra gave good reproducibility spectra and more information on peak resolving, which were helpful in the quantitative analysis in spectral regions related to the oxygenic functional groups and in depicting the process mechanism of DSE for RS.

The hydrogen bonding interaction in biological chemistry is identified as crucial and has been a challenging study [10-16]. IR spectroscopy has proved to be a promising means of quantifying the hydrogen-bonding interaction in coal [12, 17, 18] and biomass [19-22]. There is a nearly linear relationship between the wavenumber shift from the free hydroxyl-stretching vibration, $\Delta\nu_{OH}$, and that of the enthalpy change of hydrogen bond, ΔH, related to the OH-stretching region. This relationship was proposed by Drogo et al. [10]. The enthalpy change of hydrogen bond formation has been used by many investigators to interpret the average strength of hydrogen bonds [11, 23]. Miura et al. [13-15] developed the method based on this relationship to calculate the amounts of individual hydrogen bonds and estimate the strength distribution of hydrogen bonds in coal. Furthermore, this method was applied to study the dewatering mechanism of coal [24]. Based on the analytical chemistry results of the Soluble of biomass, such as the rational formula of $CH_{0.894-1.062}O_{0.065-0.114}$, it was almost completely free from ash and had high heating values (HHV) as high as 34.1–37.2 MJ/kg, so its properties were judged to be comparable to sub-bituminous coal [1]. Thus, the method for the investigation of hydrogen bonds in coal suggests a method to study the behavior of different kinds of hydrogen bonds in the Solvent-soluble of RS during the solvent treatment on the basis of the DSE of biomass. Understanding the evolution of hydrogen bonding in the Solvent-soluble of RS during solvent treatment could give insights into the mechanism of DSE.

This chapter aims at a better understanding of the transformation of oxygen-containing functional groups during the DSE and the elucidation in detail of the reaction pathway. In addition, the amount of hydroxyls contributing to each hydrogen bond and its strength were first investigated to discuss the dewatering mechanism of the DSE of RS based on the calculation.

5.2. Materials and Methods

The experiments performed in this study consisted of two parts; degradative solvent extraction and liquid membrane-FTIR. The estimation of the strength

distribution of hydrogen bonds is proposed to the study the dewater mechanism in the chapter.

Degradative solvent extraction

The degradative solvent extraction in this study was performed at various extraction temperatures as a batch experiment, the detailed procedure of the extraction experiments has been described in Chapter 2. The degradative solvent extraction was performed at four different treatment temperatures from 200, 250, 300 and 350 ^{o}C with residence time 0 minute and at 350 ^{o}C with continually heated for 60 min with constant heating rate. After the autoclave reactor was heated up to the desired temperature, the extracted products; the mixture composed of the solid extracted after precipitation at room temperature called Deposit and the extracted dissolving in the solvent (liquid phase) called Solvent-soluble, were transferred immediately to the reservoir through the opening valve. The mixture was then separated into Solvent-soluble and Deposit by a vacuum filter using 0.5 μm-PTFE filter. Each experiment of extraction temperature was performed under the same condition and procedure.

Liquid membrane-FTIR

The detailed procedure of liquid membrane-FTIR experiments has been described in Chapter 2. Liquid membrane-FTIR spectroscopy was performed to examine the changing of functional groups of solvent-soluble of biomass obtained from degradative solvent extraction. Each measurement of the background spectrum of the air was collected immediately before collecting the single-beam spectrum. The measurement spectrum was divided into two regions: the -OH (3650–3100 cm^{-1}) and oxygen-containing (1850–1500 cm^{-1}) regions shown in Figure 5.3. From the RS spectrum, first the 1-MN spectrum was subtracted as a solvent background. Because a change in the reflectance of the samples resulted when the baseline of the spectra changed with the treatment temperature, a baseline correction was performed as follows: A straight line was drawn through two points passing two absorption minima at around 3650 and 3150 cm^{-1} for the OH-stretching region, and at around 1870 and 1500 cm^{-1} for the oxygen-containing region. The IR spectrum was deconvoluted after the baseline variation was corrected. The software Igor Pro 7 was used for processing the spectrum using a multi-peak fit function with the least squares fitting algorithm. A Gaussian distribution was used as the peak shape [23-28]. The number, sub-peak position, peak width and their variation ranges were assigned as in Table 5.1. The band deconvolution was assigned regarding the spectra obtained for the FTIR analysis of coal and biomass to characteristic group frequencies. The band assignment in the -OH region [49] and the nine bands in the

oxygen-containing region (anhydride, ester, aldehydes, carboxyl groups, conjugated carbonyl groups, etc.) were assigned to resolve. The integrated peak area of each functional group was obtained from the derived peak by fitting until convergence with the original curve was nearly achieved.

To ensure the reliability and reproducibility of the method employed, each sample was prepared and analyzed through seven samplings. The standard deviations of the functional groups at different treatment temperatures are presented as the error bar illustrated in Figure 5.4(a) for the OH-stretching region and in Figure 5.4(b) for the oxygen-containing region, and the goodness of fit is represented as a chi-square value. The contribution of the functional groups to the form in each region of the spectrum was calculated by taking the integral of absorbance of the band as 100% on the basis of curve fitting.

TABLE 5.1

Peak Assignments of IR Spectra Of The Oxygen Containing Groups

No	Theoretical band center (cm^{-1})	Wavenumber of fitting (cm^{-1})*	Deviation (cm^{-1}) **	Peak Assignments	References
1	3540	3547.2	±23.0	OH-π hydrogen bonds	15, 25
2	3400	3424.8	±25.9	self-associated *n*-mers (n>3)	15, 25
3	3290	3290.4	±16.3	OH-ether O hydrogen bonds	15, 25
4	3150	3208.5	±5.0	tightly bound cyclic OH - tetramers	15, 25
5	1800	1803.7	±5.8	asymmetric anhydride ($-C(O)_2O-$)	26, 27
6	1770	1757.1	±13.7	ester (-COO)	28-31
7	1740	1762.2	±20.0	aldehydes (-CHO)	26, 27
8	1710	1712.1	±2.7	carboxylic acids (COOH)	28-32
9	1670	1689.4	±6.3	conjugated carbonyl (CO)	28-32
10	1650	1630	±6	highly conjugated carbonyl (CO)	31, 32
11	1607	1596.4	±0.3	aromatics C=C	15, 28, 31, 32
12	1580	1581.8	±2.7	aromatics stretching	15, 31, 32
13	1560	1566.4	±0.9	aromatics stretching	15, 31, 32

*, **: Wavenumber of fitting and deviation obtained from the average and standard deviation of the fitting results of all treatment temperature (Peak center shifts with different treatment temperature)

The estimation of the strength distribution of hydrogen bonds

The estimation of the strength distribution of hydrogen bonds was examined in the main region of hydrogen bonding in the hydroxyl region [49]. The curve fitting method was used to divide the FTIR spectra into six hydrogen bonded OH bands: OH-π, self-associated OH, OH-ether, tightly bound cyclic OH tetramers, OH-N, COOH dimers and the free OH if it exists; three CH stretching bands, one aromatic hydrogen and two aliphatic hydrogen [49]. In this work, OH-N, COOH dimer and three of the CH stretching bands were not observed due to the effect of interference of the solvent, which will be described in the section on the FTIR study. The IR spectra of the RS Solvent-soluble at each treatment temperature obtained from liquid membrane-FTIR were peak-resolved using the same method as in considering the change of the functional groups during solvent treatment. The amount of hydroxyls contributing to each hydrogen bond, $n_{\mathrm{OH},j}$, was estimated based on Beer's law by Equation (1), where A_i is the peak area of OH for the jth peak, $\alpha_{\mathrm{OH},0}$ is the absorptivity of the stretching vibration of the free OH, and $\Delta\nu_{OH,j}$ is the wavenumber shift of OH in hydrogen bonds relative to the position of free OH groups (3611 cm^{-1}). The $\alpha_{\mathrm{OH},0}$ value used to calculate the amount of OH was estimated referring to the slope of the free OH calibration curve with their concentrations as in the previous study [42]. The total amount of OH, $(n_{\mathrm{OH}})_{\mathrm{total}}$, related to each absorption band can be calculated by Equation (2).

$$n_{\mathrm{OH},j} = A_i/\{\alpha_{\mathrm{OH},0}(1 + 0.0147(\Delta\nu_{OH,j}))\} \quad \text{(mg-soluble.ml}^{-1}\text{-1MN)} \quad (1)$$

$$(n_{\mathrm{OH}})_{\mathrm{total}} = \sum_i n_{\mathrm{OH},j} \quad \text{(mg-soluble.ml}^{-1}\text{-1MN)} \quad (2)$$

When the bond formed is stronger, the IR wavenumber of OH-stretching vibration shifts to a lower wavenumber and releases energy ($\Delta H < 0$). The enthalpy change, ΔH, has been interpreted as the strength of the hydrogen bonds by many investigators [44, 57]. The strength of each hydrogen bond was estimated by the relationship between the enthalpy change of formation, ΔH, and the OH wavenumber shift, $\Delta\nu_{OH}$, known as 'the linear enthalpy-spectroscopic shift relations' obtained by Drago et al. [44]. The strength of the jth hydrogen bonds was calculated by Equation (3) and the total enthalpy for the formation of all OH-associated hydrogen bonds $(-\Delta H)_{\mathrm{total}}$ was calculated using Equation (4) [49].

$$(-\Delta H)_j = 0.067(\Delta\nu_{OH,j}) + 2.64 \quad \text{(kJ.mol}^{-1}\text{)} \quad (3)$$

$$(-\Delta H)_{\mathrm{total}} = \sum_j n_{\mathrm{OH},j}\,(-\Delta H)_j \quad \text{(kJ.mol}^{-1}\text{)} \quad (4)$$

5.3 Quantitative Analysis

Liquid membrane-FTIR spectroscopy was employed to obtain the IR spectra of the RS Solvent-soluble from DSE. Quantitative analyses of these spectra were used to study the evolution of the functional groups and to observe changes to the hydrogen bonding of the Solvent-soluble during the solvent treatment. The spectra for the background solvent, 1-MN, were subtracted from the as-measured spectra, and a baseline correction was performed over the regions of interest. The OH-stretching region and the carbonyl region were measured due to their relationship with the oxygenic functional groups [64]. The peak assignments are listed in Table A1. Overlapping peaks and the peak areas of different functional groups were deconvoluted and determined using Igor Pro 7.

5.3.1 FTIR Spectra of The Rice Straw Solvent-Soluble

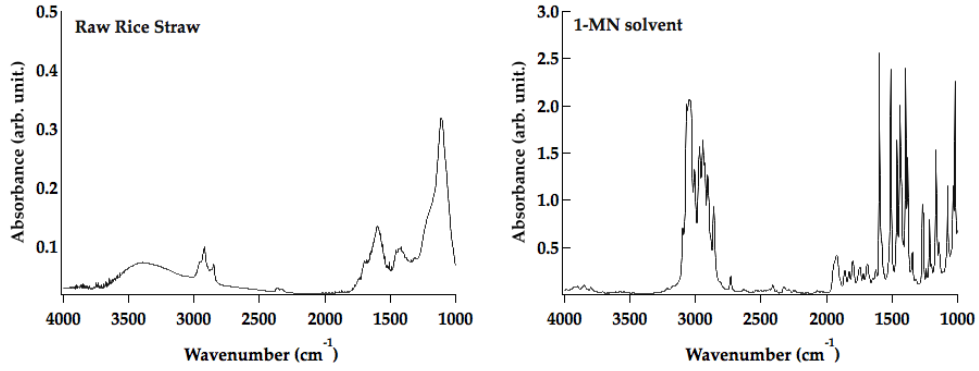

(a) (b)

Figure 5.1. FTIR spectra of (a) the raw RS obtained by the conventional KBr pellet and (b) 1-MN solvent obtained by liquid membrane-FTIR

Figure 5.1(a) illustrates the broad spectrum of the raw RS obtained from the conventional KBr pellet. The O-H stretching region (3600–3100 cm^{-1}), the C-H stretching region (3000–2800 cm^{-1}) and the C-O, C-OH, C-O-C stretching bands of cellulose (1100–1000 cm^{-1}) were identified and assigned based on published data [16]. The spectrum for 1-MN, shown in Figure 5.1(b), exhibited the aromatic C-H stretching band at 3047 cm^{-1}, the aliphatic C-H stretching band at 2980–2870 cm^{-1}, as well as a weak band at 3009 cm^{-1}. The spectrum also displayed the C-C-H in-plane ring bending region (1300–100 cm^{-1}) and the C-H in-plane bending vibration region (1420–1128 cm^{-1}).

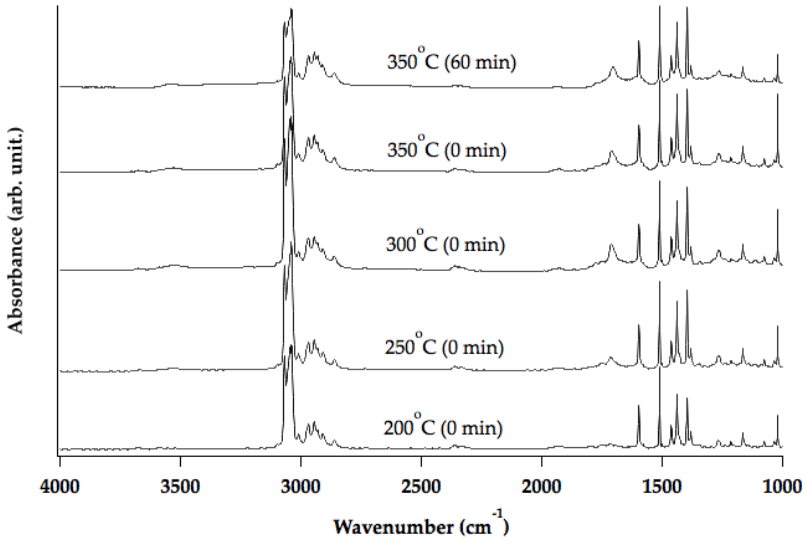

Figure 5.2. FTIR spectra of the Solvent-soluble obtained at 200, 250, 300, and 350°C with residence time 0 min and at 350°C with residence time 60 min

The spectra of the Solvent-soluble obtained at each batch extraction are shown in Figure 5.2. The figure shows the IR spectra of the Solvent-soluble of RS prepared at 200, 250, 300, and 350°C with residence time 0 min and at 350°C with residence time 60 min. The spectra characteristics are analogous to the spectrum of 1-MN. The Solvent-soluble spectra were different from those for the raw RS in that the Solvent-soluble spectra displayed weakened OH-stretching bands, more distinct bands for aromatic C-H stretching at 3050 cm^{-1}, aliphatic C-H, C-H_2, C-H_3 stretching at 2960–2850 cm^{-1}, and C=O stretching at 1700 cm^{-1}, as well as other peaks associated with bond deformation at 1500–1000 cm^{-1} [16]. The oxygen-containing region (1800–1500 cm^{-1}) increased with the solvent treatment temperature from 200 to 300°C and decreased when the treatment temperature changed from 300 to 350°C. The peak related to the C-H band of the Solvent-soluble displayed significant overlap between the different samples due to the strong C-H band for 1-MN. In order to overcome this interference of the background sample, the quantitative analysis in this study focused the absorbance region in between 3600 to 3100 cm^{-1} for the oxygen-hydrogen (-OH) stretching region and 1800 to 1500 cm^{-1} for the oxygen-containing region.

5.3.2. Quantitative Analysis of the IR Spectra of the Rice Straw Solvent-soluble

5.3.2.1. Changes of the functional groups during solvent treatment

The adjusted measurement conditions resulted in smoother FTIR spectra, reduced deviation in the wavenumber shift relative to the initial peak of the region,

and increased precision in the identification of the two absorption minima required for baseline correction. The curve-fitting results were successfully achieved with small chi-square values.

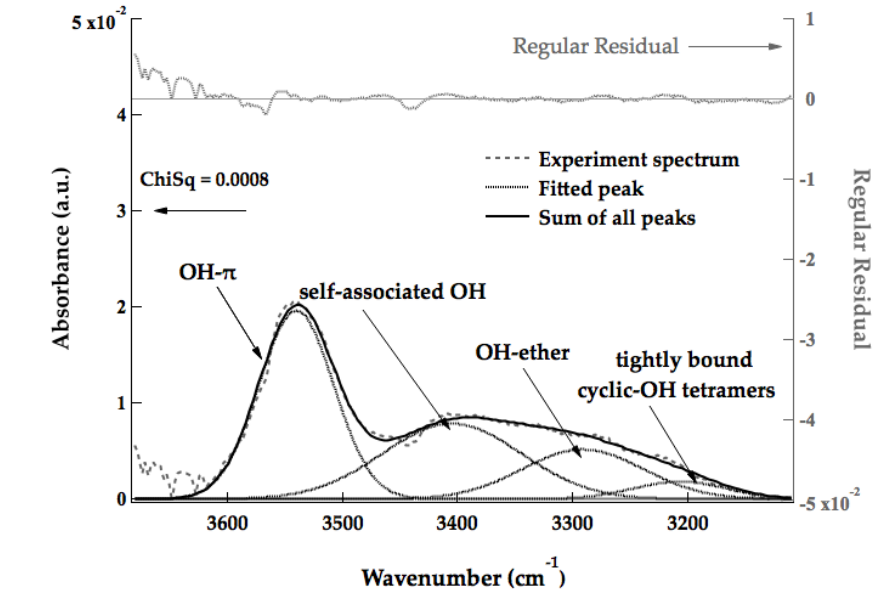

(a)

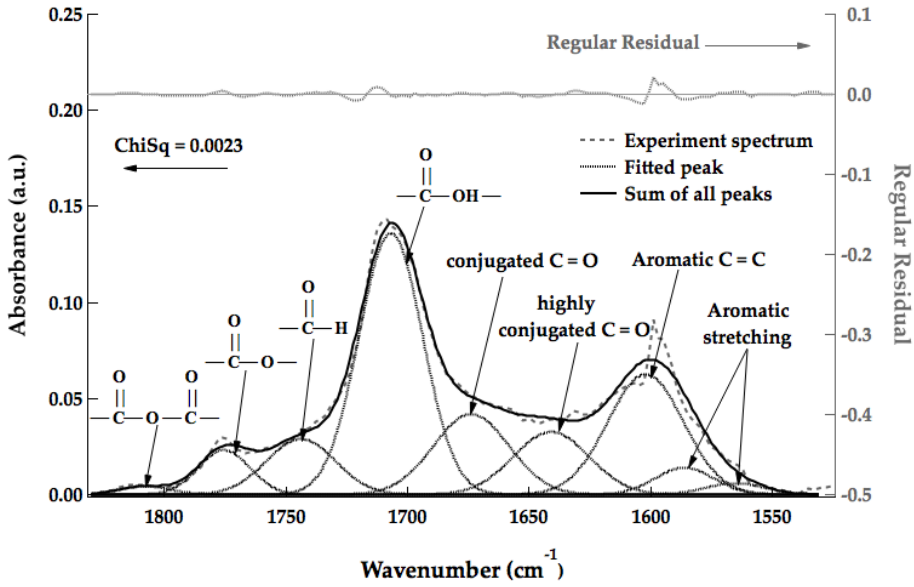

(b)

Figure 5.3. Curve-fitting of absorption bands by liquid membrane-FTIR of solvent soluble of RS at 350°C treatment temperature: (a) the OH-stretching region (3650–3100 cm^{-1}), (b) the oxygen-containing region (1850–1500 cm^{-1}).

Figure 5.3(a) shows the OH bands in the OH-stretching region (3650–3100 cm^{-1}). The wide band centred at around 3400 cm^{-1} was attributed to the hydrogen bonding of the self-associated OH n-mers and the distinct peak at 3540 cm^{-1} was

attributed to OH-π hydrogen bonding. The other two hydrogen bonds identified in the spectra were for the OH-ether O functional group and for the tightly bound cyclic-OH tetramers at 3280 and 3170 cm^{-1}, respectively. Curve-fitting was successfully used to identify peaks in the oxygen-containing region from 1850 to 1500 cm^{-1}. Figure 5.3(b) shows the bands for the nine oxygenic functional groups identified in this region. The strongest absorption band (1710 cm^{-1}) was attributed to carboxyl groups (-COOH), while shoulder bands at 1800, 1770, and 1740 cm^{-1} were assigned to anhydrides (-COOCO), esters (-COO) and aldehydes (-COH), respectively. Weak bands relative to the carboxyl groups at 1670 and 1650 cm^{-1} were attributed to conjugated carbonyl structure groups (-$C(O)_2O$). The band at 1607 cm^{-1} was attributed to aromatic C=C bonds, while the peaks at 1580 and 1560 cm^{-1} were associated with aromatic stretching bands.

Figure 5.4 illustrates the peak areas of the functional groups identified from the deconvolution of the FTIR spectra at each treatment temperature. The solid line represents the summation of the peak area of each functional group, while the dashed line represents the ratio of the total peak area to the weight percentage yield of the RS Soluble, which was obtained from the Soluble solid fraction after removal of the solvent. Figure 5.4(a) shows the absorbance area of each hydroxyl functional group in the OH-stretching region. Hydrogen bonds for OH-π and for the self-associated OH n-mers were observed from 200°C, with the area for each group increasing up to 300°C and then decreasing at higher treatment temperature. The OH-ether hydrogen bonds were first measured at 300°C and 350°C (0 min), while hydrogen bonds for the tightly bound cyclic-OH tetramers were found only at 350°C (60 min). The total peak area of hydrogen bonds at each temperature was found by summing the peak areas of the above groups. As the temperature increased from 200°C to 300°C, the total peak area of hydrogen bonds relative to the yield of RS Soluble changed little. This suggests that, as the temperature increased, the measured increase in Soluble quality was not the result of any increase in hydrogen bonds. Figure 5.4(b) shows the peak area of the various functional groups in the oxygen-containing region (1800–1500 cm^{-1}) at each treatment temperature. From 200°C to 300°C, an increase in the peak area was observed for carbonyl functional groups at 1800, 1770, 1740, 1709, 1670 and 1650 cm^{-1}. This indicates that carbonyl intermediate species in RS Solvent-soluble were formed during the solvent treatment. The aromatic C=C band at 1600 cm^{-1} and those for aromatic stretching at 1580 and 1560 cm^{-1} were found to increase slightly at 200°C, and increased further at 300°C and above. The peak areas of the carbonyl functional groups decreased from 300°C to 350°C (0 min). The percentage decreases in the peak areas for esters, highly

conjugated carbonyls, aldehydes, carboxylic groups, and conjugated carbonyls from 300°C to 350°C (0 min) were approximately 55.9, 35.2, 28.4, 19.9, and 12.8, respectively. In contrast, anhydrides increased significantly from 300°C to 350°C (0 min). From 350°C (0 min) to 350°C (60 min), anhydrides, esters, carboxylic acids, and conjugated carbonyl functional groups decreased slightly, while aldehydes, highly conjugated carbonyl groups, aromatic C=C bonds, and aromatic stretching bands were observed to increase slightly.

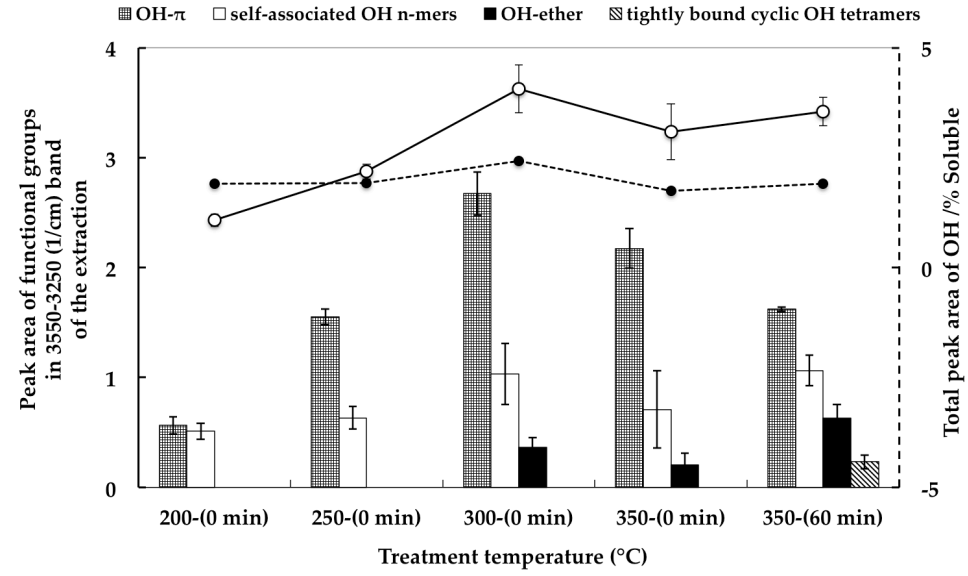

(a)

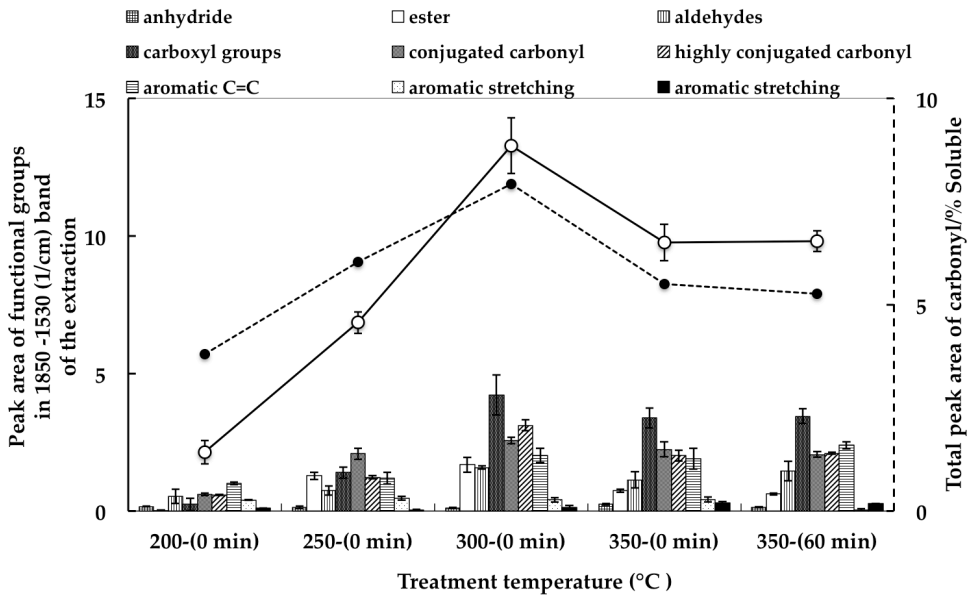

(b)

Figure 5.4. Peak areas for the different functional groups in (a) the OH-stretching region (3650–3100 cm^{-1}) and (b) the oxygen-containing region (1850–1500 cm^{-1}) with the standard error at 200, 250, 300, 350°C for 0 min and at 350°C for 60 min. Solid lines depict the total

peak area for each group and the dashed lines show the ratio of the peak area to the soluble yield.

Wannapeera et al. previously reported on the generation of CO and CO_2 in DSE from 300°C to 350°C [16]. The significant decreases in aldehydes, esters, conjugated carbonyls, and highly conjugated carbonyl groups between 300°C and 350°C not only signified the occurrence of deoxygenation, but also suggested the involvement of these groups in the release of CO and CO_2. The significant reduction of the carboxylic groups from 300°C to 350°C (0 min) also suggested the occurrence of decarboxylation. The appearance of a distinct anhydride peak at 350°C (0 min) suggests the occurrence of dehydration, as Miura et al. linked the observation of anhydrides to the decomposition of hydrogen bonds for COOH dimers in the hydroxyl region for coal with the formation of water [49].

TABLE 5.2

Peak area ratio of carboxylic groups to aromatic groups

Treatment temperature (°C)	C=O/Aromatic C=C
300 (0 min)	2.08
350 (0 min)	1.78
350 (60 min)	1.44

Table 5.2 shows the peak area ratio of the carboxylic groups (1709 cm^{-1}) to the aromatic groups (1600 cm^{-1}) at 300°C and 350°C (0 min), and at 350°C (60 min). The ratio decreased both with increased treatment temperature and with increased residence time. Previous work by Zhu et al. [18] suggested a direct link between deoxygenation and the reduction of carboxylic groups and the increase in aromatic groups during solvent extraction. Combining the results from Table 1, with the observed changes to the active oxygen-containing functional groups, such as the hydroxyl groups, which decreased from 300°C to 350°C (0 min), suggests the occurrence of aromatization from 300°C to 350°C (0 min).

5.3.2.2. Changes of hydrogen bonding during solvent treatment

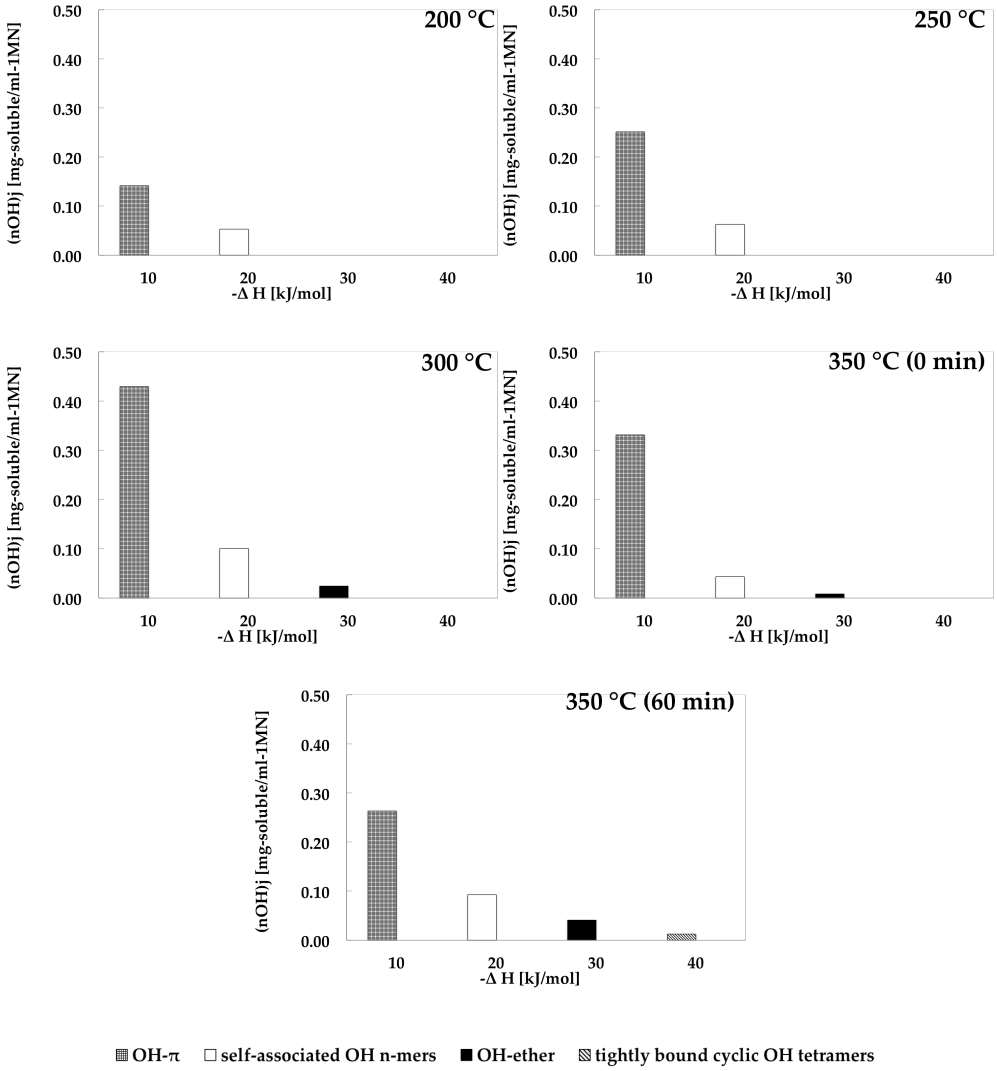

Figure 5.5 The relationship between the amount and the strength of OH associated hydrogen bonds (OH-π, self-associated OH n-mers, OH-ether and tightly bound cyclic OH tetramers) at each treatment temperature for the RS Solvent-soluble.

Figure 5.5 shows the estimated amount and strength of the OH-associated hydrogen bonds at each treatment temperature. The number of hydroxyl groups for each hydrogen bond, ($n_{OH,j}$), was estimated from each peak area, A_i, and the OH wavenumber shift, $\Delta\nu_{OH}$, using Equation (1). The strength of each hydrogen bond was interpreted from the relationship between the enthalpy change, ΔH and $\Delta\nu_{OH}$ as shown in Equation (4). In terms of the estimated bond strength, the cyclic-OH was identified as the strongest of the four types of hydrogen bonds, followed by OH-ether, the self-associated OH n-mers, and finally OH-π, which had the weakest

estimated bond strength. Only the weaker of the hydrogen bonds (OH-π and the self-associated OH n-mers) were observed at treatment temperatures of 200°C and 250°C. OH-ether was observed starting at 300°C, while the strongest of the four groups, cyclic-OH, was observed only at 350°C during the prolonged residence time. This indicates that weaker hydrogen bonds were broken at lower treatment temperatures, while the breaking of stronger hydrogen bonding groups occurred only at increased treatment temperatures and times.

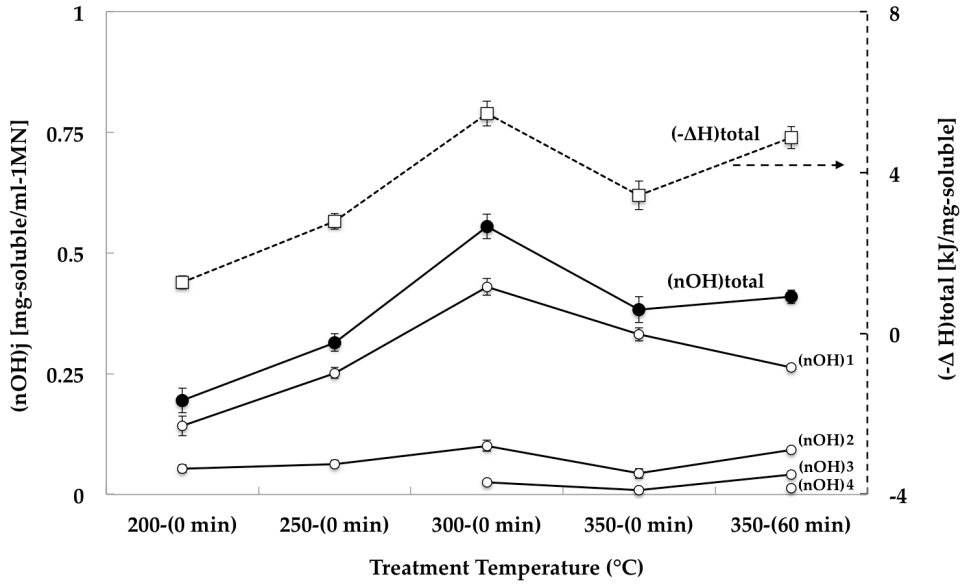

Figure 5.6. The amount of each OH-associated hydrogen bonding group $(n_{OH})_{1\text{-}4}$, the total number of hydrogen bonds $(n_{OH})_{total}$, and the total enthalpy for the formation $(-\Delta H)_{total}$ for all of the OH-associated hydrogen bonds at each treatment temperature.

Figure 5.6 shows the estimated amount of the OH-associated hydrogen bonds at the different treatment conditions. The amount of each hydrogen bond was abbreviated as follows: $n_{OH,1}$ for OH-π, $n_{OH,2}$ for the self-associated OH n-mers, $n_{OH,3}$ for OH-ether, and $n_{OH,4}$ for the cyclic-OH. At all treatment conditions, the amount of OH-π hydrogen bonds was greater than for the other OH groups. OH-π hydrogen bonds, along with those for the self-associated OH n-mers, were the only hydrogen bonds to be measured in all treatment conditions. These hydrogen bonds increased with temperature until 300°C and were then observed to decrease at 350°C (0 min). However, for the prolonged residence time at 350°C, the amount of OH-π hydrogen bonds decreased further, while the hydrogen bonds for the self-associated OH n-mers were observed to increase. The hydrogen bonds associated with OH-ether were first measured at 300°C and decreased in number at 350°C (0 min). However, like

the self-associated OH n-mers, the amount of the OH ether hydrogen bonds was seen to increase slightly during the prolonged residence time at 350°C. The hydrogen bonds associated with the cyclic-OH were only measured at the prolonged residence time at 350°C, and not in great number.

Figure 5.6 also shows the total number of hydrogen bonds associated with OH groups, as well as the total enthalpy for the formation of these bonds. Both the total number of hydrogen bonds and the total change in the enthalpy of formation were observed to increase from 200°C to 300°C, and then decrease at 350°C (0 min). For the prolonged residence time at 350°C, the total enthalpy was observed to increase slightly while the total number of hydrogen bonds remained relatively unchanged. However, in the same treatment conditions, changes were observed in the number of hydrogen bonds for the different OH groups. In combination with the observed increase in the total change in enthalpy, this suggests a release of the hydrogen bonds associated with the self-associated OH n-mers, the OH-ether, and the cyclic-OH groups, which all experienced an increase during this treatment condition.

The measured increase in the amount of hydrogen bonds related to OH-π and the self-associated OH n-mers, in combination with the observed increase in the total change in the enthalpy for the same treatment conditions, suggest that the hydrogen bonds for these two groups were released. Research by Miura et al. reported that the total number of hydrogen bonds and consequently the total change in enthalpy decreased when H_2O is produced during heat treatment [15]. This suggests that the main removal of H_2O in DSE of RS occurred from 300°C to 350°C (0 min). Similarly, the decrease in the hydrogen bonds associated with OH-π and the increase in the total change in enthalpy over the prolonged residence time at 350°C also suggests that the release of H_2O molecules is occurring during this period. This is in agreement with other research that has found that the increasing residence time increases the removal of water [18].

From the quantitative results obtained in this work, the schematic in Figure 5.7 was postulated for the reaction process of DSE of RS. Specifically, the DSE process was divided by temperature range into three stages: from 200°C to 300°C; from 300°C to 350°C (0 min); and during the prolonged residence time of 60 min at 350°C. The first stage was characterized by the release of hydrogen bonds via dehydration and the presence of aromatic compounds. The second stage was marked by the removal of the main oxygen-containing groups (H_2O, CO and CO_2) through dehydration and decarboxylation, and the occurrence of aromatization. The third stage occurred during the prolonged residence time at 350°C (0 min to 60 min), and

was characterized by aromatization and dehydration reactions. At all stages, dehydration and the presence of aromatic C=C groups were observed. This indicates that intramolecular reactions were the predominant mechanism for dehydration in RS DSE. This also signifies that polymerization of RS during the DSE process was suppressed and that the final product is composed of smaller molecular compounds. The suggestion of dehydration along with the observed presence of aromatic C=C bonds at each stage clarified that intramolecular reactions were the dominant process reactions among hydrogen bonds of RS during DSE.

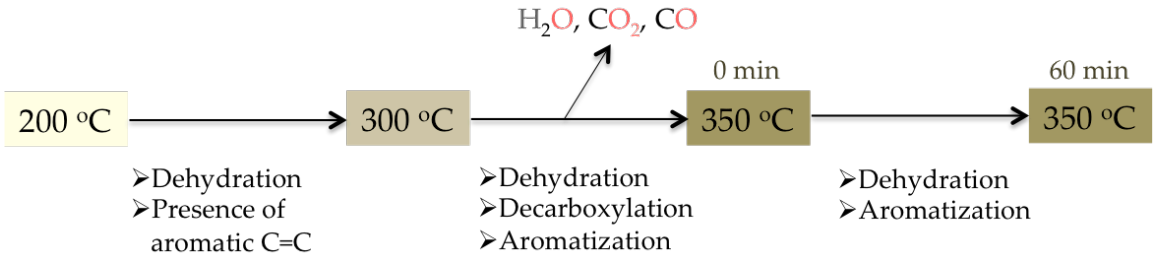

Figure 5.7. Schematic postulated for the reaction process of the DSE of RS

References

[1] Wannapeera J.; Li X.; Worasuwannarak N.; Ashida R.; Miura K. Production of high-grade carbonaceous materials and fuel having similar chemical and physical properties from various types of biomass by degradative solvent extraction. *Energy Fuels* 2012, *26*, pp. 4521–4531.

[2] Zhu X.; Xue Y.; Li X.; Zhang Z.; Sun W.; Ashida R.; Miura K.; Yao H. Mechanism study of degradative solvent extraction of biomass. *Fuel* 2016, *165*, pp. 10–18.

[3] Ashida R.; Takahashi R.; Kawase M.; Miura K. Upgrading mechanism in degradative solvent extraction of biomass wastes. 12th EMSES, 2015.

[4] Bertie J.E.; Keefe C.D.; Jones R.N. Infrared intensities of liquids VIII. Accurate baseline correction of transmission spectra of liquids for computation of absolute intensities, and the 1036 cm− 1 band of benzene as a potential intensity standard. *Canadian Journal of Chemistry* 1991, *69*(11), pp. 1609-1618.

[5] Porter J.M., Jeffries J.B., Hanson R.K. Mid-infrared absorption measurements of liquid hydrocarbon fuels near 3.4 μm. *Journal of Quantitative Spectroscopy and Radiative Transfer*, 2009, *110* (18), pp. 2135-2147.

[6] Dong A., Huang P., Caughey W.S. Protein secondary structures in water from second-derivative amide I infrared spectra. *Biochemistry 1990, 29* (13), pp. 3303-3308.

[7] Yu S., Wuu A., Basu R., Holbrook M.R., Barrett A.D., Lee J.C. Solution structure and structural dynamics of envelope protein domain III of mosquito-and tick-borne flaviviruses. *Biochemistry* 2004, *43* (28), pp. 9168-9176.

[8] Watcharakorn K., Trirat M., Janewit W., Zen H., Kii T., Miura K., Ohgaki H. Proposal of liquid membrane-FTIR spectroscopy to quantify the oxygen content in soluble fraction of degradative solvent-extraction. *Int. J. Exp. Spectroscopic Tech.* 2017, pp. 2-10.

[9] Watcharakorn K., Janewit W., Zen H., Kii T., Miura K., Ohgaki H. The mechanism study of degradative solvent extraction of biomass by liquid membrane-Fourier Transform Infrared spectroscopy. *Int. J. Physical and Mathematical Science* 2018, 12(1), pp. 9-13.

[10] Drago R.S.; Epley T.D. Enthalpies of hydrogen bonding and changes in hydroxy frequency shifts for a series of adducts with substituted phenols. *Journal of the American Chemical Society* 1969, *91* (11), pp. 2883-2890.

[11] Larsen J.W.; Gurevich I.; Glass A.S.; Stevenson D.S. A method for counting the hydrogen-bond cross-links in coal. *Energy & Fuels* 1996, *10* (6), pp. 1269-1272.

[12] Chen C.; Gao J.; Yan Y. Observation of the type of hydrogen bonds in coal by FTIR. *Energy & Fuels* 1998, *12* (3), pp. 446-449.

[13] Miura K.; Kazuhiro M.; Fumi-aki M. A new method to estimate hydrogen bonds in coal by utilizing FTIR and DSC. *Am. Chem. Soc. Fuel Div.* 1997, *42*, 209-213.

[14] Miura K.; Mae K.; Li W.; Kusakawa T. and Kumano A. In situ FT-IR measurement of the change in hydrogen bonding of coal through heat treatment. In *abstracts of papers of the american chemical society* 1999 (vol. 218, pp. U612-u612). Washington, dc: amer. Chemical soc.

[15] Miura K.; Mae K.; Li W.; Kusakawa T.; Morozumi F.; Kumano A. Estimation of hydrogen bond distribution in coal through the analysis of OH stretching bands in diffuse reflectance infrared spectrum measured by in-situ technique. *Energy & Fuels* 2001, *15* (3), pp. 599-610.

[16] Barry B.A.; Brahmachari U.; Guo Z. Tracking reactive water and hydrogen-bonding networks in photosynthetic oxygen evolution. *Accounts of Chemical Research* 2017, *50* (8), pp. 1937-1945.

[17] Solomon P.R. Relation between coal structure and thermal decomposition products. In *Coal Structure: Advances in Chemistry Series*; Gorbaty M. L.; Ouchim, K., Eds.; ACS: Washington, DC, 1981; Vol. 192, Chapter 7, pp. 95.

[18] Fuller Jr E.L.; Smyrl N.R. Chemistry and structure of coals: diffuse reflectance IR spectroscopy equipment and techniques. *Fuel* 1985, *64* (8), pp. 1143-1150.

[19] Kadla J.F.; Kubo S. Miscibility and hydrogen bonding in blends of poly (ethylene oxide) and kraft lignin. *Macromolecules* 2003, *36* (20), pp. 7803-7811.

[20] Kubo S.; Kadla J.F. Hydrogen bonding in lignin: a Fourier transform infrared model compound study. *Biomacromolecules* 2005, *6* (5), pp. 2815-2821.

[21] Poletto M.; Pistor V.; Santana R.M.C.; Zattera A.J. Materials produced from plant biomass: part II: evaluation of crystallinity and degradation kinetics of cellulose. *Materials Research* 2012, *15*(3), pp.421-427.

[22] Poletto M.; Zattera A.J. Materials produced from plant biomass: part III: degradation kinetics and hydrogen bonding in lignin. *Materials Research 2013*, *16* (5), pp. 1065-1070.

[23]Arnett E.M.; Mitchell E.J.; Murty T.S.S.R. Basicity. Comparison of hydrogen bonding and proton transfer to some Lewis bases. *Journal of the American Chemical Society* 1974, *96* (12), pp. 3875-3891.

[24]Miura K.; Mae K.; Ashida R.; Tamura T.; Ihara T. Dewatering of coal through solvent extraction. *Fuel* 2002, *81* (11-12), pp. 1417-1422.

[25]Painter P.C.; Sobkowiak M.; Youtcheff J. FT-IR study of hydrogen bonding in coal. *Fuel* 1987, 66, pp. 973-978.

[26]Painter P.C.; Starsinic M.; Coleman M.M. Determination of functional groups in coal by Fourier transform interferometry. In *Fourier Transform Infrared Spectroscopy*; Ferraro J.R.; Basile L.J., Eds. Academic Press; New York, NY, USA, 1985, pp. 169–240.

[27]Painter P.C.; Snyder R.W. The application of Fourier transform infrared spectroscopy to the characterization of coal structure. *Fuel* 1979, *58*, pp. 301-308.

[28]Supaluknari S.; Larkins F.P. An FTIR study of Australian coals: characterization of oxygen functional groups. *Fuel Processing Technology 1988*, *19*, pp. 123-140.

[29]Ibarra J.V.; Munoz E.; Moliner R. FTIR study of the evolution of coal structure during the coalification process. *Org. Geochem*. 1996, *24*, pp. 725–735.

[30]Murakami K.; Shirato H.; Nishiyama Y. In situ infrared spectroscopic study of the effects of exchanged cations on the thermal decomposition of a brown coal. *Fuel* 1997, *76*, pp. 655-661.

[31]Wang Y.; Wu J.; Xue Sh.; Wang J.; Zhang Y. Experimental Study on the Molecular Hydrogen Release Mechanism during Low-Temperature Oxidation of Coal. *Energy Fuel* 2017, *31*, pp. 5498-5506.

[32]Wenhua G.; Tsunemori N.; Hirokazu T.; Akira O. Analysis of carboxyl group in coal and coal aromaticity by Fourier transform infrared (FT-IR) spectroscopy. *Fuel* 2009, *88*, pp. 139-144.

CHAPTER 6
CONCLUSIONS AND RECOMMENDATIONS

Conclusions

The liquid membrane-FTIR technique was shown as a suitable technique for the quantitative analysis of the Soluble fraction in degradative solvent extraction (DSE). Measurements were successfully performed for the Solvent-soluble of rice straw (RS) without the removal of the solvent, thereby avoiding any modification of the sample. The IR spectra of the RS Solvent-soluble from DSE were recorded and quantitative analyses of these spectra were used to study the evolution of the oxygen-containing functional groups in the RS Solvent-soluble during the solvent treatment.

The oxygen content of the RS Soluble was calculated by analyzing the hydroxyl groups of the RS Solvent-soluble at 350°C (with 0 min residence time). The measured oxygen content of the RS Soluble was realistic with respect to reported values from the study reports of DSE. Repeated analyses confirmed these results and demonstrated the reliability of the technique. The overall results suggest a reliable quantity of oxygen-containing functional groups in the RS Solvent-soluble, which helps deepen the understanding of the biomass structure and the reaction mechanism of DSE. Furthermore, the RS Solvent-soluble spectra obtained from liquid membrane-FTIR provided additional quantitative information. The anhydrides, esters, aldehydes, and associated conjugated carbonyl groups were clearly observed in the liquid membrane-FTIR obtained spectra, but were not identifiable in the solid Soluble spectra obtained by conventional FTIR (the pellet method).

The main reactions of DSE were observed to be dehydration, decarboxylation and aromatization. To better understand the oxygen-containing functional groups and elucidate the reaction pathway of DSE for RS, the experimental conditions were adjusted to reduce the noise in the measured IR spectra. The newly obtained IR spectra possessed increased peak resolution and allowed for increased quantitative analysis. DSE of RS was performed in batches at 200°C, 250°C, 300°C and 350°C with 0 min residence times and at 350°C with a 60 min residence time. Analysis of the measured IR spectra identified three distinct stages in the DSE of RS reaction process. The first stage, between 200°C and 300°C, suggested the occurrence of

dehydration and the presence of aromatic C=C compounds. The second stage (300°C to 350°C at 0 min) was characterized by the removal of the main oxygen-containing groups (H_2O, CO and CO_2) as well as the occurrence of dehydration, decarboxylation and aromatization reactions. The third stage occurred during the prolonged residence time at 350°C (0 min to 60 min). The observed changes in the functional groups during this stage suggested the occurrence of aromatization and dehydration reactions. This indicates that intramolecular reactions were the predominant mechanism for dehydration in RS DSE. This also signifies that polymerization of RS during the DSE process was suppressed and that the final product is composed of smaller molecular compounds.

The study demonstrates the usefulness of liquid membrane-FTIR in the quantitative examination of the reaction process of DSE of RS., and suggests the applicability of this technique for the analysis of other solvent–carbon based interactions in a variety of disciplines.

Recommendations

- The prolonged residence time indicates the necessity for biomass upgrading by DSE and enhanced oxygen removal.
- Liquid membrane-FTIR is not suitable for analyzing the structural dependence of CH bond absorptivity of the Solvent-soluble in a C-H bond-containing solvent. Thus, for reliable analysis of C-H bonds in the Solvent-soluble, a solvent with no C-H bonds is recommended.
- Liquid membrane-FTIR can be applied to real-time and in-situ analysis for DSE or other solvent processes
- Liquid membrane-FTIR is suitable for the analysis of other solvent–carbon based interactions in a variety of disciplines
- The combination the other non-destructive techniques for in-situ analysis such as Laser-Induced Fluorescence (LIF) and/or Photoacoustic spectroscopy (PAS) in analyzing the aromatic hydrocarbon evolution and other functional groups in fingerprint regions, respectively, could reduce analysis time. In addition, the observation without sample modification by using the spectroscopic technique could be reliable in predicting the reaction process and optimizing the DSE condition.

LIST OF PUBLICATIONS

Journal Publications

1. Watcharakorn K*., Trirat M., Janewit W., Zen H., Kii T., Miura K., Ohgaki H. Proposal of liquid membrane-FTIR spectroscopy to quantify the oxygen content in soluble fraction of degradative solvent-extraction. *Int. J. Exp. Spectroscopic Tech.* **2017**, pp. 2-10
2. Watcharakorn K*., Janewit W., Zen H., Kii T., Miura K., Ohgaki H. The mechanism study of degradative solvent extraction of biomass by liquid membrane-Fourier Transform Infrared spectroscopy. *Int. J. Physical and Mathematical Science* **2018**, 12(1), pp. 9-13.
3. Watcharakorn K*., Zen H., Ashida R., Kii T., Miura K., Ohgaki H. Investigation on Conversion Pathway in Degradative Solvent Extraction of Rice Straw by Using Liquid Membrane-FTIR Spectroscopy. *Energies* (*Submitted) Date of submission : Dec 3, **2018**. Status : under review*

Conference proceedings and Oral presentations

1. Watcharakorn K*., Janewit W., Zen H., Kii T., Miura K., Ohgaki H. **Liquid Membrane-Fourier Transform Infrared Spectroscopy Application on The Mechanism Study of Degradative Solvent Extraction.** *The 14th Eco-Energy and Materials Science and Engineering Symposium **2018 (**Oral presentation**)***
2. Watcharakorn K*., Janewit W., Zen H., Kii T., Miura K., Ohgaki H. **The Mechanism Study of Degradative Solvent Extraction of Biomass by Liquid-Membrane Fourier-Transform.** *ICOLS 2018: 20th International Conference on Optics, Lasers and Spectroscopy. **2018** (Proceeding and oral presentation)*
3. Watcharakorn K*., Trirat M., Janewit W., Zen H., Kii T., Miura K., Ohgaki H. **Proposal of Liquid Membrane FTIR Spectroscopy for Investigation of Soluble Fraction of Degradative Solvent-Extraction**. *13th Eco-Energy and Materials Science and Engineering Symposium, Udonthani,Thailand,* 1-3 December **2016** (*Proceeding and oral presentation*)

Posters

1. Watcharakorn K*., Trirat M., Janewit W., Zen H., Kii T., Miura K., Ohgaki H. **The Liquid Membrane-FTIR Spectroscopy for Examine of Soluble Fraction of Degradative Solvent Extraction**. *The Japan Society of Infrared Science and Technology* **2016**
2. Watcharakorn K*., Trirat M., Janewit W., Zen H., Kii T., Miura K., Ohgaki H. **Proposed Technique of Liquid Membrane-FTIR Spectroscopy for Investigation of Soluble Fraction of Degradative Solvent Extraction.** *Ajou-Kyoto-Zhejiang Joint Symposium on Energy Science* **2016**

List of Contributed Poster

1. Chandrashekhar . R , Watcharakorn . K , Zen . H. , Hideaki. O **The appliction of photoacoustic spectroscopy technique to investigate the solvent-soluble of biomass using MID-IR KU-FEL.** *The 9th International Symposium of Advanced Energy Science - Interplay for Zero-Emission Energy* September 3rd - 5th, **2018**

Award

1. Watcharakorn K*., Trirat M., Janewit W., Zen H., Kii T., Miura K., Ohgaki H. **Proposed Technique of Liquid Membrane-FTIR Spectroscopy for Investigation of Soluble Fraction of Degradative Solvent Extraction.** *Ajou-Kyoto-Zhejiang Joint Symposium on Energy Science* **2016** ***(Best Poster Award)***

APPENDIX

ADDITIONAL UNSUCCESSFUL PROTOCOL

A. Investigation on C=C and C-H Bonds of Solvent-soluble of Rice Straw by Using Liquid Membrane-FTIR

Figure A1 showed that the chemical structure of solvent-soluble of biomass, the components presented in the absorbance spectra of this study were in approximate 3600-2500 cm^{-1} (the OH stretching region) and 1800-1000 cm^{-1} (the carbonyl region, 1800-1500 cm^{-1} and the fingerprint region at 1500-1000 cm^{-1}). The significant processes of degradative solvent extraction are involving the removing of the oxygen-containing functional group, the deoxygenation and decarboxylation [1-3]. In order to study the mechanism or characterize chemical components of solvent-soluble, the extend study of C=C and C-H stretching or bending groups could give more information. As the raw sample is a grasses biomass, the typical components are cellulose, hemicellulose and lignin which consist of mainly carbohydrate and aromatic polymer. It can be basically observed that samples are most likely consisted of acid, methanol, alkyl, aliphatics, aromatics and ketone with different oxygen-containing functional groups observed, e.g., O-H (3500–3200 cm^{-1}), COOH (1700 cm^{-1}), C-O (1735–1727 cm^{-1}), C-O-C (1250–1270 cm^{-1}, 1170 cm^{-1}), and C-O(H) (1050 cm^{-1}), etc. [4]. Still, they were rich in compounds with C=C (aromatic skeleton mode) and C-H stretching or bending function groups.

Important regions are generally used for quantitative IR spectrum evaluation on relating C=C and C-H bonds;

Peak (cm−1)	Assignments
3055−3030	aromatic C−H stretching
3000−2800	aliphatic C−H stretching
1650−1520	aromatic C=C ring stretching
1520−1350	aliphatic −CH2 and −CH3 deformation
1350−1250	aromatic ether C−O−C, phenolic C−O, and ester C−O−O−C stretching
1150−950	aliphatic ether C−O−C and alcohol C−O stretching

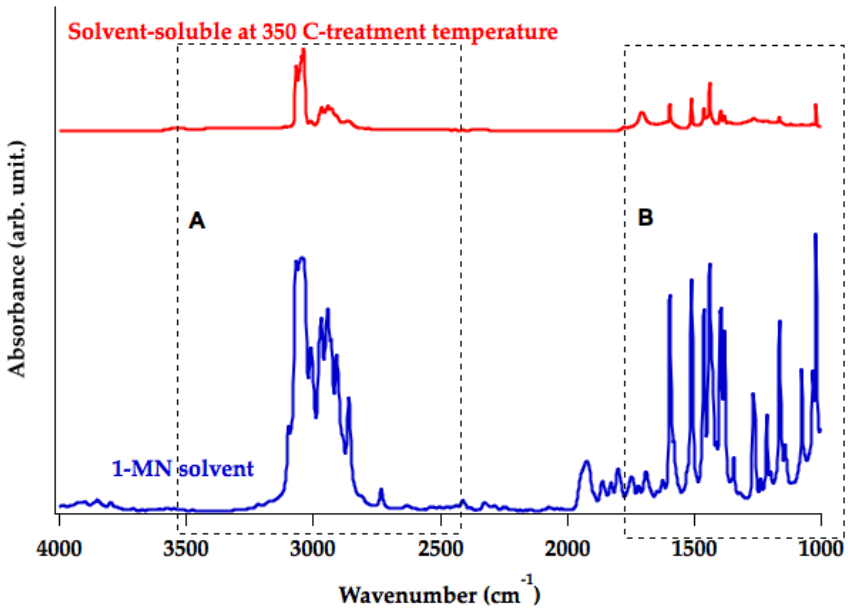

Figure A1. Comparing solvent-soluble and 1-MN solvent spectrum; A:3600-2500 cm^{-1} region and B:1800-1000 cm^{-1} region.

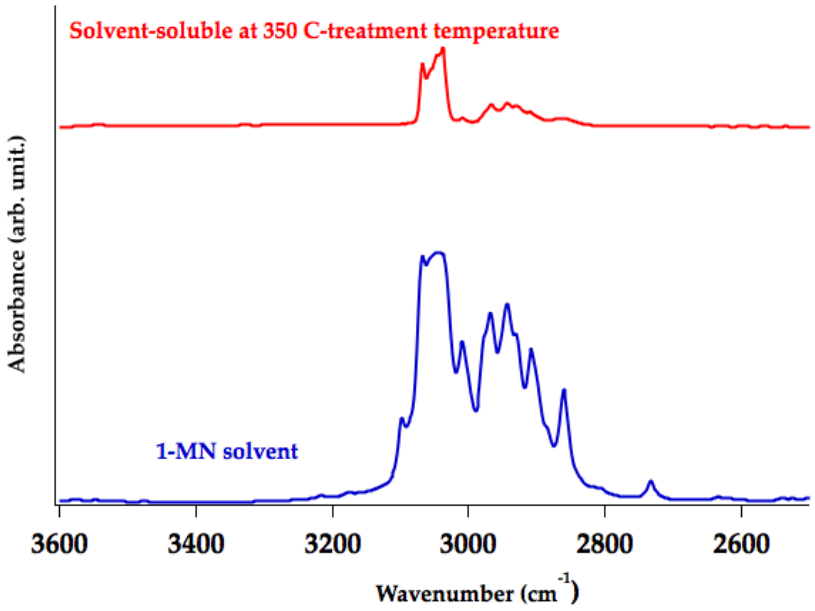

Figure A2. Zooming of 3600-2500 cm^{-1} region in comparing solvent-soluble and 1-MN solvent spectrum.

Figure A2 is the enlarge of Figure A1(A) showing the comparison of solvent-soluble and 1-MN spectrum, the similar shape of both spectrum can observe at ~3200-2800 cm^{-1}. This region relates to aromatic-aliphatic C-H region. The significant

IR peaks concerning in coal/biomass is at 3050-3058 cm^{-1} of aromatic-CH bond, and 2920-2926 cm^{-1} and 2840-2855 cm^{-1} of aliphatic-CH bond.

The effect of 1-MN spectrum to solvent-soluble sprctrum is observed by dilution solvent-soluble at 350 C-treatment temperature with 1-MN into 3 concentrations. They are 0.0023, 0.0047 and 0.0093 g-solvent-soluble/ml-1MN. IR sprectrum of 3 dilution solution are measured by liquid membrane-FTIR. The measurement is performed for 5 samplings (Figure A3). The spectrum are curve-fitted which their hidden peak positions in this region are assigned base on the IR spectra of coal, solid-soluble, solvent-soluble and 1-MN as shown in Table A1. The spectra are peak deconvolted in order to eastimate the total peak area (Figure A4). The overlap IR peaks of solvent-soluble and 1-MN related to aromatic-aliphatic CH bonds are observed, and their total peak area are presented in Table A2.

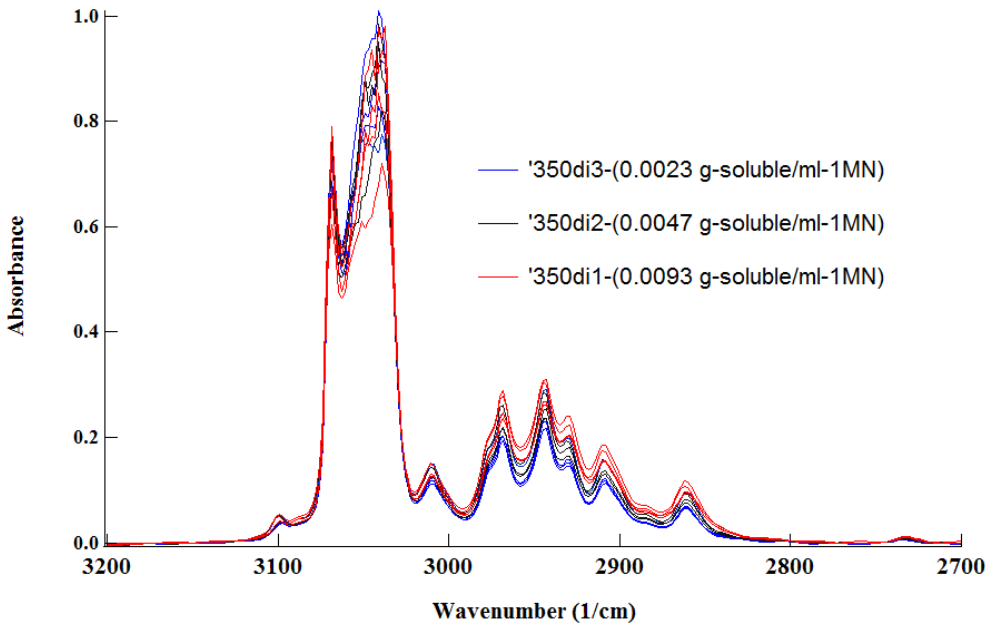

Figure A3. Spectra of the dilution solution of solvent-soluble at 350 C-treatment temperature with 1-MN.

TABLE A1

Theoritical wavenumber and peak assignments

Coal	Solid-soluble	1-MN	Solvent-soluble
3050-3058	3058	3047	3049
		3010	3009
2950-2960		2967	2968
		2943	2944
2920-2926	2923	2922	2929
2855-2900		2872	2909
2870-2874			2879
2840-2855	2852		2858
2811-2822			2822
	2795		

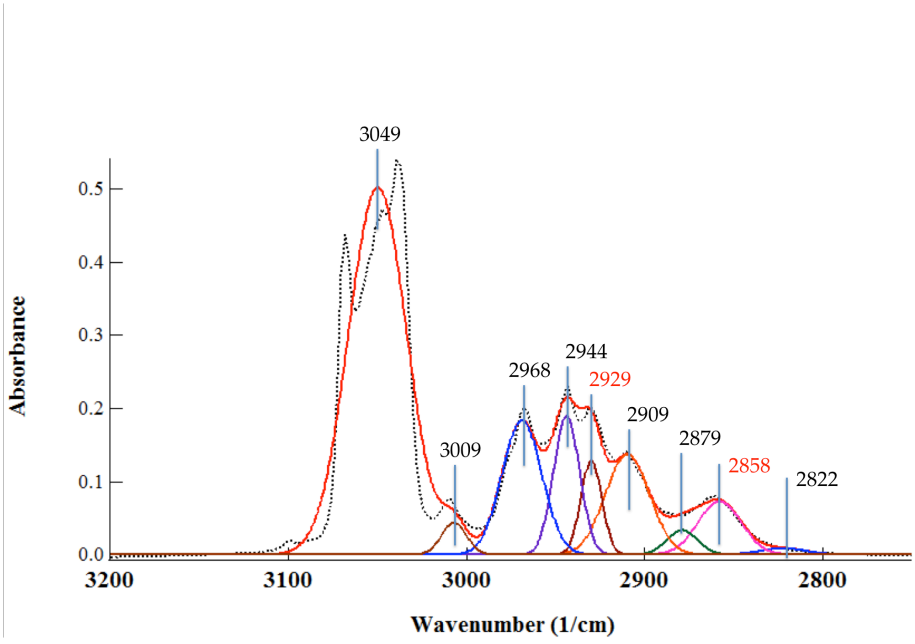

Figure A4 Peak deconvolution of solvent-soluble in the aromatic-aliphatic region

TABLE A2

Peak Area of Diluted Solvent-soluble in

Aromatic-Aliphatic CH region

Dilution solution (g-solvent-soluble/ml-1MN)	Avg. Peak Area	STD
0.0023	***33.75***	**0.03**
0.0047	***33.70***	**0.03**
0.0093	***32.60***	**0.01**

The overlap peak in aromatic-aliphatic CH region of solvent-soluble and 1-MN are observed, the related prominent peaks are at 3050 cm^{-1} of aromatic-CH, and 2928 and 2858 cm^{-1} contributing to aliphatic-CH bands. The average value of total peak area of the dilution solution of solvent-soluble suggests that the quantity in the aromatic-aliphatic CH region of solvent-soluble results from 1-MN.

As the results of this study, due to the 1-MN solvent and the sample considered in the study are the structural dependence of CH bond absorptivity. The examination on the overlapping of aromatic-aliphatic CH peaks of the solvent-soluble suggested most of 1-MN existing in solvent-soluble. The evaluation of aromatic-aliphatic CH can be greatly affected by 1-MN solvent which contains a highly aliphatic material with a high absorptivity of aliphatic CH bonds. For reliable analysis of CH bond in solvent-soluble by using liquid membrane-FTIR technique was not recommended for the CH bond-containing solvent. This technique cannot apply to investigate CH bonds of solvent-soluble in this study.

References

[1] Janewit W., Li X., Nakorn W., Ashida R., Miura K., "Production of high-grade carbonaceous materials and fuel having similar chemical and physical properties from various types of biomass by degradative solvent extraction," *Energy Fuels*, vol. 26, pp. 4521–31, 2012.

[2] Ashida R., Takahashi R., Kawase M., Miura K., "Upgrading mechanism in degradative solvent extraction of biomass wastes," 12thEMSES, 2015.

[3] Zhu X., Zhang Z., Zhou Qi, Cai T., Qiao E., Li X, Yao H. "Upgrading and multistage separation of rice straw by degradative solvent extraction," *J Fuel Chem Technol*, vol. 43, 4, pp. 422-428, 2015.

[4] H. Yang, R. Yan, H. Chen, D.H. Lee, C. Zheng, Characteristics of hemicellulose, cellulose and lignin pyrolysis, Fuel 86 (12–13) (2007) 1781–1788.